EPFL

Thèse n° 7384

Chemistry and Analysis of Nanoparticle-Modified Living Cells

Présentée le 24 septembre 2020

à la Faculté des sciences et techniques de l'ingénieur
Laboratoire des polymères
Programme doctoral en science et génie des matériaux

pour l'obtention du grade de Docteur ès Sciences

par

Tanja THOMSEN

Acceptée sur proposition du jury

Prof. D. Damjanovic, président du jury
Prof. H.-A. Klok, directeur de thèse
Prof. B. Engelhardt, rapporteuse
Prof. B. Rothen-Rutishauser, rapporteuse
Prof. E. Amstad, rapporteuse

École polytechnique fédérale de Lausanne

2020

The work described in this Thesis has been performed at the École Polytechnique Fédérale de Lausanne from August 2015 until August 2020 under the supervision of Prof. Harm-Anton Klok.

This work was financially supported by Swiss National Science Foundation (SNSF).

Acknowledgments

First, I would like to thank Harm-Anton Klok for giving me the opportunity to work on this interesting and challenging project in his lab. During the last 5 years, I appreciated a lot that you gave me help and support when I needed it but also the freedom to explore and to become the person I am now.

A special thanks goes to my committee members, Britta Engelhardt, Barbara Rothen-Rutishauser and Esther Amstad for their helpful feedback and extremely inspiring discussions. Dragan Damjanovic I would like to thank for making sure that my defense via Zoom went smoothly.

I want to express my gratitude to Britta Engelhardt and her whole lab for all the insightful discussions and lessons on cell related topics. A sincere thanks goes to all people who helped me with preparing and performing my transmigration assays: Regina Reissman, Elisa Kaba, Mariana Castro Dias, Luca Marchetti, Sasha Soldati and Daniela Ivan. In general, thanks to everybody in the Theodor Kocher Institute in Berne for being so welcoming and comforting after my long night's experiments. I appreciated our collaboration a lot, Ahmed B. Ayoub, Elizabeth Antoine and Demetri Psaltis (Optics Laboratory, EPFL). I think we had a very successful project and good example how people can learn from each other. Thanks to Ahmed of not getting tired of explaining optics over and over to me! Furthermore, I would like to acknowledge Olivier Burri for helping me with the image analysis. Acknowledgements also to the Arne Seitz and the whole Bio Imaging & Optics Platform and also the Flow Cytometry Core Facility at EPFL.

Thank you for proofreading my thesis, Corey and Kuljeet! A big thanks goes to Maxime who introduced me to this project, trained and helped me to overcome initial problems. Thank you for making me smile even in the most difficult situations! Claudia and Nariye, you were always there for me during my first years at EPFL. Thanks for all the gossip, cheering up and smiles and hugs! Jacques, you have been a big pillar of LP and helped me with endless things inside and outside the lab, if it was your task or not! I don't know what I would have done without you! Julian, thanks for the adventurous trips in the mountains and all the beers and nice food! Cristina, I really enjoyed sharing an office with you. Thank you so much for all the nice time we had and for always finding time to gossip and discuss the whole world (very loudly) with me! Lisa, thank you for always having an open ear, for our cappuccino breaks with Jacques and all the help with French! Corey, you have been an immense support for me in terms of scientific advices but also in terms of discussions about sports or random life problems. I will miss our conversations! Maria, you brought a lot of positive energy to the lab. I had great fun with you learning together how to snowboard! I hope we will be able to repeat this at some point! Alex, thank you for being such a motivated member of LP with a lot of crazy ideas! A big thanks goes also to Cindy and Susanne for all the help with administrative issues and the coffee! Philippe, merci beaucoup pour toujours avoir une porte ouverte et pour toutes les discussions. C'était vraiment un plaisir!

I want to thank all Laboratoire des Polymères (LP) members which I have met during the last years: Ana, Justin, Ioana, Arda, John, Thomas, Yasushi, Jirawan, Thawinda, Michael, Piotr, Jan, Mark, Fabio, Tina, Sabrina, Feng, Xinyue, Zhao, Jian, Markus, Alice, Frieda, Ghezae, Yann, Anna Lena and Sophia. It has been a great pleasure working with you in the last years!

It has been an adventurous journey and I was lucky to meet so many amazing people during my years at EPFL and would like to thank everybody for being part of this chapter of my life. Åsa and Anne-Flore, without you I wouldn't have survived the first years at EPFL. Thanks for being so supportive and understanding! Giuseppe, it was great having you around. Without you MX was never the same anymore. Lukas, Louis, Sergio and Jorge for our swimming/biking and beer sessions. You did a great job distracting me when things got very stressful! The whole DNH running team, I really enjoy my Tuesday and Thursday evenings! Thanks also to Lorenz, Chris, Mathieu and the rest of their lab for all the shared beers and laughter's!

Another big thank you goes to my friends in chemistry: Natalia, Sean and Bruno and the rest of your group with who I enjoyed a lot of aperos and public defenses. Natalia, I am extremely grateful that were coincidentally in the same French class. Thank you so much for all the fun we had together! You made my life in Lausanne so much brighter! Sean and Bruno, thank you for your support and your amazing humor! You were always there for me – especially during the crazy confinement times, Anne and Flo, I value your support. You always had an open ear for my worries and reduced my stress, thanks for being amazing flatmates! My biggest gratitude to my dearest friends from my Master studies, Clarissa and Frauke, thank you for your warm words in the last months and for all the amazing trips we did in the last years! I hope there are many more to come!

Finally, I want to thank my family for their constant support, understanding and patience during my studies and the years of my PhD. Thank you for spoiling me whenever I managed to go home!

Table of Contents

Summary **1**

Zusammenfassung **3**

1. Chemical Cell Surface Modification and Analysis of Nanoparticle-modified living cells **5**

1.1. Introduction 5

1.2. Chemical Cell Surface Modification 8
1.2.1. Covalent nanoparticle immobilization 9
1.2.2. Non-covalent nanoparticle immobilization 14
1.2.3. *In vitro* analysis of nanoparticle-modified cells 21

1.3. Challenges and Opportunities 28

1.4. References 29

2. Fluorescence-based and Fluorescent label-free Characterization of Polymer Nanoparticle Decorated T cells **36**

2.1. Introduction 36

2.2. Experimental Section 38
2.2.1. Materials 38
2.2.2. Methods 38
2.2.1. Procedures 41

2.3. Results and Discussion 43
2.3.1. Nanoparticle preparation 44
2.3.2. Cell surface modification and analysis 45

2.4. Conclusions 59

2.5. References 60

2.6. Supporting Information 64

3. Chemical Nanoparticle Conjugation to T lymphocytes and their Influence on Viability and functional Properties **71**

3.1. Introduction 71

3.2. Experimental Section 73
3.2.1. Materials 73
3.2.2. Methods 74
3.2.1. Procedures 76

3.3. Results and Discussion 83
3.3.1. Nanoparticle preparation and modification 85
3.3.2. Nanoparticle conjugation to the cell surface 87
3.3.3. Detailed analysis of nanoparticle-modified cells 91

3.4. Conclusions 101
3.5. References 102
3.6. Supporting Information 106

4. Conclusions and Perspectives 114

Curriculum vitae……..…a

Summary

Conventional therapeutics are often limited by their targeting ability, resulting in harmful and potential fatal side-effects for the patients. Recently, new strategies have been developed to improve target specificity of drugs in order to generate more efficient therapeutics. An innovative concept, examined in this thesis, is the use of cells as therapeutic carriers. This concept termed cell-mediated drug delivery, relies on the intrinsic targeting properties of cells to transport the therapeutic drug to the target location. The conjugation of nanoparticles, loaded with drugs or adjuvants, to the surface of cells enables the transport to the desired location and increases the local drug concentration, reducing the required therapeutic leading to further attenuation of side effects. Explicitly, the work presented in this thesis explores the conjugation of biodegradable polymer (poly(lactic acid), (PLA)) nanoparticles to the surface of T cells (human T lymphocytes (Jurkat cells) and mouse $CD4^+$ effector/memory T cells (SJL-PLP7 cells)) via different covalent and non-covalent chemical conjugation strategies and highlights the importance of a thorough *in vitro* characterization of nanoparticle- modified cells.

Chapter 1 introduces the concept of cell-mediated drug delivery. It highlights the advantages of using cells decorated with nanoparticles as carriers for therapeutics as opposed to free (polymer) nanoparticles. Examples of various covalent and non-covalent conjugations strategies are discussed and an overview of all approaches, which have been used previously to attach nanoparticles to the cell surface, is presented. For the cell to act as a drug carrier, cell viability, cell proliferation, and other essential cellular functions including motility, should remain unaffected by the nanoparticle conjugation. Therefore, the importance of a thorough *in vitro* characterization of nanoparticle-modified cells is emphasized. The use of common characterization techniques such as flow cytometry, UV-Vis and fluorescence spectroscopy, fluorescence and electron microscopy, and radiolabeling is discussed in detail and examples of qualitative and quantitative *in vitro* analysis of nanoparticle- modified cells are reviewed.

Chapter 2 contains an extensive *in vitro* analysis of cell–nanoparticle conjugates using fluorescent- and fluorescent label- free methods. The stability of nanoparticles loaded with cargo attached to cells was investigated by encapsulating three different green fluorescent dyes into nanoparticles and tracking the fluorescence signal over 24 h. Two of the dyes revealed a complete loss of fluorescence of a time period of 24 h, suggesting

detachment from the cell surface. A third entrapped dye and a covalently attached dye did not have a decrease in fluorescence over 24 h. Taken together, these results reveal that dye physically entrapped within polymer nanoparticles can leach, leading to a decrease in cell-associated fluorescence. Three-dimensional reconstruction of confocal microscopy images and subsequent image analysis aided in quantification and localization of the nanoparticles with respect to the cell body and the cell membrane. Finally, we developed a fluorescent label-free method as an alternative to characterize nanoparticle-decorated cells without the need for any fluorescent label.

Chapter 3 systematically explores conjugation chemistries to immobilize two platforms of functional biodegradable polymer nanoparticles (PEG-PLA (poly(ethylene glycol) - poly(lactide)) nanoparticles and PLA-COOH nanoparticles) on T cells as potential carrier across the blood-brain barrier (BBB). We compared a series of covalent and non-covalent immobilization strategies by flow cytometry (FACS), confocal microscopy, and impact on cell proliferation and cellular viability. We found that T-cell surface coupling of nanoparticles is dependent on the ratio of nanoparticles to cells and that higher ratios led to more particles attached to cells. Furthermore, the most efficient strategy to attach nanoparticles was via ligand-receptor interactions (lectin – sialic acid and biotin – NeutrAvidin). In addition, nanoparticle-decorated T cells were investigated for their ability to cross an *in vitro* mouse BBB model under static conditions in a two-chamber assay. Decorating the cells with nanoparticles does not affect their ability to bind ICAM-1 (a protein involved in the transmigration process) or to cross the model biological barrier. This study demonstrates a variety of nanoparticle immobilization strategies with minimal impact on cellular viability and migration, paving the way for tunable and robust cell-mediated drug delivery.

Keywords: cell-mediated drug delivery, T lymphocytes, PLA nanoparticles, chemical cell surface modification, *in vitro* characterization of surface-modified cells, optical diffraction tomography, endothelial T cell transmigration.

Zusammenfassung

Aufgrund der nicht zielgerichteten Wirkung der verabreichten therapeutischen Mittel erfordert die Behandlung vieler Krankheiten eine hohe Medikamentendosis. Die Wirkstoffe verteilen sich gleichmäßig im Körper, ohne sich am gewünschten Wirkungsort anzureichern. Die Folge dieses Verhalten ist, dass hohe Wirkstoffkonzentrationen verabreicht werden müssen, um einen therapeutischen Effekt zu erzielen, was zu schweren Nebenwirkungen für die Patienten führen kann. In den letzten Jahren wurden neue Strategien entwickelt, die durch die eine selektivere and zielgerichtetere Anreicherung Therapien effizienter machen und somit die Nebenwirkungen verringen sollen. Ein Beispiel eines innovativen Konzepts ist die Verwendung von Zellen als aktive Wirkstofftransporter. Zellen sind in der Lage, gewissen körpereigenen Signalen zu folgen. Sie können sich zielgerichtet in verschiedenen Organen und Geweben anreichern und dabei biologische Barrieren überwinden. Die Modifikation von Zellmembranen mit Nanopartikeln ermöglicht den gezielten Transport zum gewünschten Wirkungsort, wo die Wirkstoffe in hoher lokaler Konzentration freigesetzt werden können. Im Rahmen der vorliegenden Thesis wird die Konjugation von bioabbaubaren PLA (Polylactid)-Polymernanopartikeln an die Oberfläche von T-Zellen (menschliche T-Lymphozyten (Jurkat-Zellen) und $CD4^+$-T-Maus-Gedächtniszellen (SJL-PLP7-Zellen)) untersucht. Zur Befestigung der Nanopartikel wurden verschiedene chemische kovalente und nicht-kovalente Konjugationsstratgien genutzt und verglichen, um die Bedeutsamkeit einer gründlichen In-vitro Charakterisierung von Nanopartikel-modifizierten Zellen zu demonstrieren.

Kapitel 1 führt in das Konzept der zielgerichteten Zelltherapie (*cell-mediated drug delivery*) ein. Es hebt die Vorteile der Verwendung von mit Nanopartikeln dekorierten Zellen als Träger für Therapeutika im Gegensatz zu freien (Polymer-)Nanopartikeln hervor. Beispiele verschiedener kovalenter und nicht-kovalenter Konjugationsstrategien werden diskutiert und ein Überblick über alle Ansätze, die bisher zur Anheftung von Nanopartikeln an die Zelloberfläche verwendet wurden, gegeben und die Bedeutung einer gründlichen In-vitro-Charakterisierung von Nanopartikel-modifizierten Zellen betont. Der Einsatz gängiger Charakterisierungstechniken wie Durchflusszytometrie, UV-Vis- und Fluoreszenzspektroskopie, Fluoreszenz- und Elektronenmikroskopie sowie Radiomarkierung wird ausführlich diskutiert und Beispiele für die qualitative und quantitative In-vitro-Analyse von Nanopartikel-modifizierten Zellen werden erklärt.

Kapitel 2 enthält eine umfassende In-vitro-Analyse von Zell-Nanopartikel-Konjugaten mit fluoreszenz- und fluoreszenzmarkierungsfreien Methoden. Die Stabilität von Nanopartikeln, die mit an Zellen anhaftender Fracht beladen waren, wurde untersucht, indem drei verschiedene grüne Fluoreszenzfarbstoffe in Nanopartikel eingekapselt und das Fluoreszenzsignal über 24 Stunden verfolgt wurde. Zwei der Farbstoffe zeigten einen vollständigen Verlust der Fluoreszenz über einen Zeitraum von 24 Stunden, was auf eine Ablösung der Nanopartikel von der Zelloberfläche schließen lässt. Ein dritter eingeschlossener Farbstoff und ein kovalent gebundener Farbstoff zeigten über 24 Stunden keine Abnahme der Fluoreszenz. Zusammengenommen zeigen diese Ergebnisse, dass Farbstoff, der physikalisch in Polymernanopartikeln eingeschlossen ist, auslaugen kann, was zu einem Rückgang der zellassoziierten Fluoreszenz führt. Die dreidimensionale Rekonstruktion von konfokalen Mikroskopiebildern und die anschließende Bildanalyse halfen bei der Quantifizierung und Lokalisierung der Nanopartikel in Bezug auf den Zellkörper und die Zellmembran. Schließlich entwickelten wir eine fluoreszenzmarkierungsfreie Methode als Alternative zur Charakterisierung von Zellen, die mit Nanopartikeln dekoriert sind, ohne dass eine Fluoreszenzmarkierung notwendig ist.

Kapitel 3 untersucht systematisch Konjugationschemien zur Immobilisierung von zwei Plattformen funktioneller biologisch abbaubarer Polymernanopartikel (PEG-PLA (Poly(ethylenglykol)- Poly(lactid))-Nanopartikel und PLA-COOH-Nanopartikel) auf T-Zellen als potenziellem Träger über die Blut-Hirn-Schranke. Wir verglichen eine Reihe von kovalenten und nicht-kovalenten Immobilisierungsstrategien mittels Durchflusszytometrie, konfokaler Mikroskopie und studierten den Einfluss auf die Zellproliferation und Zellviabilität. Die Anbindung von Nanopartikeln an die Zelloberfläche hängt vom Verhältnis von Nanopartikeln zu Zellen ab und höhere Verhältnisse führen zu mehr an Zellen gebundenen Nanopartikeln. Zusätzlich wurden mit Nanopartikeln dekorierte T-Zellen in einem Zwei-Kammer-Assay auf ihre Fähigkeit untersucht, durch ein In-vitro-Maus-Blut-Hirn-Schranken-Modell unter statischen Bedingungen zu migrieren. Die Dekoration der Zellen mit Nanopartikeln hat keinen Einfluss auf ihre Fähigkeit, ICAM-1 (ein am Transmigrationsprozess beteiligtes Protein) zu binden oder die biologische Barriere des Modells zu durchqueren.

Schlüsselwörter: Zielgerichtete zellbasierte Therapy, T-Lymphozyten, PLA-Nanopartikel, chemische Zellmembranmodifikation, In-vitro-Charakterisierung von oberflächenmodifizierten Zellen, optische Beugungstomographie, endotheliale T-Zell-Transmigration.

1. Chemical Cell Surface Modification and Analysis of Nanoparticle-modified living cells

1.1. Introduction

Conventional therapies often suffer from severe side effects, especially when the treatment involves a frequent drug administration. These side effects stem from the accumulation of small or low-molecular weight therapeutics in off-target organs, resulting in a decrease in the bioavailability of drugs in the target organs, further necessitating a higher drug dose or recurrent administration. Furthermore, the efficient transport of small molecular weight therapeutics is often hindered by their lack of ability to cross biological barriers (i.e. endothelial, epithelial, and cellular barriers). In addition, the circulation time of small drug molecules in the blood is limited due to rapid clearance by the mononuclear phagocytotic system (MPS) and excretion by the liver and kidneys. Further exacerbating the issue; the lack of target specificity of small drug molecules leads to distribution throughout the body, decreasing its concentration in a specific tissue. These factors require special consideration for therapies which require repeated administration of highly toxic compounds such as chemotherapy. Therefore, there is a need for improved therapeutics with efficient target-specific drug delivery minimizing the interaction with off-target organs or tissues.[1-3]

One strategy to overcome the above mentioned drawbacks of conventional small molecule therapeutics is the conjugation of drugs to polymers. Polymer therapeutics are drugs (proteins, peptides, antibodies, cytokines, growth factors, or small-molecule drugs) conjugated to a polymer chain that can be either linear, branched, or assembled into polymer nanoparticles. The attachment of a synthetic moiety (like polymers) to a drug provides an opportunity to tailor the body's reaction toward the therapeutic by manipulating its biodistribution, pharmacokinetics, and pharmacodynamics.[4-7] Several drugs and drug tracking compounds can also be included within the polymer therapeutics. Additionally, polymers that respond to environmental changes, like pH or temperature, can lead to "smart" conjugates, altering drug activity and release. Polymers can also be modulated with

regard to their molecular structure, molecular weight, and architecture, enabling a control over *in vivo* fate of the drug, drug release profile, and its interactions with cells. PEG is widely used to modify drugs because of its hydrophilicity and bio-compatibility. Attaching PEG to a therapeutic increases its solubility, reduces immunogenicity, and prevents renal clearance due to the increase in size and hence, prolongs plasma half-life.[8] Biodegradable polyesters such as PLA, poly(lactic-co-glycolic acid) (PLGA) or polycaprolactone (PCL) can prevent the necessity to remove non-biodegradable therapeutics like PEG.

Polymers can assemble into nanoparticles, which provides an opportunity for a rational nanoparticle design with distinct chemical, physical, and biological properties (nanoparticle shape, size, compound loading (therapeutics or dye molecules), surface (charge, functionality, and ligand density), rigidity, stimuli-responsive behavior).[9,10] Macromolecules and nanoparticles have been observed to accumulate in tumor tissue based on the EPR (enhanced permeability and retention) effect. The basis of this theory is the hyperpermeability and fenestration of tumor vasculature, in combination with impaired lymphatic drainage which makes the tumor tissue accessible for nanomedicine (10 – 100 nm) penetration, retention, and therefore accumulation.[11,12] However, extensive data analysis revealed that only 1 % of the administered nanoparticles reached the tumor tissue in animal solid-tumor models.[13] While a majority of the administered nanoparticles accumulate in the liver, spleen and lungs.[14] Therefore, the EPR effect is currently debated and alternative tumor targeting mechanisms, such as active transcytosis, are currently being investigated.[15,16] Moreover, the introduction of targeting ligands (antibodies, carbohydrates, small molecules, peptides, aptamers) can enhance the targeting abilities through specific interactions with overexpressed molecules in the targeted cells/tissues.[17] However, the targeting of nanomedicines to tumor tissues is limited by endothelial cell barriers, which the therapeutics cannot actively cross.[8,10]

Instead of manipulating nanoparticles to overcome endothelial barriers, a more efficient approach is the use of cells as active carriers for the nanoparticles. Cells, as endogenous compounds possess inherent biological properties and do not elicit an immune response, in contrast to synthetic materials. Cells are highly specific and versatile in sensing biological cues and responding in a dynamic manner, which makes them ideal drug carriers. Various cells have specific functions in the body and therefore, provide a variety of advantages in terms of mobility, circulation time, interaction with other cells and molecules, drug loading capacity, and their ability to overcome biological barriers.[18] The therapeutic cargo (which can be small molecules, polymers or micro/ nanoparticles) can be

encapsulated inside the cell or attached to the cell membrane. By making use of wide variety of cell types, the targeting ability can be extended to several tissues, which further increases the therapeutic potential to a broader disease spectrum than cancer targeting. Circulatory cells (erythrocytes, monocytes, macrophages, lymphocytes, neutrophils, platelets, leukocytes, dendritic cells, stem cells, and extracellular vesicles) have long blood circulation times and are interesting candidates for cell-mediated drug delivery. For example, red blood cells (RBCs) are the most abundant cells in the body and are responsible for the oxygen transport. Because of their inherent properties such as excellent biocompatibility, low immunogenicity, and long blood circulation half-life (~120 days in humans), RBCs are suited for sustained drug delivery. In addition to the large and flexible surface area for cargo immobilization, the cells lack a nucleus as well as many organelles providing a large encapsulation volume.[19-22] RBC-hitchhiking, the immobilization of nanoparticles on the cell membrane has become a popular drug delivery strategy. RBCs decorated with polymer nanoparticles have shown to enhance the nanoparticle delivery to organs of interest such as lungs[23-25] brain[26] and kidneys. Organs of the MES (liver, spleen, and bone marrow) can also be selectively targeted. Neutrophils, a part of the innate immune system, are the most abundant type of white blood cells in the body and are among the first cells which respond to infections or tissue damage, creating an inflammation by migrating from the blood stream to infection sites and crossing endothelial barriers.[27, 28] *In vivo* hitchhiking of active neutrophils by nanoparticles has been reported as a strategy for nanoparticles to overcome endothelial cell barriers.[29] Neutrophils can also transport nanoparticles to the tumor site.[30] Monocytes are circulatory cells which move through the vasculature and target pathological tissues, whereas macrophages are terminally differentiated cells permanently residing in various tissues.[31] Both cell types, being phagocytotic cells, can be loaded with therapeutic cargo. Monocytes and macrophages can target and penetrate into inflammation sites and are capable of providing the drug release in the center of a tumor. T cells are used for cell- mediated drug delivery because they are able to cross biological membranes, reside into tumors, and provoke an immune response as part of the adaptive immune system and immunological memory. A cellular response is created by $CD4^+$ helper T cells activating other immune cells and $CD8^+$ cytotoxic T cells killing infected/ target cells.[32] Dendritic cells are the link between the innate and the adaptive immune response and can present tumor-associated antigens to T cells. Stem cells also have targeting capabilities, are self-renewable, can differentiate into specialized cells, home to injured sites, and disseminate into solid tumors.[33-35]

1.2. Chemical Cell Surface Modification

Cell membranes are composed of a very complex network of thousands of different proteins, carbohydrates, and lipids. Proteins associated with the cell membrane are of significant importance, since they account for over a third of a cell's surface.[36] Cell membranes display a large variety of functional groups such as $–NH_2$, –SH, (originating from amino acid side chains, such as lysine and cysteine) and carbonyl groups (as part of the glycocalyx carbohydrates), which allow for the direct covalent and non-covalent immobilization of nanoparticles. Furthermore, the introduction of biorthogonal groups can be realized through the reaction with biotin modified molecules or the metabolic introduction of $–N_3$ groups. Additional nanoparticle conjugation strategies exploit the physicochemical nature of the cell membrane by using electrostatic and lipophilic interactions. The cell glycocalyx offers further possibilities for nanoparticle anchorage through the specific interactions of carbohydrates and lectins. Even though, the chemical conjugation of nanoparticles to the cell surface depends on the availability of the functional groups and their reactivity under physiological conditions, it provides universal cell surface modification strategies, which can be extended to various cell types.

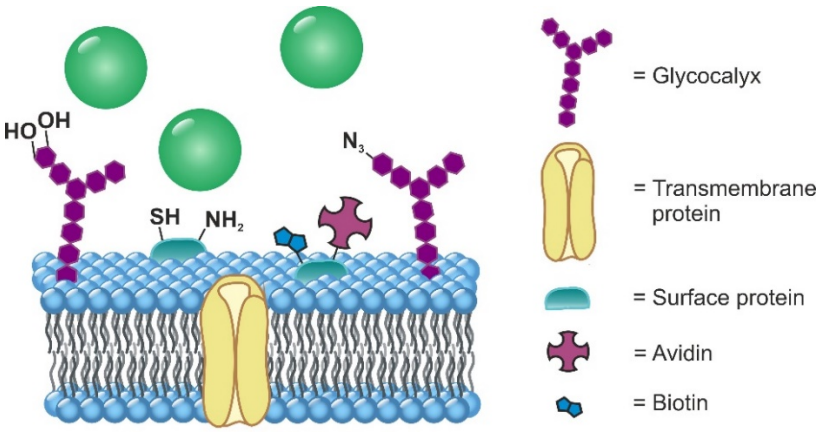

Figure 1: Scheme of the cell membrane illustrating the diversity of functional groups (native and non- native) expressed on cell surfaces.

1.2.1. Covalent nanoparticle immobilization

Table 1 lists various covalent approaches, which have been utilized to conjugate polymer nanoparticles to the cell surface. Nanoparticles functionalized with activated esters can target native amine groups on the cell membrane, resulting in the formation of a stable amide bond between the nanoparticle and the cell surface. A range of different sized hyper-branched polyglycerols (HPG) have been grafted to the surface of RBCs using succinimidyl / succinate activated HPGs without impairing the cell viability.[37] The conjugation of HPGs led to a reduction in detection of the cell surface Rhesus antigens, which is beneficial for the formation immunocamouflaged cells. Furthermore, HPGs can also be used as multifunctional delivery agent. This was demonstrated by attaching fluorescent markers to the HPG via degradable linkages prior to grafting on RBCs.[37, 38] Xie *et al.* designed redox-responsive adjuvant nanogels and conjugated these nanogels to the amino groups of the surface of T cells. The interleukin-2/Fc (Il-2/Fc) nanogels bound to the surface of T cells were tested for controlled release of Il-2 as an example of safe administration of repeated doses against melanoma metastases. This type of cell-mediated delivery of Il-2 resulted in a more than 80 fold increase in tumor-reactive T cells than when free Il-2/Fc was systematically administered at an equivalent dose.[39]

Surface thiol groups, in the reduced state as –SH groups and in the oxidized state as disulfide bridges, are part of proteins associated with the cell membrane. The –SH groups are often used for cell surface modifications and the number accessible surface thiol groups can be increased through reduction of disulfide bridges using mild reducing agents such as tris(2-carboxyethyl)phosphine (TCEP). It has been reported that such cell pretreatment does not impair the cell viability.[40] Kim *et al.* attached fluorescent mesoporous silica nanoparticles (MSNs) onto TCEP treated cells via maleimide- thiol coupling. This type of covalent conjugation is stable under physiological conditions and does not compromise viability, metabolism, or functional properties of various cell types i.e. of a human cancer cell line (HeLa cells), human mesenchymal stem cells (hMSC) and mouse myoblasts cells (C2C12 cells). The surface modified cells showed potential applications in localized drug delivery.[41] In another approach cells were used as carriers for adjuvant drug- loaded nanoparticle in order to enhance the efficiency of adoptive cell therapy, Stephan *et al.* covalently attached liposomes to the surface of various cell types used in cell therapy, including $CD8^+$ T lymphocytes or hematopoietic stem cells (HSCs). The nanoparticles were conjugated to the cell membrane via maleimide- thiol coupling followed by a subsequent PEGylation of the unreacted maleimide groups on the nanoparticles through

the addition of a thiol-modified PEG. A sustained adjuvant drug release from the membrane- bound nanoparticles of donor cells enabled continuous stimulation of transferred cells *in vivo*. The stable conjugation of up to 140 (± 30) nanoparticles to the cell surface (~ 3% of the surface of a typical 7-µm-diameter T cell) did not compromise cell viability and showed no alteration of key cellular functions (such as the formation of an immunological synapse, killing of target cells, secreting cytokines, and transmigration across an endothelial cell layer). T-cell transmigration was studied with an *in vitro* transwell co-culture system. It was shown that T cells retained 83% (± 3%) of the original cargo, indicating formation of a strong thioether bond between nanoparticles and cells.[42] Similarly, CAR (chimeric antigen receptor) T cells have been modified with maleimide functionalized cross-linked multilamellar liposomes to deliver adjuvants to the immune suppressive tumor microenvironment. The covalent attachment did not impair the cell viability or functions and resulted in a stable conjugation of 287 ± 49 nanoparticles/ cell with an average conjugation efficiency of 55.9 %.[43] Another reversible and pH-responsive strategy to conjugate nanoparticles to the cell surface for intratumoral drug delivery by T cells was investigated by Wayteck *et al.* They studied the reaction of liposomes and nanogels modified with a pyridyldithiopropionate head group, with surface thiols of $CD8^+$ effector T cells resulting in reducible disulfide bond. A dependency of liposome coupling on the T cell activation status was shown and indicated the correlation of the expression of certain surface marker (such as CD25) as part of the phenotypical cell changes during the T cell activation process facilitates optimal liposome conjugation. Additionally, the conjugation didn't impact the cell viability, proliferation, or cytotoxic effector functions.[44]

Saccharides which contain diols in the cis- configuration, such as sialic acid or glucose, react with phenylboronic acid modified nanoparticles in a reversible esterification to form covalent boronic esters. This reaction was used to reversibly encapsulate single yeast cells.[45] An alternative strategy reported by Holden *et al.* utilized aldehydes, derived from oxidation of hydroxyl groups of sialic acid (using e.g. sodium periodate), to conjugate amine-derivatized PEG coated polyamidoamine dendrimers via Schiff base formation. Further, the labile imine (-C=N-) bond was reduced to a more stable -C-NH- bond (e.g using sodium cyanoborohydride). In a proof-of-principle study it was shown that the non-specific uptake of the covalently bound dendrimers by macrophages was retarded through the second step, the reduction to stabile amine bonds. A potential application of these surface modified macrophages is the targeted delivery of anticancer drug to hypoxic tumor tissue.[46]

The display of bioorthogonal groups on the cell surface is achieved by the metabolic introduction of modified sugars. N-azidoacetylmannosamine (Ac_4ManNAz) is taken up by the cell, metabolized, and transformed into N-azidoacetyl-sialic acid which is displayed in the glycocalyx. Metabolic glycoengineering provides a strategy for *in vivo* cell targeting. The first step is the delivery and metabolism of unnatural sugars carrying bioorthogonal groups (e.g. azide groups) to cancer cells, followed by a strain-promoted, copper-free alkyne-azide cycloaddition (SPAAC) between an alkyne (e.g. dibenzocyclooctyne (DBCO)) bearing nanoparticles and azido groups in the glycocalyx of the cell. This two-step bioorthogonal approach for cell surface engineering is used for *in vivo* targeting and binding of polymer nanoparticles to cancer cells. However, most studies don't include an *in vitro* characterization of nanoparticle binding to the target cells.[47-51] A second bioorthogonal reaction used for *in vivo* cell targeting with nanoparticles is the Diels-Alder reaction between trans-cyclooctene (TCO) modified cells (previously modified with TCO functionalized anti-CD11b) and tetrazine functionalized PEGylated MSNs. Confocal microcopy images of TCO modified $CD11b^+$ cells incubated with tetrazine functionalized nanoparticles showed a successful *in vitro* chemo-selective click reaction. Furthermore, the selectivity of the click reaction was investigated using dual-color fluorescence cross-correlation spectroscopy (FCCS). This method allows the sensitive quantification of the interaction between the two spectrally distinct fluorophores and analysis of the kinetics of chemical bond formation in real-time. A strong cross-correlation provides evidence for the selective reaction of tetrazine nanoparticles with TCO-functionalized antibodies in complex biological media.[52] The azido targeting ability of glycol chitosan nanoparticles, which were modified with bicyclo[6.1.0]nonyne was demonstrated by Lee *et al.*. The nanoparticle-cell conjugates were characterized using flow cytometry and confocal microscopy. Time-dependent cellular binding and subsequent cellular uptake indicates the feasibility of intracellular drug delivery.[48] Zhang *et al.* reported a study where they showed that azido- labeled cells can also be targeted with triarylphosphine modified nanoparticles to react in a Staudinger ligation. The polyoxazoline-block-polycaprolactone (POX-PCL) nanoparticles target tumors metabolically labeled with azido groups and thus enhance the *in vitro* and *in vivo* tumor targeting ability of nanoparticles. The *in vitro* targeting of POX-PCL nanoparticles and subsequent nanoparticle uptake was quantitatively analyzed by flow cytometry and confocal microscopy.

Table 1: Covalent conjugation chemistries which have been used to immobilize (polymer) nanoparticles to the cell surface, nanoparticle compositions, diameter and the (potential) application of the nanoparticle-cell conjugates.

Funct. group (cell)	Cell pretreatment	NP reactive groups	NP composition	d(NP) [nm]	Application	Ref.
-NH_2		NHS ester	Fluorescein-labeled HPGs	Radius of hydration: 2.3 – 4.7	RBC antigen masking, chronic transfusion	[37], [38]
		1. covalent coupling: NHS ester (BS3 linker, NHS-SS-NHS) 2. electrostatic: PEG-PLL (introduction of positive charges)	Alexa Fluor 647 labeled redox-responsive interleukin-2 (IL-2)/Fc nanogels	100	Adjuvant anti-cancer adoptive T-cell transfer immunotherapy	[39]
-SH	Reduction of disulfides using TCEP	Maleimide	FITC-, Cy5-, or Cy5.5-labeled PEG- coated MSNs	104	Localized drug delivery	[54]
		1. Maleimide NP coupling, 2. In situ PEGylation with SH-PEG	Liposomes, multilamellar lipid nanoparticles and lipid-coated DiD- labeled PLGA nanoparticles	100 - 300	Adjuvant drug delivery in adoptive T cell therapy for cancer and hematopoietic stem cell grafts	[42]
			DiD-loaded multilamellar liposomal vesicles	N/A	CAR T-cell therapy for treatment of solid cancers	[43]
		Maleimide	Rhodamine and DiD- labeled multilamellar lipid vesicles and polystyrene NPs	200	Drug delivery into T cell immunological synapse for anti-tumor immunity	[55]
			Alexa Fluor 647-conjugated ovalbumin multilamellar crosslinked lipid capsules	244 ± 17	T cell- mediated immunotherapeutic agent	[56]

					delivery to an anatomical site of viral replication	
			DiD- labeled multilamellar lipid capsule, 2. In- situ PEGylation	340 ± 12	T cell active targeting of chemotherapy tumor metastases	[57]
			DiD loaded polydisperse multilamellar lipid vesicles	496 ± 5	In utero hematopoietic cell transplantation	[58]
		Pyridyldithiopopionate	DiD- labeled liposomes	150	Intratumoral drug delivery by T cells	[44]
Sialic acid (cis-diols)		Phenylboronic acid	MSNs	51 – 1417	Reversible encapsulation of single yeast cells	[45]
	1. Oxidation to aldehyde groups by NaIO4	1. Amine group to form a Schiff base 2. reduction to secondary amine using $NaBH_3CN$	PEG-conjugated 5-(aminoacetamido) fluorescein-labeled polyamidoamine dendrimer	N/A	Macrophage hypoxia-targeted drug delivery	[46]
$-N_3$	Cancer cell treatment with $Ac_4ManNAz$	Bicyclo[6.1.0]nonyne	FITC-labeled glycol chitosan nanoparticle	200	*In vivo* NP tumor targeting	[48]
		Triarylphosphine	FITC-labeled polyoxazoline-block-polycaprolactone micelles	~ 74	*In vivo* NP tumor targeting	[53]

1.2.2. Non-covalent nanoparticle immobilization

Non-covalent bonds are usually less strong than covalent bonds, but multivalent binding can realize a strong nanoparticle immobilization to the cell surface. A summary of various approaches which have been utilized to non-covalently attach polymer nanoparticle to the surfaces of cells is shown in **Table 2**.

A popular strategy for the nanoparticle adhesion on cell surfaces is based on electrostatic interactions between the surface of the nanoparticles and the cell membrane. Although positively charged nanoparticles are reported to show an increased adsorption compared to negatively charged nanoparticles due to the net negative charge of the cell membrane[59], cell-immobilized negatively charged nanoparticles are also widely used as drug carriers. Particularly, RBCs are decorated with nanoparticles via electrostatic interactions. The electrostatic interactions between the cell surface and the nanoparticles are reversible and can be used for *in vivo* applications such as the detachment of drug-loaded nanoparticles through shear forces in epithelium for drug delivery to lungs. Adsorption of negatively charged polystyrene nanoparticles onto the surface of RBCs increase their blood circulation time compared to free nanoparticles and allow for an accumulation in the lungs while reducing the nanoparticle uptake by liver and spleen.[25, 60-62]. On the contrary, Zhao *et al.* used a slightly positive PLGA nanoparticles for conjugation to the RBCs. The nanoparticle-modified cells increased the drug delivery to the lungs by 10-fold as compared to the free nanoparticles.[63] A control over macrophage polarization towards the antitumor phenotype and a localized cytokine release is obtained by the conjugation of PLGA- polyvinyl alcohol (PVA) backpacks to the surfaces of macrophages. The contact regions of the backpacks are made of modified hyaluronic acid and poly(allylamine) hydrochloride, which creates a cell adhesive layer and adsorbs on the surface of macrophages through a combination of electrostatic interactions and the binding of hyaluronic acid to CD44 receptors on the macrophage membrane. The backpacks were able to evade a significant phagocytosis by the macrophages over time.[64]

The lipophilic nature of the plasma membrane is the basis for the insertion of lipophilic molecules, i.e. cholesterol or alkyl chains into the cell membrane. Jeong *et al.* modified MSCs with octadecyl chain-functionalized HPGs through hydrophobic chain insertion into the cell membrane. The HPGs contained vasculature binding peptides to overcome the incapability of stem cells to bind to inflamed endothelium. The conjugation of the bioactive polymer nanostructures to cells significantly increased the cellular affinity

for the vascular cell adhesion molecule (VCAM), a protein which is overexpressed in inflamed blood vessels. Only a small decrease in the metabolic activity in comparison to uncoated mesenchymal stem cell was found.[65] Myoglobin-polymer–surfactant complexes which were modified nonylphenyl chains are reported to insert into the cell membrane of hMSCs. The cells act as a carrier of the oxygen-binding protein to enhance tissue oxygenation. The insertion of the complex into the cell membrane showed no cytotoxic effect and cell self-renewal and differentiation was not impaired.[66]

Another type of biologically relevant interactions are the ligand- receptor interactions. They are characterized by a high specificity, affinity, and avidity. Ligand-receptor interactions, which have been used to immobilize nanoparticles to the cell surface include: antibody and antigen, avidin (or the analogs of avidin like streptavidin and NeutrAvidin) and biotin or lectins and carbohydrates of the glycocalyx. The interaction between avidin and biotin is one of the strongest non-covalent interactions occurring in nature and has been widely used in biochemistry. Avidin is a tetrameric protein which consists of four identical subunits, each of which binds to biotin with high specificity and affinity (K_d ~10^{-15} M).[67] Biotin moieties can be introduced into the cell membrane by covalently coupling modified biotin molecules to the amino groups of the cell surface using e.g. NHS ester chemistry or through oxidation of native sialic acid hydroxyl groups to non-native aldehydes and subsequent reaction with a hydrazide modified biotin.[68,69] Other strategies include the attachment of biotin molecules to the cell membrane using antibodies.[70] The biotinylation of MSCs and conjugation with avidin coated nanoparticles has been used by several groups to benefit from the tumortropic properties of these stem cells.[68,71] Tumor cells were conjugated with nanoparticles via biotin- streptavidin binding to act as a cancer vaccine. Ahmed *et al.* developed hybrids of tumor cells and PLGA nanoparticles, which had the ability to co-deliver the antigen (through the cell) and the adjuvant drug (loaded inside the nanoparticles) to dendritic cells.[70] Mooney *et al.* conjugated streptavidin-modified fluorescent polystyrene nanoparticles to the surface of tumor-tropic neural stem cells which (NSCs) derive from specific neurogenic regions of the brain as a strategy for the drug transport across the blood- tumor barrier.[72]

The strong binding of lectins such as wheat germ agglutinin (WGA) to carbohydrates of the cell glycocalyx (N-acteylglucosamine and sialic acid) is result of a combination of the specific interaction between the carbohydrates and binding sites of WGA, the charge on WGA (WGA has a high isoelectric point), and an avidity effect. The WGA homodimer has in total, 8 independent biding domains (four unique binding sites per

unimer) for binding carbohydrates.[73] The antiparallel orientation of the monomers creates non-cooperative domain pairs of two binding sites resulting in four high affinity (principal binding sites) and four low affinity binding sites (helper binding sites).[74] The K_d of WGA and N-actylgucosamine was determined in total as ~10^{-5} M.[75] WGA modified PLGA nanoparticles have been employed for *in vitro* studies of nanoparticle binding to the cell surface and its subsequent uptake.[76] Fillafer *et al.* investigated the adhesion and uptake of WGA modified PLGA nanoparticles by human colon cells and discussed its potential application for drug delivery.[76-78] Selective nanoparticle binding with monosaccharide imprinted nanoparticles can be achieved by first covalently attaching the monosaccharides and then removing them in an etching process, to generate the negative imprint which will selectively interact with saccharides of the cell glycocalyx such as sialic acid, mannose, and fucose. It serves as strategy to selectively bind to different cancer cell lines.[79,80] Furthermore nanoparticles saccharides such as lactose and D-galactosamine interact with lectins interact on the cell surface.[81,82] Nanoparticle binding via host-guest recognition of azobenzene and β-cyclodextrin enables a light-controllable reversible reaction between nanoparticles and the cell surface. The β-cyclodextrin moiety has been introduced by glycoengineering and subsequent reaction with an alkyne modified cyclodextrin. The spatiotemporal control over cell- cell interaction and immobilization of nanoparticles shows a great potential for drug delivery applications.[83]

Table 2: Non- covalent conjugation chemistries which have been used to immobilize (polymer) nanoparticle to the cell surface, nanoparticle compositions, diameter and the (potential) application of the nanoparticle- cell conjugates.

Funct. group (cell)	Cell pretreatment	NP reactive groups	NP composition	d(NP) [nm]	Application	Ref.
Charges on the cell membrane		Negatively charged carboxyl	^{3}H-radiolabeled polystyrene NPs	200 and 500	Improvement of blood pharmacokinetics and lung targeting	[25]
			polystyrene particles	200, 500 and 750	Reduction in MPS clearance	[84]
			FITC-labelled poly-styrene nanoparticle,	750	Retarded targeted drug delivery with a long lifetime of the particles in the blood circulation	[85]
		Plain, carboxyl groups, PEI modified nanoparticles, aldehyde modified. PEGylation after NP binding	Fluorescently labeled polystyrene NPs, ^{3}H-oleic acid radiolabeled PS NPs	110, 200, 220, 250, 450, 830 and 1100	Prolonged blood circulation	[61], [62]
		Carboxyl, ICAM-antibody-coated	^{3}H-oleic acid radiolabeled spherical and rod-shaped polystyrene NPs	200	Lung targeting and reduction in MPS clearance	[24]
		Pristine and IgG-conjugated	^{3}H conjugated oleic acid labeled polystyrene NPs and ^{125}I- labeled lysozyme-dextran nanogels	~200 and ~300	Prolonged blood circulation	[60]
		Pristine and IgG and BSA conjugated	Fluorescently labeled and ^{125}I- labeled polystyrene, PLGA NPs nanogels, albumin NPs, Liposomes,	N/A	Targeted lung and brain delivery	[26]

	Alternating layers of hyaluronic acid modified with aldehyde and poly(allylamine) hydrochloride	PLGA-PVA backpacks	Thickness: 1490, width: 756	Control of macrophage polarization toward antitumor phenotypes and cytokine release	[64]
	Positively charged	DOX fluorescence loaded PLGA nanoparticles	136.0 ± 2.7	Targeted delivery of chemotherapeutic to lung metastasizes	[63]
Phospholipid bilayer	Octadecyl chains	Fluorescein-conjugated hyperbranched Polyglycerol (HPG)	N/A	Stem cell targeting to inflamed tissue	[65]
	Nonylphenyl tail	myoglobin-polymer–surfactant complexes	4 - 9	Mesenchymal stem cell-mediated oxygen delivery to hyaline cartilage	[66]
Glycocalyx carbohydrates (N-acteylglucosamine and sialic acid)	WGA	PLGA NPs, covalently conjugated with a fluorescein-derivative	360- 621	Drug delivery to the human intestine	[76]
		BODIPY 493/503 labeled PLGA NPs	160	Drug delivery to the human intestine	[77], [78]
		FITC labeled- cyclodextrin-modified liposomes	110 – 140	Drug delivery to oral cells	[86]
	Sialic acid imprinted	Fluorescent conjugated polymers (poly(fluorene-alt-benzothiadiazole))	30	Selective NP cancer cell targeting	[79]
	Monosaccharide-imprinted (sialic acid, mannose, fucose)	FITC doped silica NPs	50	Selective NP cancer cell targeting	[80]
Lectin (Galectin)	Lactose	Rhodamine B pyridine based labeled polymeric nanospheres	282 - 766	Galectin targeting	[81]
	D-galactosamine	Nile Red incorporating polystyrene- polypeptide NPs	100–150	Specific and reversible NP binding to Chinese	[82]

					hamster ovary cells (CHO)	
Avidin – biotin	1. Oxidation of sialic acid moieties to aldehyde groups by $NaIO_4$ 2. reaction with hydrazide-biotin	Streptavidin	Nile red- loaded polystyrene NPs	798	Neural stem cell-mediated delivery to brain tumors	[72]
	1. Cell treatment with Ac_4ManNAz 2. reaction with an DNA initiator modified DBCO 3. Addition of biotin conjugated to DNA		Quantum dots	10 nm	NP surface concentration increase through polyvalent interactions	[87]
	Tumor cell surface modification with a biotinylated antibody targeting the β1 integrin		Rhodamine B- loaded PLGA NPs	~ 500	Adjuvant delivery of tumor cells for use as cancer vaccines	[70]
	1. Oxidation of sialic acid moieties to aldehyde groups by NaIO4 2. reaction with hydrazide-biotin	Avidin	PLA-PEG-biotin microparticles surface engineered with rhodamine-labeled avidin	1400	Self-assembly of cell with microparticles	[69]
	Biotinylation using Sulfo-NHS-LC-Biotin	NeutrAvidin	Fluorescent polystyrene NPs	40	Mesenchymal stem cell-mediated tumor tropic drug delivery, endothelial cell multicellular structure formation	[68]
	1. Oxidation of sialic acid moieties to aldehyde groups by NaIO4 2. reaction with hydrazide-biotin 3. Cell coating with avidin	Biotin	pH- responsive nile red-loaded poly(ethylene glycol)-poly((diisopropyl amino)ethyl methacrylate (PEG-PDPAEMA) NPs	400	Neural stem cell-mediated intratumoral drug delivery	[88]

	1. Biotinylation using Sulfo-NHS-LC-Biotin 2. Addition of Streptavidin		Curcumin loaded chitosan polymer NPs	377.0 ± 14.6	Mesenchymal stem cell-mediated tumor tropic drug delivery	[71]
Host- guest interaction	1. Cell treatment with $Ac_4GalNAz$ 2. alkynyl-PEG-β-CD conjugation	Azobenzene host- guest interaction	PEG- conjugated FITC-doped silica nanoparticles	50	Light-controllable reversible binding of NPs to cell surface	[83]

1.2.3. *In vitro* analysis of nanoparticle-modified cells

Experimental techniques, which are used to qualitatively and quantitatively analyze nanoparticle-decorated cells, include the use of fluorescent labels for flow cytometry and fluorescence spectroscopy and UV-Vis active dyes or assays. Imaging methods frequently employed to visualize nanoparticle localization and cellular properties are optical microscopy, differential interference contrast microscopy (DICM), fluorescence microscopy, confocal laser scanning microscopy (CLSM), and electron microscopy (scanning electron microscopy (SEM) and transmission electron microscopy (TEM)). Furthermore, nanoparticles modified with molecules containing radionuclides (e.g. ^{3}H, ^{125}I) enables an accurate quantification of nanoparticles associated with cells *in vitro*, as well as their *in vivo* biodistribution.[89] All the techniques which have been used to study nanoparticle-cell association *in vitro* and the impact of nanoparticle conjugation on cellular properties, (such as cell viability, cell proliferation, and intrinsic functional cell properties, e.g. target cell killing or endothelial cell transmigration) are summarized **in Table 3**. **Table 3** also highlights that the analysis of nanoparticle-modified cells relies most frequently on flow cytometric methods, fluorescence and confocal microcopy, SEM, and radiolabeling. Flow cytometry and fluorescence / confocal microscopy are complementary methods and thus require only one cell staining procedure.

1.2.1. Flow cytometry

Flow cytometry (FACS) is a multiparametric high-throughput analysis tool based on the intrinsic light scattering properties of the cells and fluorescent emission from cell associated fluorophores after irradiation with a laser beam in a fluidics system. The direction of the scattered light provides information about the viability of the cells, different cell populations that can be identified, and cell debris excluded from the analysis.[90] Fluorophores can be internalized by the cell or attached to the cell surface using antibodies, proteins, fluorescent dyes, or nanoparticles. Cell surface conjugation with polymer nanoparticles loaded with fluorescent dyes enable the analysis by flow cytometry, comparing the relative increase in cell fluorescence intensity distribution caused by nanoparticle association compared to the autofluorescence of the control cells. Nanoparticle- associated fluorescence is used as a measure for the nanoparticle surface concentration and often used to qualitatively measure the nanoparticle attachment to the

cell membrane as well as the nanoparticle coupling efficiency. However, to quantify the number of nanoparticles per cell, a calibration of the instrument is required, for example, by using calibration beads containing a known amount of fluorophores (provided by the manufacturer or experimentally determined).[85] Additional information that can be obtained by the analysis of nanoparticle- associated fluorescence is nanoparticle binding as function of nanoparticle/ cell incubation ratio, incubation time or incubation temperature, nanoparticle attachment stability, and binding specificity. The addition of trypan blue to nanoparticle- conjugated cells quenches the extracellular fluorescence and a qualitative analysis of the surface-conjugated and internalized nanoparticles can be performed via FACS.[42] Flow cytometry is a standard tool for the observation of cellular properties, such as cell viability and cell proliferation. Proliferation of nanoparticle- conjugated cells is measured by analyzing the dilution of a cytosolic stain (e.g. carboxyfluorescein succinimidyl ester (CFSE)) over the daughter cells at varying time points. The impact of nanoparticle decoration and nanoparticle cell surface concentration on cell viability can be evaluated by the detection of DNA- intercalating dyes and phosphatidylserine, which binds to Annexin V. Moreover, functional assays aid to determine potential impairment of functional properties after nanoparticle conjugation. Stephan *et al.* reported that nanoparticle conjugation to T cell doesn't alter key cellular functions. T cells were able to form an immunological synapse, kill target cells, and secrete cytokines. When T cell were decorated with 100 nanoparticles/ cell, the transmigration in transwell co-culture system across an endothelial monolayer was not altered and 83% (± 3%) of the nanoparticles were retained.[42] In summary, flow cytometry provides a fast high-throughput acquisition of nanoparticle- modified cells and allows the analysis of various cell properties and cell functions. Yet, using flow cytometry, no exact nanoparticle localization, i.e. either associated to the cell membrane or inside the cytosol/ cellular organelles, can be obtained and additional analytical tools have to be consulted.

1.2.2. UV-Vis absorbance and fluorescence emission spectroscopy

UV-Vis and fluorescence spectroscopy has been utilized to measure the nanoparticle cell association. Using UV-Vis spectroscopy, a proportion of membrane-bound nanoparticles has been estimated by an indirect colorimetric enzyme-substrate assay. When streptavidin functionalized nanoparticles are bound to biotinylated cells, a reaction with a biotinylated alkaline phosphatase, which binds to streptavidin on the nanoparticle surface, produces a colored enzyme-substrate product detectable by UV-Vis.[70]

Approximately 25% - 30 % of the initial amount of nanoparticles added remained on the cell surface after three washing steps. Moreover, cell proliferation of nanoparticle-decorated cells was studied by absorbance-based cell counting assay and cell viability relying on the enzymatic reduction of MTT (3-(4,5-dimethylthiazol-2-yl)-2,5-diphenyltetrazolium bromide) or MTS (3-(4,5-dimethylthiazol-2-yl)-5-(3-carboxymethoxyphenyl)-2-(4-sulfophenyl)-2H-tetrazolium) to formazan. Especially, RBCs cell modifications with nanoparticle are evaluated by cell compatibility assays, such as oxidative stress, cell lysis and osmotic stress, and cell deformability via UV-Vis spectroscopy.

Fluorescence outputs of nanoparticle-decorated cells[72], lysed nanoparticle-decorated cells[58] or the supernatant nanoparticles[39] have been analyzed to estimate the number of nanoparticles per cell using standard NP stock solutions. In a study by Mooney *et al.*, streptavidin coated and Nile Red-loaded polystyrene nanoparticles were conjugated to biotinylated neural stem cells and the number of nanoparticles per cell were quantified by recording a nanoparticle fluorescence standard curve in the presence of cells. They observed a dose-dependent increase in nanoparticle binding to the cell surface. Up to 175 ± 12 nanoparticles/ cell were found to be coupled to the cell surface without negatively impacting the cell viability. Additionally, in a transmigration experiment, the number of nanoparticles before and after the transmigration were analyzed using this quantitative fluorescent approach and revealed that 169 ± 11 NPs/ cell were retained at maximum.[72]

1.2.3. Optical and differential interference contrast microscopy

For optical and differential interference contrast microscopy, no additional staining is needed, as this technique relies on differences in refractive index. Properties of nanoparticle-decorated cells, including cell shape, agglutination, and cell differentiation can be obtained via this method of microscopy.

1.2.4. Widefield fluorescence and confocal microscopy

Fluorescent microscopy uses laser emission of fluorophores to visualize cellular compartments and nanoparticles associated with the cell and therefore, requires the labeling of nanoparticles with fluorophores. A disadvantage of this technique is that fluorescent molecules can alter the properties of the nanoparticles and their interactions with cells.

Moreover, they can leach out of the nanoparticles, can be bleached, or quenched. Fluorescence microscopy allows to simultaneously stain various cellular compartments and thus, to study the subcellular nanoparticle localization. Confocal microscopy enables a three dimensional (3D) live cell imaging of conjugated nanoparticle to the cell surface and surface-bound and internalized nanoparticles can be presented by z-stack images of individual cells. High-resolution confocal microscopy enables the acquisition of z-stacks and quantitative determination of nanoparticle tethered to the cell membrane.[42] Previous studies use widefield fluorescence and confocal microscopy to confirm the nanoparticle association with the cell membrane, analyze the nanoparticles localization, and observe the nanoparticle behavior (cell internalization, clustering/ change localization in response to certain stimuli). Single cell 3D reconstruction confocal microscopy enables the localization of the membrane-bound as well as internalized nanoparticles.[43] In a study by Stephan *et al.* the spatiotemporal distribution of T cell conjugated multilamellar crosslinked lipid capsules during T cell transmigration across the vasculature and showed the reorganization of membrane-bound nanoparticles during tumor cell engagement due to certain stimuli. To simulate the T cell migration across the vasculature they employed an *in vitro* transwell co-culture setup in which nanoparticle-conjugated T cells migrate across an endothelial cell layer in response to a chemoattractant in the lower chamber. As part of the process of T cell transmigration the T cell polarizes and shifts the surface- bound nanoparticles to the rear of the cell (i.e. the uropod) as observed by confocal microscopy. Post migration and during tumor cell encounter, the nanoparticles concentrated at the uropod are redistributed as the T cells encounter the tumor cells into the immunological synapse contact zone.[55]

1.2.5. Electron microscopy

A major drawback of florescence microscopy is the limited resolution of ~ 200 nm. Electron microscopy, SEM and TEM can achieve much higher resolutions and does not required fluorescent labels used in confocal or widefield microscopy. However, polymer nanoparticles and cells are organic material, which typically provide only a low contrast images via TEM or SEM, making precise nanoparticle localization analysis on nanoparticle-decorated cells a challenge. Nonetheless, SEM is a widely used technique to visualize nanoparticle localization and distribution, nanoparticles clustering, and morphological changes of the cell in response to the nanoparticle coupling. Polymer nanoparticles with sizes from 200 nm and different shapes can be resolved on a single particle level.[24] Brenner *et al.* studied the adsorption of clinically translatable nanocarrier

(PLGA nanoparticles, albumin nanogels and liposomes) and qualitatively analyzed the binding of polystyrene nanoparticles and nanogels to the surface of murine RBCs by SEM.

1.2.6. Nanoparticle radiolabeling

In several studies, it has been reported that the use of a scintillation counter enables the detection of radiolabeled nanoparticles, which can be transformed into number of nanoparticles per cell for a quantitative nanoparticle analysis. Anselmo *et al.* demonstrated the attachment of polystyrene nanoparticles to RBCs and the analysis of RBC- bound average nanoparticle numbers by radiolabeling with increasing nanoparticle concentration. At a feed nanoparticle/ cell ratio of 100, an average nanoparticle conjugation of 24 nanoparticles per cell was detected. FACS analysis shows that > 99% of all cell were labeled with nanoparticles. The determination of the exact amount of nanoparticles associated with cells is necessary to study the influence of nanoparticle cell surface concentration on cell viability, i.e. RBC lysis, as well as morphological changes resulting from nanoparticle attachment. *In vivo* biodistribution of radiolabeled nanoparticles conjugated to RBCs show a 3-fold increase in the blood over 24 h and 7-fold higher accumulation of nanoparticles in the lungs while reducing the uptake in liver and spleen.25 Pan *et al.* moved from model systems such as polystyrene nanoparticles to clinically more relevant nanogels and studied the adsorption of ^{125}I- labelled lysozyme-dextran nanogels to the surface of RBCs. The number of nanoparticles and their adsorption efficiency on murine and human RBCs was assessed. Furthermore, the impact of nanoparticles binding (cell agglutination, osmotic and oxidative stress, cell deformability and exposure of phosphatidylserine) was investigated as function of the initial nanoparticle concentration.[60]

Table 3: Analysis of nanoparticle- modified cells, techniques, analyzed properties and methods.

Technique	Analyzed properties	Method	Ref.
FACS	NP- associated fluorescence	Relative increase of nanoparticle- associated fluorescence in comparison to control cells, NP coupling efficiency, study of cell binding, NP attachment stability, binding specificity	[37, 38, 39, 54, 42, 56, 57, 43, 44, 48, 53, 25, 60, 61, 62, 84, 64, 63, 66, 76, 77, 78, 80, 81, 72, 88, 69, 87, 71, 70]
	Reduction in NP-associated fluorescence	Percentage of antigens or functional groups blocked	[37, 38, 42]
	Trypan blue extracellular fluorescence quenching	Surface- conjugated and internalized nanoparticles	[42]
	FACS calibration with standard beads	Number of NPs/ cell	[85]
	Cell proliferation	Dilution of the cytosolic stain (e.g. CFSE)	[42, 44]
	Cell viability	Annexin V/PI, ViaCount assay, viability as a function of cell stimulation and the number of NP/ cell	[42, 60, 81, 72, 88]
	Functional properties	Detection of surface markers	[43]
		T cells: *in vitro* formation of immunological synapse, killing target cells	[42, 43, 44]
		Cytokine secretion, cytotoxicity assay	[42, 43, 44]
		Transmigration efficiency across endothelium and NP retention	[42, 43, 72, 88]
Fluorescence spectroscopy	NP association	Number of NPs/ cell NP by recording standard curve and recording of NPs fluorescence (lysed cells, nanoparticle-decorated or NPs in supernatant)	[39, 43, 58, 72]
		Qualitative NP binding to the cell	[86]
	Cell compatibility	*In vitro* serum stability and shear studies	[63]
UV-Vis spectroscopy	NP association	Number of NPs/ cell by indirect quantitative NP binding analysis using a colorimetric enzyme- substrate assay	[70]
		Qualitative NP binding	[71]
	Cell proliferation	Cell counting assay (CellTiter 96 solution)	[66]
	Cell viability	MTT or MTS cytotoxicity	[65, 66, 79, 71]
	Cell compatibility	Oxidative stress, cell lysis and osmotic stress and cell deformability	[37, 38, 25, 60]
Optical microscopy	Cell properties	Cell shape, agglutination, cell differentiation	[37, 38, 60, 26, 66]
DICM	Cell properties	Cell shape	[85, 70]

Fluorescence microscopy	NP association	Qualitative NP binding, distribution and uptake	[84], [85], [65], [77], [78], [70]
		Number of microparticles	[69]
	Viability assay	Calcein-AM and ethidium homodimer solution, fluorescein diacetate/propidium iodide (FDA/PI) staining	[54], [45]
	Functional properties	Tumor tropism, response and polarization to tumor spheroids in collagen gels, transmigration efficiency across endothelium, cell count	[68], [71]
Confocal microscopy	NP association	Qualitative NP visualization, surface bound or internalized	[54], [42], [57], [44], [25], [64], [63], [66], [76], [86], [79], [80], [81], [82], [72], [88], [68], [71], [83]
High- resolution confocal		Number of NPs/ cell	[42]
	Qualitative colocalization assay	Time course nanoparticle distribution analysis, NP uptake, ratio of fluorescence between the cell walls versus the cell interior	[46], [48], [53], [64], [86]
Live cell confocal		Nanoparticle localization and time-lapse redistribution (during cell activation)	[55], [56], [66], [82]
SEM	Qualitative NP visualization	NP localization and distribution, clustering and morphological changes of cell	[45], [25], [60], [62], [26], [24], [84], [85], [63], [72], [88], [69], [68], [70]
TEM		NP localization and distribution, clustering	[54], [45], [25], [87]
Scintillation counter	Radiolabeled nanoparticles	Number of NPs per cell in dependence of initial NP/ cell concentration	[25], [60], [26]

1.3. Challenges and Opportunities

As described in the previous chapter, cells are attractive carriers for the transport and delivery of polymer nanoparticles. However, many fundamental challenges and questions related to the modification of cells with nanoparticulate cargo and the characterization of these systems remain open. For instance, moving from model nanoparticles (e.g. PS nanoparticles which are well-defined, well-dispersed, morphological uniform and have a narrow size distributions) to more clinically relevant biodegradable polymer nanoparticles such as PLA. Does nanoparticle conjugation, i.e. the conjugation chemistry play a role for using nanoparticle-decorated cells as targeted carrier? How does the nanoparticle surface concentration change with the conjugation chemistry? What is the effect of conjugation chemistry and nanoparticle surface concentration on cell viability? Are the nanoparticles located in the cell membrane or are they internalized by the cell? Does the conjugation chemistry change the intrinsic cellular behavior in response to certain stimuli (cytokine dependent tropism, homing properties, and migration across cellular barriers)?[91] An extensive characterization of nanoparticle-decorated cells is essential for a more complete understanding of nanoparticle-cell interactions. This includes the precise determination of numbers of nanoparticles/cell, identifying the location with where nanoparticles are attached, i.e. surface proteins or carbohydrates of the glycocalyx. Which functional groups are involved in the nanoparticle conjugation and what effect does the nanoparticle localization have on the cell viability and cell function? Precise quantification of nanoparticles on the cell surface enables the estimation of drug loading per cell. For the safe use of cells as targeted drug carriers, possible interactions between nanoparticles and nanoparticle cargo and the biological environment need to be studied and to be insure that drug-loading of the nanoparticles is robust enough to reach the target tissue.

The objectives of this thesis is to precisely characterize nanoparticle-modified cells using fluorescent and fluorescent label-free methods. The influence of the encapsulation of a fluorescent dye on the physicochemical properties of the nanoparticles will be studied and the impact of fluorescent bleaching/leaching on the characterization of the nanoparticle-modified cells investigated. Nanoparticle localization and distribution on the cell surface will be qualitatively and quantitatively evaluated. A second objective is the understanding of the effect of conjugation chemistries (covalent and non-covalent

nanoparticle conjugation) and their influence on nanoparticle cell surface concentration, cell viability and functional cell properties.

1.4. References

(1) Duncan, R., *Nat. Rev. Cancer* **2006,** *6* (9), 688-701.

(2) Zhao, Z.; Ukidve, A.; Kim, J.; Mitragotri, S., *Cell* **2020,** *181* (1), 151-167.

(3) Barua, S.; Mitragotri, S., *Nano today* **2014,** *9* (2), 223-243.

(4) Ekladious, I.; Colson, Y. L.; Grinstaff, M. W., *Nature Reviews Drug Discovery* **2019,** *18* (4), 273-294.

(5) Simpson, D. J.; Smith, A. S.; Thurecht, J. K.; Such, G., *Polymers* **2019,** *11* (9).

(6) Ferrari, R.; Sponchioni, M.; Morbidelli, M.; Moscatelli, D., *Nanoscale* **2018,** *10* (48), 22701-22719.

(7) Chamundeeswari, M.; Jeslin, J.; Verma, M. L., *Environmental Chemistry Letters* **2018**.

(8) Davis, M. E.; Chen, Z. G.; Shin, D. M., *Nat. Rev. Drug Discov.* **2008,** *7* (9), 771-82.

(9) Elsabahy, M.; Wooley, K. L., *Chem. Soc. Rev.* **2012,** *41* (7), 2545-61.

(10) Nicolas, J.; Mura, S.; Brambilla, D.; Mackiewicz, N.; Couvreur, P., *Chem. Soc. Rev.* **2013,** *42* (3), 1147-1235.

(11) Maeda, H.; Wu, J.; Sawa, T.; Matsumura, Y.; Hori, K., *J. Controlled Release* **2000,** *65* (1–2), 271-284.

(12) Bertrand, N.; Wu, J.; Xu, X.; Kamaly, N.; Farokhzad, O. C., *Adv Drug Deliv Rev* **2014,** *66*, 2-25.

(13) Wilhelm, S.; Tavares, A. J.; Dai, Q.; Ohta, S.; Audet, J.; Dvorak, H. F.; Chan, W. C. W., *Nat. Rev. Mater.* **2016,** *1* (5), 16014.

(14) Bae, Y. H.; Park, K., *J. Controlled Release* **2011,** *153* (3), 198-205.

(15) Sindhwani, S.; Syed, A. M.; Ngai, J.; Kingston, B. R.; Maiorino, L.; Rothschild, J.; MacMillan, P.; Zhang, Y.; Rajesh, N. U.; Hoang, T.; Wu, J. L. Y.; Wilhelm, S.; Zilman, A.; Gadde, S.; Sulaiman, A.; Ouyang, B.; Lin, Z.; Wang, L.; Egeblad, M.; Chan, W. C. W., *Nature Materials* **2020,** *19* (5), 566-575.

(16) Pandit, S.; Dutta, D.; Nie, S., *Nature Materials* **2020,** *19* (5), 478-480.

(17) Yoo, J.; Park, C.; Yi, G.; Lee, D.; Koo, H., *Cancers* **2019,** *11* (5), 640.

(18) Yoo, J.-W.; Irvine, D. J.; Discher, D. E.; Mitragotri, S., *Nat. Rev. Drug Discovery* **2011,** *10* (7), 521-535.

(19) Yan, J.; Yu, J.; Wang, C.; Gu, Z., *Small Methods* **2017,** *1* (12), 1700270-n/a.

(20) Han, X.; Wang, C.; Liu, Z., *Bioconjugate Chem.* **2018**.

(21) Villa, C. H.; Anselmo, A. C.; Mitragotri, S.; Muzykantov, V., *Adv. Drug Del. Rev.* **2016,** *106*, 88-103.

(22) Villa, C. H.; Cines, D. B.; Siegel, D. L.; Muzykantov, V., *Transfusion Medicine Reviews* **2017,** *31* (1), 26-35.

(23) Zelepukin, I. V.; Yaremenko, A. V.; Shipunova, V. O.; Babenyshev, A. V.; Balalaeva, I. V.; Nikitin, P. I.; Deyev, S. M.; Nikitin, M. P., *Nanoscale* **2018**.

(24) Anselmo, A. C.; Kumar, S.; Gupta, V.; Pearce, A. M.; Ragusa, A.; Muzykantov, V.; Mitragotri, S., *Biomaterials* **2015,** *68*, 1-8.

(25) Anselmo, A. C.; Gupta, V.; Zern, B. J.; Pan, D.; Zakrewsky, M.; Muzykantov, V.; Mitragotri, S., *ACS Nano* **2013,** *7* (12), 11129-11137.

(26) Brenner, J. S.; Pan, D. C.; Myerson, J. W.; Marcos-Contreras, O. A.; Villa, C. H.; Patel, P.; Hekierski, H.; Chatterjee, S.; Tao, J.-Q.; Parhiz, H.; Bhamidipati, K.; Uhler, T. G.; Hood, E. D.; Kiseleva, R. Y.; Shuvaev, V. S.; Shuvaeva, T.; Khoshnejad, M.; Johnston, I.; Gregory, J. V.; Lahann, J.; Wang, T.; Cantu, E.; Armstead, W. M.; Mitragotri, S.; Muzykantov, V., *Nat. Commun.* **2018,** *9* (1), 2684.

(27) Chu, D.; Dong, X.; Shi, X.; Zhang, C.; Wang, Z., *Adv. Mater.* **2018**, e1706245.

(28) Han, Y.; Zhao, R.; Xu, F., *Small* **2018,** *14* (42), 1801674.

(29) Chu, D.; Gao, J.; Wang, Z., *ACS Nano* **2015,** *9* (12), 11800-11811.

(30) Chu, D.; Dong, X.; Zhao, Q.; Gu, J.; Wang, Z., *Adv. Mater.* **2017,** *29* (27), 1701021.

(31) Anselmo, A. C.; Gilbert, J. B.; Kumar, S.; Gupta, V.; Cohen, R. E.; Rubner, M. F.; Mitragotri, S., *J. Controlled Release* **2015,** *199*, 29-36.

(32) von Andrian, U. H.; Mackay, C. R., *N Engl J Med* **2000,** *343* (14), 1020-34.

(33) Ayer, M.; Klok, H. A., *J. Controlled Release* **2017,** *259*, 92-104.

(34) Fliervoet, L. A. L.; Mastrobattista, E., *Adv. Drug Del. Rev.* **2016,** *106*, 63-72.

(35) Su, Y.; Xie, Z.; Kim, G. B.; Dong, C.; Yang, J., *ACS Biomater. Sci. Eng.* **2015,** *1* (4), 201-217.

(36) Mager, M. D.; LaPointe, V.; Stevens, M. M., *Nature Chemistry* **2011,** *3*, 582.

(37) Rossi, N. A. A.; Constantinescu, I.; Kainthan, R. K.; Brooks, D. E.; Scott, M. D.; Kizhakkedathu, J. N., *Biomaterials* **2010,** *31* (14), 4167-4178.

(38) Chapanian, R.; Constantinescu, I.; Medvedev, N.; Scott, M. D.; Brooks, D. E.; Kizhakkedathu, J. N., *Biomacromolecules* **2013,** *14* (6), 2052-62.

(39) Xie, Y.-Q.; Arik, H.; Wei, L.; Zheng, Y.; Suh, H.; Irvine, D. J.; Tang, L., *Biomater. Sci.* **2019,** *7*, 1345-1357.

(40) Cha, J.; Kim, H.; Hwang, N. S.; Kim, P., *ACS Applied Materials & Interfaces* **2018,** *10* (42), 35676-35680.

(41) Metcalfe, C.; Cresswell, P.; Ciaccia, L.; Thomas, B.; Barclay, A. N., *Open Biology* **2011,** *1* (3), 110010.

(42) Stephan, M. T.; Moon, J. J.; Um, S. H.; Bershteyn, A.; Irvine, D. J., *Nat. Med.* **2010,** *16* (9), 1035-41.

(43) Siriwon, N.; Kim, Y. J.; Siegler, E.; Chen, X.; Rohrs, J. A.; Liu, Y.; Wang, P., *Cancer Immunology Research* **2018,** *6* (7), 812-824.

(44) Wayteck, L.; Dewitte, H.; De Backer, L.; Breckpot, K.; Demeester, J.; De Smedt, S. C.; Raemdonck, K., *Biomaterials* **2016,** *77*, 243-254.

(45) Geng, W.; Jiang, N.; Qing, G. Y.; Liu, X.; Wang, L.; Busscher, H. J.; Tian, G.; Sun, T.; Wang, L. Y.; Montelongo, Y.; Janiak, C.; Zhang, G.; Yang, X. Y.; Su, B. L., *ACS Nano* **2019**.

(46) Holden, C. A.; Yuan, Q.; Yeudall, W. A.; Lebman, D. A.; Yang, H., *Int. J. Nanomed.* **2010,** *5*, 25-36.

(47) Koo, H.; Lee, S.; Na, J. H.; Kim, S. H.; Hahn, S. K.; Choi, K.; Kwon, I. C.; Jeong, S. Y.; Kim, K., *Angew. Chem. Int. Ed.* **2012,** *51* (47), 11836-11840.

(48) Lee, S.; Koo, H.; Na, J. H.; Han, S. J.; Min, H. S.; Lee, S. J.; Kim, S. H.; Yun, S. H.; Jeong, S. Y.; Kwon, I. C.; Choi, K.; Kim, K., *ACS Nano* **2014,** *8* (3), 2048-2063.

(49) Layek, B.; Sadhukha, T.; Prabha, S., *Biomaterials* **2016,** *88*, 97-109.

(50) Du, L.; Qin, H.; Ma, T.; Zhang, T.; Xing, D., *ACS Nano* **2017,** *11* (9), 8930-8943.

(51) Lee, S.; Jung, S.; Koo, H.; Na, J. H.; Yoon, H. Y.; Shim, M. K.; Park, J.; Kim, J.-H.; Lee, S.; Pomper, M. G.; Kwon, I. C.; Ahn, C.-H.; Kim, K., *Biomaterials* **2017,** *148*, 1-15.

(52) Lee, S. H.; Park, O. K.; Kim, J.; Shin, K.; Pack, C. G.; Kim, K.; Ko, G.; Lee, N.; Kwon, S.-H.; Hyeon, T., *J. Am. Chem. Soc.* **2019**.

(53) Zhang, P.; Zhang, X.; Li, C.; Zhou, S.; Wu, W.; Jiang, X., *ACS Applied Materials & Interfaces* **2019**.

(54) Kim, H.; Shin, K.; Park, O. K.; Choi, D.; Kim, H. D.; Baik, S.; Lee, S. H.; Kwon, S.-H.; Yarema, K. J.; Hong, J.; Hyeon, T.; Hwang, N. S.-Y., *J. Am. Chem. Soc.* **2017**.

(55) Stephan, M. T.; Stephan, S. B.; Bak, P.; Chen, J.; Irvine, D. J., *Biomaterials* **2012,** *33* (23), 5776-87.

(56) Jones, R. B.; Mueller, S.; Kumari, S.; Vrbanac, V.; Genel, S.; Tager, A. M.; Allen, T. M.; Walker, B. D.; Irvine, D. J., *Biomaterials* **2017,** *117*, 44-53.

(57) Huang, B.; Abraham, W. D.; Zheng, Y.; Bustamante López, S. C.; Luo, S. S.; Irvine, D. J., *Science Translational Medicine* **2015,** *7* (291), 291ra94-291ra94.

(58) Loukogeorgakis, S. P.; Fachin, C. G.; Dias, A. I. B. S.; Li, H.; Tang, L.; Kim, A. G.; Vrecenak, J. D.; Stratigis, J. D.; Ahn, N. J.; Nissim, I.; Nissim, I.; Moron, A. F.; Martins, J. L.; Peranteau, W. H.; De Coppi, P.; Irvine, D. J.; Flake, A. W., *Blood* **2019,** *134* (22), 1983-1995.

(59) Dias, A.; Werner, M.; Ward, K.; Fleury, J. B.; Baulin, V. A., *Nanoscale* **2018**.

(60) Pan, D. C.; Myerson, J. W.; Brenner, J. S.; Patel, P. N.; Anselmo, A. C.; Mitragotri, S.; Muzykantov, V., *Sci. Rep.* **2018,** *8* (1), 1615.

(61) Chambers, E.; Mitragotri, S., *Exp. Biol. Med.* **2007,** *232* (7), 958-966.

(62) Chambers, E.; Mitragotri, S., *J. Controlled Release* **2004,** *100* (1), 111-119.

(63) Zhao, Z.; Ukidve, A.; Gao, Y.; Kim, J.; Mitragotri, S., *Science Advances* **2019,** *5* (11), eaax9250.

(64) Shields, C. W.; Evans, M. A.; Wang, L. L.-W.; Baugh, N.; Iyer, S.; Wu, D.; Zhao, Z.; Pusuluri, A.; Ukidve, A.; Pan, D. C.; Mitragotri, S., *Science Advances* **2020,** *6* (18), eaaz6579.

(65) Jeong, J. H.; Schmidt, J. J.; Kohman, R. E.; Zill, A. T.; DeVolder, R. J.; Smith, C. E.; Lai, M.-H.; Shkumatov, A.; Jensen, T. W.; Schook, L. G.; Zimmerman, S. C.; Kong, H., *J. Am. Chem. Soc.* **2013,** *135* (24), 8770-8773.

(66) Armstrong, J. P. K.; Shakur, R.; Horne, J. P.; Dickinson, S. C.; Armstrong, C. T.; Lau, K.; Kadiwala, J.; Lowe, R.; Seddon, A.; Mann, S.; Anderson, J. L. R.; Perriman, A. W.; Hollander, A. P., *Nat. Commun.* **2015,** *6* (1), 7405.

(67) Green, N. M., *The Biochemical journal* **1963,** *89* (3), 585-591.

(68) Cheng, H.; Kastrup, C. J.; Ramanathan, R.; Siegwart, D. J.; Ma, M.; Bogatyrev, S. R.; Xu, Q.; Whitehead, K. A.; Langer, R.; Anderson, D. G., *ACS Nano* **2010,** *4* (2), 625-631.

(69) Krishnamachari, Y.; Pearce, M. E.; Salem, A. K., *Adv. Mater.* **2008,** *20* (5), 989-993.

(70) Ahmed, K. K.; Geary, S. M.; Salem, A. K., *J. Controlled Release* **2017,** *248*, 1-9.

(71) Xu, M.; Asghar, S.; Dai, S.; Wang, Y.; Feng, S.; Jin, L.; Shao, F.; Xiao, Y., *Int. J. Biol. Macromol.* **2019,** *134*, 1002-1012.

(72) Mooney, R., Weng, Y., Tirughana-Sambandan, R., Valenzuela, V., Aramburo, S., Garcia, E., Li, Z., Gutova, M., Annala, A. J., Berlin, J. M., Aboody, K. S. , *Future Oncol.* **2014,** *10* (3), 401-415.

(73) Monsigny, M.; Roche, A. C.; Sene, C.; Maget-Dana, R.; Delmotte, F., *Eur. J. Biochem.* **1980,** *104* (1), 147-53.

(74) Wright, C. S., *J. Biol. Chem.* **1992,** *267* (20), 14345-52.

(75) Itakura, Y.; Nakamura-Tsuruta, S.; Kominami, J.; Tateno, H.; Hirabayashi, J., *International journal of molecular sciences* **2017,** *18* (6).

(76) Gabor, F.; Trimmel, K.; Ratzinger, G.; Kerleta, V.; Fillafer, C.; Wirth, M., *J. Drug Deliv. Sci. Technol.* **2008,** *18* (1), 51-57.

(77) Weissenböck, A.; Wirth, M.; Gabor, F., *J. Controlled Release* **2004,** *99* (3), 383-392.

(78) Fillafer, C.; Friedl Daniela, S.; Wirth, M.; Gabor, F., *Small* **2008,** *4* (5), 627-633.

(79) Liu, R.; Cui, Q.; Wang, C.; Wang, X.; Yang, Y.; Li, L., *ACS Applied Materials & Interfaces* **2017,** *9* (3), 3006-3015.

(80) Wang, S.; Yin, D.; Wang, W.; Shen, X.; Zhu, J.-J.; Chen, H.-Y.; Liu, Z., *Sci. Rep.* **2016,** *6* (1), 22757.

(81) Hou, Y.; Cao, S.; Li, X.; Wang, B.; Pei, Y.; Wang, L.; Pei, Z., *ACS Applied Materials & Interfaces* **2014,** *6* (19), 16909-16917.

(82) Jacobs, J.; Byrne, A.; Gathergood, N.; Keyes, T. E.; Heuts, J. P. A.; Heise, A., *Macromolecules* **2014,** *47* (21), 7303-7310.

(83) Shi, P.; Ju, E.; Yan, Z.; Gao, N.; Wang, J.; Hou, J.; Zhang, Y.; Ren, J.; Qu, X., *Nat. Commun.* **2016,** *7*, 13088.

(84) Wibroe, P. P.; Anselmo, A. C.; Nilsson, P. H.; Sarode, A.; Gupta, V.; Urbanics, R.; Szebeni, J.; Hunter, A. C.; Mitragotri, S.; Mollnes, T. E.; Moghimi, S. M., *Nat. Nanotechnol.* **2017,** *12* (6), 589-594.

(85) Barbul, A.; Singh, K.; Horev-Azaria, L.; Dasgupta, S.; Auth, T.; Korenstein, R.; Gompper, G., *ACS Appl. Nano Mater.* **2018,** *1* (8), 3785-3799.

(86) Wijetunge, S. S.; Wen, J.; Yeh, C.-K.; Sun, Y., *Colloids Surf. B. Biointerfaces* **2020,** *185*, 110572.

(87) Shi, P.; Zhao, N.; Lai, J.; Coyne, J.; Gaddes, E. R.; Wang, Y., *Angew. Chem.* **2018**, *57* (23), 6800-6804.

(88) Mooney, R.; Weng, Y.; Garcia, E.; Bhojane, S.; Smith-Powell, L.; Kim, S. U.; Annala, A. J.; Aboody, K. S.; Berlin, J. M., *J Control Release* **2014,** *191*, 82-9.

(89) Farzin, L.; Sheibani, S.; Moassesi, M. E.; Shamsipur, M., *J. Biomed. Mater. Res. A* **2019,** *107* (1), 251-285.

(90) Adan, A.; Alizada, G.; Kiraz, Y.; Baran, Y.; Nalbant, A., *Crit. Rev. Biotechnol.* **2017,** *37* (2), 163-176.

(91) Panyam, J.; Labhasetwar, V., *Pharm. Res.* **2003,** *20* (2), 212-20.

2. Fluorescence-based and Fluorescent label-free Characterization of Polymer Nanoparticle Decorated T cells

2.1. Introduction

Conventional therapies that use low molecular weight drugs are often compromised by off-target delivery and consequently significant side-effects for patients. The use of polymer- or (polymer) nanoparticle-based carriers provides a strategy to improve control over drug biodistribution and can also allow a controlled release.[1-7] Polymers and polymer nanoparticle based-carriers, furthermore, can also protect the drug from hydrolysis, reduce systemic toxicity and enhance solubility. Nevertheless, for a variety of medical conditions, most notably cancer, very often only a fraction of the administered drug reaches the target site and there is a great interest in and need for strategies that allow to even better control the biodistribution of drug-loaded polymers and polymer nanoparticles.[8-10]

One interesting and powerful strategy to enhance control over the biodistribution of drug-loaded polymers and polymer nanoparticles is the use of cells as carriers.[11-21] Various cell types have unique properties that make them attractive as carriers for polymers and polymer nanoparticles. Red blood cells, for example, are able to circulate in the blood stream for extended periods of time.[22] Several cells of the immune system, such as macrophages,[23] monocytes and B- and T cells,[24-26] possess tumor targeting properties and are attractive carriers for the targeted delivery of anti-cancer polymer nanomedicines. Mesenchymal stem cells also possess tumor-tropic and –migratory characteristics in the tumor microenvironment and have also been used as nanoparticle carriers.[27] Loading of cell-based carriers with polymers or polymer nanoparticles can be achieved by internalization of the payload (in particular in case of macrophages) or via immobilization on the cell surface.[28] A broad range of chemical conjugation strategies has been used to

immobilize polymer nanoparticles on cell surfaces. This includes non-covalent approaches such as the use of electrostatic[29-31] or ligand-receptor interactions (e.g. biotin-streptavidin).[32,33] Cell surfaces on the other hand, also can be modified following a broad range of covalent chemistries that can target both natural and non-natural functional groups.[34-38]

The surface modification of cells with nano- or microparticles or the internalization of nanoparticles by cells is often monitored with fluorescence-based techniques, such as flow cytometry (FACS) and confocal microscopy. These techniques require the use of fluorescent-labelled particles. By using calibrated beads that contain a known amount of dye, FACS allows to quantitatively determine the average number of nanoparticles that are associated to the cell.[39] Also, nanoparticle standard curves are utilized to determine the number of nanoparticles bound per cell.[40] Confocal laser scanning microscopy allows to visualize nanoparticle decorated and nanoparticle containing cells and can provide insight into the localization, distribution and number of nanoparticles per cell.[24,41] If an appropriate fluorescent label is selected, nanoparticle-modified or -loaded cells can be simultaneously analyzed by FACS and confocal microscopy. In addition to FACS and confocal microscopy, there are also techniques to monitor the decoration of cell surfaces with nanoparticles that do not require the use of fluorescent-labeled particles. The use of radiolabeled particles, for example, represents one approach that allows to quantify the nanoparticle load per cell without the need for fluorescent labels.[29, 42, 43] Scanning electron microscopy (SEM) is another method that is frequently used to characterize nanoparticle decorated cells.[42-44] It enables high-resolution imaging of three-dimensional cellular structures. The detection of polymer nanoparticles on the surface of cells can be challenging, however, due to a low contrast of the nanoparticles. Additionally, SEM is limited to fixed, dehydrated samples that are modified with a thin, conductive coating.[42,44]

While the characterization of nanoparticle-decorated cells still predominantly relies on the use of fluorescent-labeled particles, the use of fluorescent labels also poses some risks and has several drawbacks. Fluorescent dyes may bleach or leach from the nanoparticles.[45] If this happens, how does this impact the characterization of the nanoparticle modified cells? In some cases, the use of fluorescent labels has been reported to alter the physicochemical properties of nanoparticles and their interactions and uptake by cells.[46,47] This manuscript investigates the use of fluorescent dye labelled nanoparticles to monitor cell surface conjugation processes and to characterize surface-modified cells. It

is shown that the use of fluorescent dyes that are physically entrapped in the nanoparticles can lead to false negative or erroneous results. The use of nanoparticles that contain covalently tethered fluorescent dyes, instead, was found to provide a robust approach to monitor cell surface conjugation reactions and to quantitatively analyze nanoparticle-decorated cells. Finally, it will be demonstrated that optical diffraction tomography allows to characterize nanoparticle-decorated cells without the need for fluorescent labels.

2.2. Experimental Section

2.2.1. Materials

All chemicals were used as received unless described otherwise. Acid terminated poly (D,L-lactide) (Resomer R202H, M_w: 10000 – 18000 g/ mol), Coumarin 6 (3-(2-benzothiazolyl)-N,N-diethylumbelliferylamine), poly(L-lysine) solution (0.1 % (w/v) in H_2O, Mw: 150 000 – 300 000 g/mol) and dimethyl sulfoxide (Hybri-Maxe, sterile-filtered, BioReagent, suitable for hybridoma) were purchased from Sigma Aldrich. BODIPY 493/503 (4,4-difluoro-1,3,5,7,8-pentamethyl-4-bora-3a,4a-diaza-s-indacene), DPBS (Dulbecco's phosphate-buffered saline, no calcium, no magnesium), RPMI 1640 medium, GlutaMAX supplement, FBS (fetal bovine serum, qualified, E.U.-approved, south America origin), penicillin-streptomycin, CellTrace Violet (Cell Proliferation Kit, for flow cytometry), wheat germ agglutinin Texas Red-X conjugate and ProLong Gold Antifade Mountant were purchased at Thermo Fisher Scientific. DiOC18(3) (3,3'-dioctadecyloxacarbocyanine perchlorate) was obtained from Biotium. Poly(D,L-lactic acid)-Cyanine 5 (M_n: 14631 g/mol, Đ = 1.7) was purchased at PolySciTech. Precision cover slips (diameter 12 mm) were purchased at Roth. For ODT experiments 24 x 50 mm^2 cover slips (Menzel Glaser inc.) were used. Jurkat cells (clone E6-1, cat. no. TIB-152) were obtained from ATCC.

2.2.2. Methods

UV-Vis Absorption and fluorescence emission spectra. UV-Vis absorption and fluorescence emission spectra were recorded on a Tecan Infinite M200 Pro platereader.

Spectra were recorded using 0.1 mg/mL solutions of Coumarin 6, BODIPY 493/503 and DiO in DMSO. UV-vis absorption spectra were recorded from 320 to 800 nm. For the fluorescence spectra, the excitation wavelength was set at 488 nm and the emission was recorded from 488 to 800 nm. Spectra are included in **Supporting Information Figure S1**.

Particle size and zeta potential measurements. Particle sizes and zeta potentials were measured using a Zetasizer Nano Zs instrument (Malvern). Size measurements were performed at room temperature in DPBS at a nanoparticle concentration of 0.02 mg/mL. Zeta-potential measurements were performed in 1 mM NaCl using a nanoparticle concentration of 0.056 mg/mL. All measurements were performed in triplicate and the standard deviation is reported.

Flow cytometry (FACS). Flow cytometry was performed using a Beckman Coulter Gallios cytometer with violet (405 nm), blue (488 nm), green (561 nm) and red (640 nm) lasers. For FACS analysis, the cells were resuspended in FACS buffer (DPBS containing 2.5% FBS and 0.1% sodium azide) at a concentration of 1 mio cells/mL. Ten thousand events were analyzed per experiment. The gating strategy that was applied for the analysis of the cells is shown in **Supporting Information Figure S2**. The data were analyzed using FlowJo software.

Laser scanning confocal microscopy. Confocal microscopy images were acquired on a Zeiss LSM700 microscope with a Plan-Apochromat 63×/1.40 oil objective. Z-stacks were taken with a distance of 130 nm between each focal plane. The resolution of the images are 26.2 pixel per µm and the voxel size 38.2 x 38.2 x 130 nm^3. Images were acquired sequentially (Channel 1 and channel 2 together and channel 3 separately) in order to avoid excitation and emission bleed-through with the following settings for the individual channels. Channel 1 excitation: 405 nm, detection: 405–490 nm, channel 2 excitation: 555 nm, detection: 555–588 nm and channel 3 excitation: 488 nm, detection: 488–555 nm. The pinhole was adjusted for each channel individually to obtain the same optical slice thickness of 0.4 µm. For channels 1 and 2, the pinhole was set in order to obtain the same optical slice thickness as in channel 3 as 0.33 AU. The zoom was adjusted to 1.3. For images with 4 channels the same settings as for 3 channels were used just an

additional channel was added and recorded together with channel 3 (639 nm, recording: above 640 nm).

Confocal microscopy image analysis. Microscopy images were deconvolved using Huygens Remote manager and processed using Image J 1.52p and Imaris. The matlab code is available, see reference.[48] Nanoparticle localization with respect to the cell membrane and cell body was analyzed with the help of the Imaris spot detection and a distance transform operation. Nanoparticles are detected as spots based on the fluorescence signal above the threshold and their size using Imaris' built-in spots detector (smoothing: 0.15, quality: 20, spot XY: 0.2 µm, spot Z: 0.4 µm (detect ellipsoid), perform region growing, threshold: 2). To quantify the number of nanoparticles per cell, for the image analysis in this paper, an average particle size of 200 nm was used. Larger spots were considered as aggregates of multiple 200 nm diameter nanoparticles. Surfaces are detected using Imaris' built-in surface detector (smoothing: 0.25, surface threshold: 200 (auto), largest sphere: 0.5 µm, min. volume 80 μm^3). Cell bodies are detected using Imaris' built-in surface detector (smoothing: 0.2, surface threshold: 500 (auto), largest sphere 10 µm, min. volume 100 μm^3. For each detected surface, a Euclidean distance map is computed. In the distance map, each pixel contains its distance to the nearest surface edge. Then, the average distance to the surface edge for each spot by measuring the mean intensity around the spot in the Euclidean distance map was computed. Negative values represent objects inside the surface and positive values outside the surface. Nanoparticle agglomerates were fitted with several nanoparticles based on the nanoparticle size.

Optical diffraction tomography (ODT). Nanoparticle-modified cells and unmodified control cells were fixed 20 min in 4 % paraformaldehyde solution in PBS, washed twice with PBS and sedimented on a cover slip by centrifugation (3 min, 200 g). The experimental data were taken from an optical diffraction tomography (ODT) configuration setup (**Supporting Information Figure S3**) in which Galvo-mirrors were used to control the illumination angle. 360 holograms were recorded for each sample in a circular pattern with 1° resolution at an incidence angle of 45°. ODT involves the following procedures: (1) measuring the hologram of the scattering object (i.e. T-cells with PLA nanoparticles) for each illumination angle (projection), (2) the complex amplitude of the scattered field is extracted from each hologram, (3) the 2D map of the scattered field in mapped into the 3D Fourier space by its own incident k-vectors, (4) repeating the previous

step for all the projections, (5) finally, inverse 3D Fourier transform is applied to get the 3D reconstruction in spatial domain. In this work, the absolute value of the field was used instead of the complex amplitude. This novel technique resulted in images that highlight the nanoparticles.

2.2.1. Procedures

Nanoparticle preparation. Nanoparticles were prepared by slowly precipitating a total volume of 1 mL of an acetone solution, which contained 10 mg acid terminated poly(D,L-lactide) as well as 5 µL of a 1 mg/mL acetone solution of the appropriate dye (Coumarin 6, BODIPY 493/503 or DiO) into 2 mL DPBS. For the preparation of nanoparticles that incorporate a covalently attached dye, 1 mL of an acetone solution was used, which contained 9 mg acid terminated poly(D,L-lactide) and 1 mg cyanine 5 terminated poly(D,L-lactide) together with 5 µL of a 1 mg/mL acetone solution of the appropriate dye. The nanoparticle suspension was stirred for 5 min and subsequently the organic solvent was removed under reduced pressure at room temperature. Nanoparticles were washed 2 x (centrifugation at 30000 g, 5 min) with 2 mL DPBS and resuspended in DPBS at a concentration of 1 mg/mL. The number of nanoparticles per volume was estimated using the nanoparticle diameter as determined by DLS and the bulk density of PLA (ρ_{PLA} = 1.25 g/cm^3 [49]). To minimize dye leaching, the nanoparticles were prepared fresh at the same day before every experiment. UV-Vis analysis of nanoparticles generated from 9 mg acid terminated poly(D,L-lactide) and 1 mg cyanine 5 terminated poly(D,L-lactide) using the Cy5 absorbance at 648 nm indicated that these mixed nanoparticles are composed of 12 wt% of the cyanine 5 terminated poly(D,L-lactide), which is in good agreement with the feed composition of the polymers in the nanoparticle preparation.

Dye encapsulation efficiency. To determine the dye encapsulation efficacy, nanoparticles were washed twice with MilliQ-water, lyophilized and dissolved in DMSO at a concentration of 1 mg/mL. The fluorescence of the DMSO solution was determined using a Tecan Infinite M200Pro plate reader. Fluorescence calibration curves for Coumarin 6 (excitation wavelength: 444 nm, emission: 515 nm), BODIPY 493/503 (excitation: 444 nm, emission wavelength: 500 nm) and DiO: (excitation wavelength: 444 nm, emission wavelength: 500 nm) in DMSO were recorded. The unknown dye concentration of the

nanoparticles dissolved in DMSO was determined from the calibration curves. The encapsulation efficiency was calculated by comparing the input dye concentration (500 ng dye/mg polymer) with the experimentally determined dye concentrations. The encapsulation efficiency was calculated as 95 % (476 ng dye/mg polymer) for Coumarin 6 loaded nanoparticles, 65 % (324 ng dye/mg polymer) for BODIPY 493/503 loaded nanoparticles and 95 % (475 ng dye/mg polymer) for DiO loaded nanoparticles (**Supporting Information Figure S4**).

Nanoparticle dye release. One fraction of nanoparticles encapsulating Coumarin 6, BODIPY 493/503 or DiO was lyophilized directly after the preparation, the other fraction was incubated in 50 mL DPBS at 37 °C for 24 h. Next, the nanoparticles were washed twice with Milli-Q water and lyophilized. Comparison of the relative fluorescence of the dissolved nanoparticles in DMSO (2 mg/mL) directly after the preparation and after 24 h incubation indicated a reduction of relative fluorescence by 15 % for Coumarin 6 loaded nanoparticles, by 7 % for BODIPY 493/503 loaded nanoparticles and by 44 % for DiO loaded nanoparticles.

Cell culture. Jurkat cells were cultured in RPMI 1640 Medium supplemented with 10% fetal bovine serum (FBS) and 1% penicillin/streptomycin. Cells were maintained in a humidified atmosphere containing 5% (v/v) of CO_2 at 37 °C and split every 3-4 days until they reached a concentration of maximal 1 mio cells/mL in complete cell culture medium. The cells were used up to the 5^{th} passage for the experiments described here.

CellTrace Violet staining. Cells were washed 2 x with DPBS and resuspended at a concentration of 1 mio cells/mL. Then, CellTrace violet (5 µM, 1 mg/mL in DMSO) was added to the cell suspension and incubated for 20 min. Subsequently, an excess of cell growth medium was added for 5 min followed by a resuspension in cell culture medium and additional incubation of at least 30 min.

Cell-surface modification. Cells were washed 2 x with DPBS and suspended in DPBS at a concentration of 5 mio cells/mL. Then, a 1 mg/mL nanoparticle suspension in DPBS (5000 nanoparticles/cell) was added to the cell suspension and incubated for 30 min. The suspension was gently mixed every 10 min. After that, the cells were washed 3 x with 10 mL DPBS to remove free nanoparticles. After cell-surface modification, the surface

decorated, CellTrace Violet-stained cells were prepared for flow cytometry analysis, proliferation assay and confocal microscopy. To this end, the cell suspension was divided into three fractions. One fraction was prepared for flow cytometry analysis at t = 0 h and thus resuspended in FACS buffer, another part was prepared for flow cytometry proliferation analysis at t = 24 h and therefore resuspended in cell culture medium. The third fraction was prepared for WGA Texas Red membrane staining for microscopy slide preparation and resuspended in DPBS.

Flow cytometry proliferation assay. Surface decorated, CellTrace Violet-stained cells were resuspended in cell culture medium at a concentration of 0.5 mio cells/mL and incubated for 24 h. Cells were analyzed by FACS analysis both t = 0 h and after 24 h. Cell proliferation was assessed by comparison of the CellTrace violet mean fluorescence intensity at t = 0 h and after 24 h (**Supporting Information Figure S5**).

WGA Texas Red staining and microscopy slide preparation. To 0.5 mL of a DPBS suspension containing 1 mio cells/mL, 25 µL of WGA Texas red in DPBS (1 mg/mL) was added. After incubation for 30 min on ice, cells were washed twice with DPBS and fixed in 4 % paraformaldehyde solution in DPBS at room temperature for 20 min. After two washing steps, the cells were resuspended in DPBS at a concentration of 1 mio cells/mL and sedimented on a poly(L-lysine) coated cover slip (diameter 12 mm) by centrifugation (200 g, 3 min). The supernatant was discarded and the cover slip mounted with mounting media on a microscopy slide. The slides were cured for 24 h and sealed.

2.3. Results and Discussion

As a model system, this study has investigated the cell surface modification of Jurkat cells with carboxylic acid functionalized poly(D,L-lactic acid) (PLA) nanoparticles (**Figure 1**). Jurkat cells are immortalized cells that are used as model T lymphocytes. T lymphocytes are non-phagocytic cells, which makes them ideal candidates to study cell surface modification with nanoparticles, with a minimal risk of internalization. PLA nanoparticles were chosen as a model system representing a widely used class of degradable nanocarriers.[1-7] There have been several previous reports that have shown that

negatively charged nanoparticles can adsorb to cell membranes and in which such nanoparticle-decorated cells have been successfully used *in vivo*, for example, to increase nanoparticle circulation times.[39,42,50,51] The binding of negatively charged nanoparticles to cell surfaces can be driven by two mechanisms. First, nanoparticle attachment to the cell membrane can result from electrostatic interactions between the negatively charged nanoparticles and cationic sites on the cell membrane.[52-54] A second mechanism that may help to drive the adsorption of negatively charged nanoparticles onto the cell membrane is entropy gain-driven depletion.[55-57]

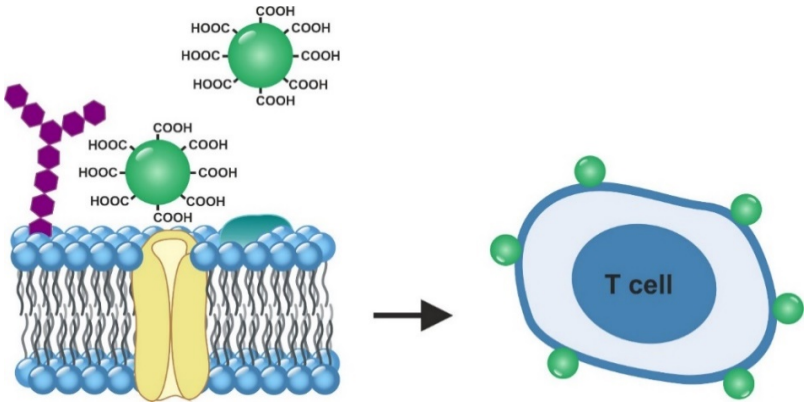

Figure 1: Schematic illustration of the surface modification of T-cells via electrostatic binding of PLA nanoparticles. Carbohydrates of the glycocalyx are shown in purple, a protein channel in yellow, a surface protein in turquoise and nanoparticles in green.

2.3.1. Nanoparticle preparation

PLA nanoparticles with a diameter of ~ 200 - 220 nm, which contained a physically entrapped fluorescent dye, were prepared by nanoprecipitation of an acetone solution containing the polymer and the dye into DPBS. As fluorescent dyes, Coumarin 6, BODIPY 493/503 and DiO were selected. These dyes have similar spectral properties (absorption in DMSO λ_{max}: Coumarin 6 = 464 nm, BODIPY 493/50 3= 492 nm, DiO = 496 nm; emission in DMSO λ_{max}: Coumarin 6 = 520 nm, BODIPY 493/503 = 518 nm, DiO = 516 nm, see also **Supporting Information Figure S1**) but different lipophilicities. For each of the three types of nanoparticles, **Table 1** lists the chemical structure of the dye and their calculated log p value, which is a measure of lipophilicity, together with the hydrodynamic diameter, polydispersity index (PDI) and zeta-potential of the particles as well as the dye

encapsulation efficiency (EE). While DiO and Coumarin 6 could be encapsulated almost quantitatively, for BODIPY the EE was ~ 65 %. As illustrated by the results in **Table 1**, encapsulation of the dyes did not result in any major changes in particle size, polydispersity or zeta-potential.

Table 4: Chemical structures and calculated log P values (clogP, calculated by ChemDraw based on the algorithm described in[58]) of the dyes DiO, BODIPY 493/503 and Coumarin 6 and the physicochemical properties of the corresponding dye-loaded PLA nanoparticles.

Fluorophore	clog P	d_H [nm]	PDI	ζ-pot. [mV]	Dye content [ng/mg polymer]	Encapsulation efficiency [%]
None	-	216	0.2	-80 ± 6.9	-	-
Coumarin 6 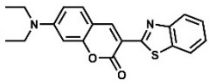	5.4	209	0.2	-79 ± 7.6	476	95
BODIPY 493/503 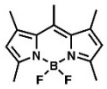	5.0	216	0.2	-72 ± 7.6	324	65
DiO 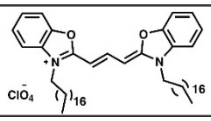	19.1	199	0.1	-73 ± 9.2	475	95

2.3.2. Cell surface modification and analysis

In a first series of experiments, surface modification of the Jurkat cells with PLA nanoparticles was monitored with flow cytometry. For these experiments, the cell cytosol was first stained with CellTrace Violet, prior to the conjugation of the dye-loaded nanoparticles to the cell surface (**Supporting Information Figure S6**). The use of CellTrace Violet to stain the cytoplasm in combination with the Coumarin 6, BODIPY and DiO labeled nanoparticles allowed to simultaneously monitor cell proliferation by following the CellTrace Violet fluorescence, as well as the cell surface nanoparticle conjugation by tracking the nanoparticle associated fluorescence with FACS and confocal microscopy. Cell surface conjugation of the PLA nanoparticles was performed by incubating Jurkat cells at a concentration of 5 million cells/mL with an equivalent of 5000

nanoparticles/cell for 30 min in DPBS at 37 °C. After that, the excess unbound nanoparticles was removed in 2 washing steps with DPBS. To assess the potential impact of nanoparticle attachment on proliferation and viability, an aliquot of the surface-modified cells was incubated for a period of 24 h in cell culture medium.

Nanoparticle surface modification of the Jurkat cells was monitored by FACS by analyzing the nanoparticle-associated fluorescence. **Figure 2** summarizes the results of the flow cytometry analyses of nanoparticle decorated cells directly after cell surface modification as well as after 24 h incubation and proliferation of the cells. Analysis of the surface modified cells directly after the nanoparticle conjugation reaction reveals a significant shift in the nanoparticle-associated fluorescence as compared to the non-modified control cells, which reflects the successful immobilization of the PLA nanoparticles on the cell surface. Analysis of the PLA nanoparticle modified cells after incubation for 24 h in cell culture medium, however, reveals dramatic changes. The flow cytometry histograms of Jurkat cells modified with Coumarin 6 and BODIPY 493/503 loaded nanoparticles recorded after 24 h incubation were identical to those of the unmodified control cells, which suggests a complete loss of the surface attached nanoparticle payload. For Jurkat cells modified with DiO loaded nanoparticles, incubation in cell culture medium for 24 h results in a 2.7 x decrease in the mean fluorescence intensity as compared to the cells directly after the cell surface modification. While the decrease in the mean fluorescence intensity that is observed for the DiO loaded nanoparticle modified cells is much less as compared to the Coumarin 6 and BODIPY 493/503 loaded nanoparticle decorated cells, it is still larger than the two-fold decrease that would be expected as a consequence of the cell proliferation. This also indicates an, at least partial, loss of the DiO-loaded PLA nanoparticle payload.

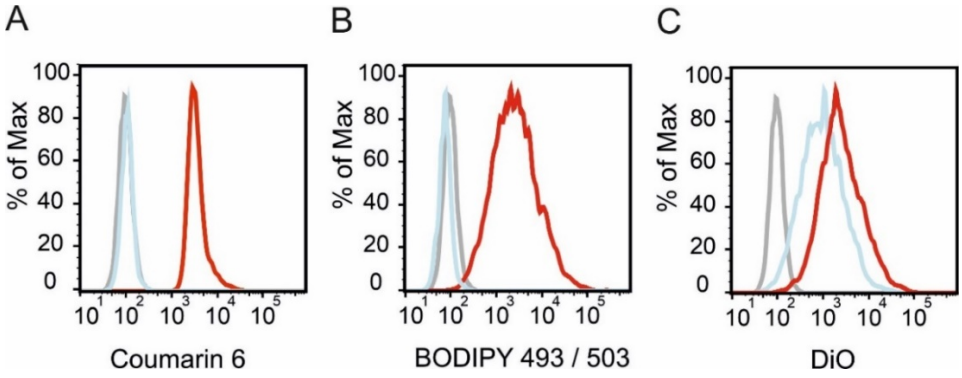

Figure 2: Representative flow cytometry histograms showing the nanoparticle-associated fluorescence directly after cell surface modification (red) and after an incubation period of 24 h (blue) for Jurkat cells modified with (A) Coumarin 6; (B) BODIPY 493/503 and (C) DiO-loaded nanoparticles. Shown in grey is the nanoparticle-associated fluorescence for unmodified control cells.

FACS was subsequently used to investigate the influence of nanoparticle surface modification on the proliferation and viability of the Jurkat cells. **Supporting Information Figure S5** presents flow cytometry histograms that compare the CellTrace Violet associated fluorescence of Jurkat cells modified with the different dye loaded nanoparticles at t = 0 h and t = 24 h. Analysis of unmodified control cells at t = 0 and t = 24 h shows a 1.98 fold reduction in the CellTrace Violet associated fluorescence, which is consistent with a single cycle of proliferation. FACS analysis of the nanoparticle-modified cells provided similar changes in the CellTrace Violet associated fluorescence, viz. a 1.82, 1.86 and 1.95 fold decrease for Coumarin 6, BODIPY 493/503 and DiO indicating that the presence of the nanoparticle payload does not impair cell proliferation. Flow cytometry analysis of the CellTrace Violet-associated fluorescence also allows to assess and compare the viability of the nanoparticle-decorated cells with that of unmodified control cells. **Supporting Information Figure S7** compares flow cytometry scatter plots of Jurkat cells modified with the different nanoparticles, both directly after cell surface modification as well as after 24 h incubation. These analyses, both directly after cell surface modification (t = 0) as well as after 24 h, do not reveal any significant differences in viability between the non-modified control cells and the nanoparticle-decorated cells.

To visualize the distribution of the nanoparticles on the cell surface and to quantitatively characterize the nanoparticle surface concentration, the surface modified Jurkat cells were studied with confocal microscopy. For these experiments, cells were

stained with CellTrace Violet to visualize the cell body and with WGA Texas Red, which was used as membrane stain. **Figure 3** compares confocal microscopy images of Jurkat cells modified with Coumarin 6, BODIPY 493/503 and DiO loaded PLA nanoparticles, both directly after the cell surface modification (**Figure 3A – C**), as well as after 24 hours (**Figure 3D – F**). **Figure 3A-C** show that directly after cell surface modification, the dye-loaded nanoparticles are either co-localized with the cell membrane or attached to the outer periphery of the cell membrane. Internalization of the nanoparticles does not occur to a significant extent. After 24 h incubation, confocal imaging of cells decorated with Coumarin 6 and BODIPY 493/503 loaded nanoparticles no longer reveals the nanoparticle-associated fluorescence. Images of cells modified with DiO labeled nanoparticles, in contrast, still show nanoparticle-associated fluorescence, albeit to a lesser extent as compared to the images taken at t = 0. These confocal microscopy observations are consistent with the results of the FACS analyses that were discussed above (**Figure 2**) and suggest a complete loss of Coumarin 6 and BODIPY 493/503 loaded nanoparticles and a partial loss of DiO-labeled nanoparticles from the cell surface.

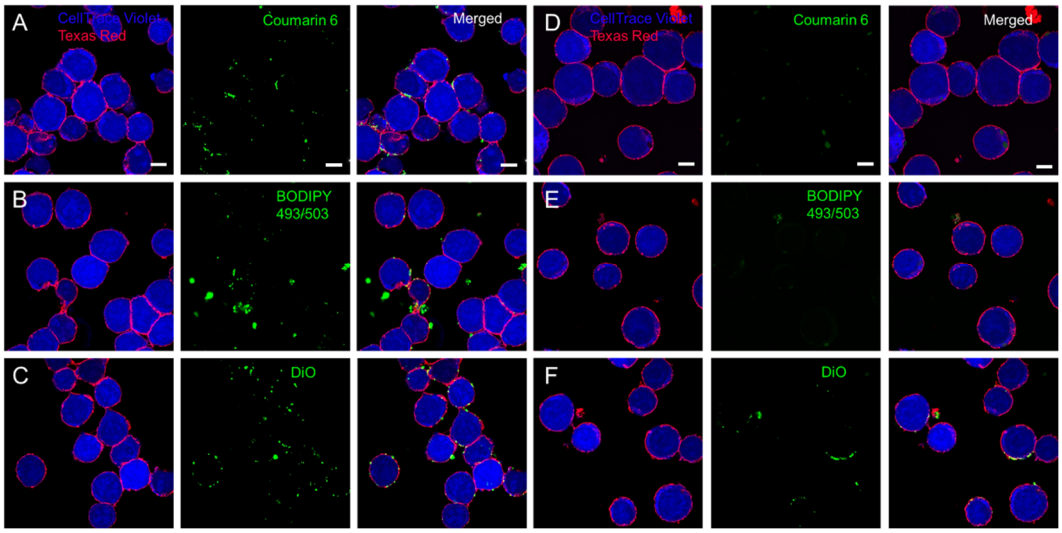

Figure 3: Laser scanning confocal microscopy images of cells decorated with nanoparticles. The cell membrane was stained with WGA Texas Red, the cytosol (blue) with CellTrace Violet and nanoparticles are shown in green. Panel A, B and C present images of Jurkat cells modified with Coumarin 6, BODIPY 493/503 and DiO-loaded nanoparticles directly after surface-modification. Panels D, E and F are confocal images of Jurkat cells modified with Coumarin 6, BODIPY 493/503 and DiO-loaded nanoparticles after an incubation time of 24 h (scale bar = 5 µm).

To quantitatively analyze the nanoparticle distribution on the cell surface, z-stacks of single nanoparticle-decorated cells were imaged and reconstructed in 3D. For each of the three different types of nanoparticles, **Figure 4** shows, for a single, selected cell directly after cell surface modification, three images that represent 2D projections of that cell in the xy, zx and zy planes. To help highlight the nanoparticles, the images in **Figure 4** only present the CellTrace Violet-associated fluorescence that visualizes the cell body as well as that of the nanoparticles, but not of the WGA-Texas Red stained cell membrane. The z-stacks of single cells were analyzed by creating distance maps, which illustrate the localization of the nanoparticle with respect to the cell body and the cell membrane. The results of these image analyses are summarized in **Figure 5** for Jurkat cells directly after surface modification with Coumarin 6 (**Figure 5A**) and BODIPY 493/503 loaded nanoparticles (**Figure 5B**) and well as for Jurkat cells decorated with DiO-loaded nanoparticles directly after surface modification (**Figure 5C**) and after 24 h (**Figure 5D**). In **Figure 5**, each sphere represents a single nanoparticle (from in total 12 single cell z-stacks). Nanoparticles that co-localize with the cell membrane are colored red, while nanoparticles that are located at the periphery of the cell are represented in black. Image analysis of the Jurkat cells directly after surface modification reveals surface concentrations of 103 ± 62, 103 ± 64 and 98 ± 55 nanoparticles/cell for the Coumarin 6, BODIPY 493/503 and DiO-loaded nanoparticles. Analysis of the data in **Figure 5** further reveals that 77 ± 5 % of the Coumarin 6 loaded nanoparticles, 66 ± 6 % of the BODIPY 493/503 loaded nanoparticles and 83 ± 5 % of the DiO loaded nanoparticles overlap with the WGA Texas red signal and co-localize with the cell membrane. After incubation for 24 h in cell culture medium, confocal microscopy images of Jurkat cells modified with Coumarin 6 and BODIPY loaded nanoparticles did no longer reveal any fluorescence due to the nanoparticle payload (see **Figure 3D and 3E**). In the confocal images of Jurkat cells modified with DiO loaded nanoparticles, in contrast, nanoparticle fluorescence was still detectable after 24 h, yet, less as compared to the images recorded directly after the cell surface modification (**Figure 3F**). After 24 h incubation, confocal image analysis indicates an average number of 32 ± 19 DiO-loaded nanoparticles on the cell surface, which represents a reduction by a factor 3 as compared to the analysis directly after cell surface modification (**Figure 5D**). A slight increase in membrane co-localization of DiO loaded nanoparticles was observed. After an incubation period of 24 h, 86 ± 13% of the DiO loaded nanoparticles colocalize with the cell membrane. **Supporting Information Figure S8** presents for each of the different dye-loaded nanoparticle decorated cells, histograms that

show for each nanoparticle the distance to the cell body. Most nanoparticles that stain WGA positive, i.e. that are co-localized with the cell membrane, are found at distances very close to the cell body. Nanoparticles that stain negative for WGA show a broader range of distances from the cell body and are predominantly located at the outer periphery of the cell. The nanoparticle distribution curves show that at t = 0 h more than 80 % of all Coumarin 6- and DiO labeled particles are localized in a distance from -0.5 to 0.5 µm with respect to the cell membrane. For BODIPY 403/503 labeled nanoparticles more than 60 % of all nanoparticles were found within this distance. Incubation for a period of 24 h leads to a broadening of the DiO-loaded nanoparticle distribution. No significant nanoparticle internalization is observed, however, and 64 % of all nanoparticles are located between -0.5 to 0.5 µm. Overall, these results are in agreement with those of the flow cytometry experiments discussed above, which also suggested a complete loss of Coumarin 6 and BODIPY 493/503 loaded nanoparticles and a decrease in the number of surface-bound DiO loaded PLA nanoparticles (**Figure 2**).

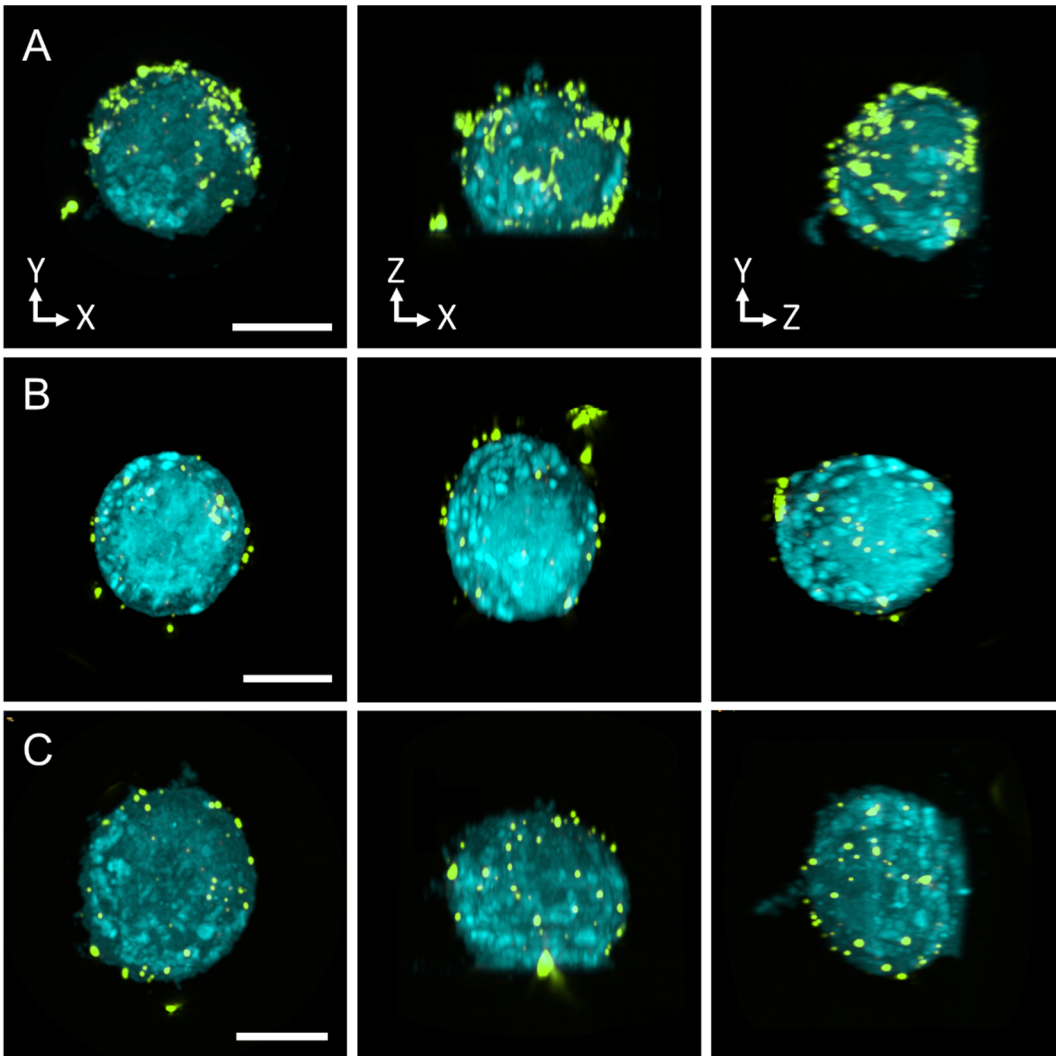

Figure 4: Single cell 2D projections in the yx-, zx- and yz- direction of 3D reconstructions of Jurkat cells directly after surface modification with (A) Coumarin 6 loaded nanoparticles; (B) BODIPY 493/503 loaded nanoparticles and (C) DiO loaded nanoparticles. Cell cytosol (blue) is stained with CellTrace Violet. To help highlight the nanoparticles, the images present only the CellTrace Violet-associated fluorescence that visualizes the cell body as well as that of the nanoparticles, but not of the WGA-Texas Red stained cell membrane (scale bar = 5 µm).

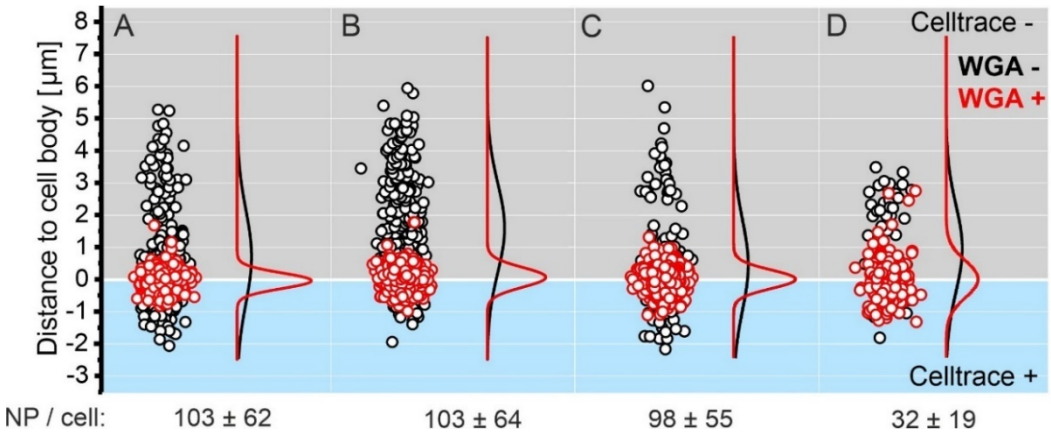

Figure 5: Distribution of Coumarin 6 (A, t = 0), BODIPY 493/503 (B, t = 0) or DiO loaded nanoparticles (C, t = 0 and D, t = 24 h) on the surface of cells. Nanoparticles that colocalize with the cytosol stain CellTrace violet are considered to be inside the cell (black dots, Celltrace +). Nanoparticles negative for CellTrace violet (Celltrace -) are inside the cell membrane (red dots, WGA +) or attached to the cell periphery (black, WGA -). The plot represents the nanoparticle distribution on the cell surface over 12 single cells and the standard deviation.

Next, as an alternative, fluorescent-label free technique, optical diffraction tomography (ODT) was explored to monitor the surface modification of the Jurkat cells with PLA nanoparticles. Cells that were used for these experiments were prepared as described above using Coumarin 6, BODIPY 493/503 or DiO loaded nanoparticles and a ratio of 5000 nanoparticles per cell. ODT enables label-free cell imaging down to a resolution of 100 nm. The method analyses differences in refractive index (RI) and can provide a 3-D refractive index distribution of optically transparent materials such as cells.[59,60] A modified method was used in this study where the 3D reconstruction was obtained from amplitude only measurements of the 2D projections, yielding images which highlight small features (i.e. the nanoparticles). By using the intensity, the 3D reconstruction highlights the small features of the nanoparticle decorated cells (i.e. it shows the nanoparticle), which enables better localization capability of the nanoparticles on the cell membrane. **Figure 6** shows representative images of single cells recorded by ODT and reconstructed in 3D from different perspectives. Nanoparticles can be identified as spots with increased intensity, which are located at the cell periphery. To exclude that these spots are cellular components or artefacts, unmodified cells were imaged with the same technique

(**Figure 6A**). ODT analysis of the unmodified cells did not reveal spots with increased intensity. As a consequence, on cells modified with nanoparticles, intensity increased signal in size range of the utilized nanoparticles indicates the existence of cell-associated nanoparticles. Furthermore, the localization of the nanoparticles in the cell membrane is highlighted by drawing an intensity profile of a cell cross-section. Nanoparticles can be identified by an intensity increase above 1.34. Label-free ODT image acquisition consistently shows that nanoparticles are associated to the cell membrane directly after surface modification (**Figure 6B, 6D and 6F**) and are also detectable after an incubation period of 24 h (**Figure 6C**, **6E** and **6G)**. The ODT analyses suggest that the results of the FACS and confocal microscopy analysis that were presented earlier may not be due to a loss of nanoparticles from the cell surface, but could be false negative results and due to, for example, leaching of the dyes from the nanoparticles.

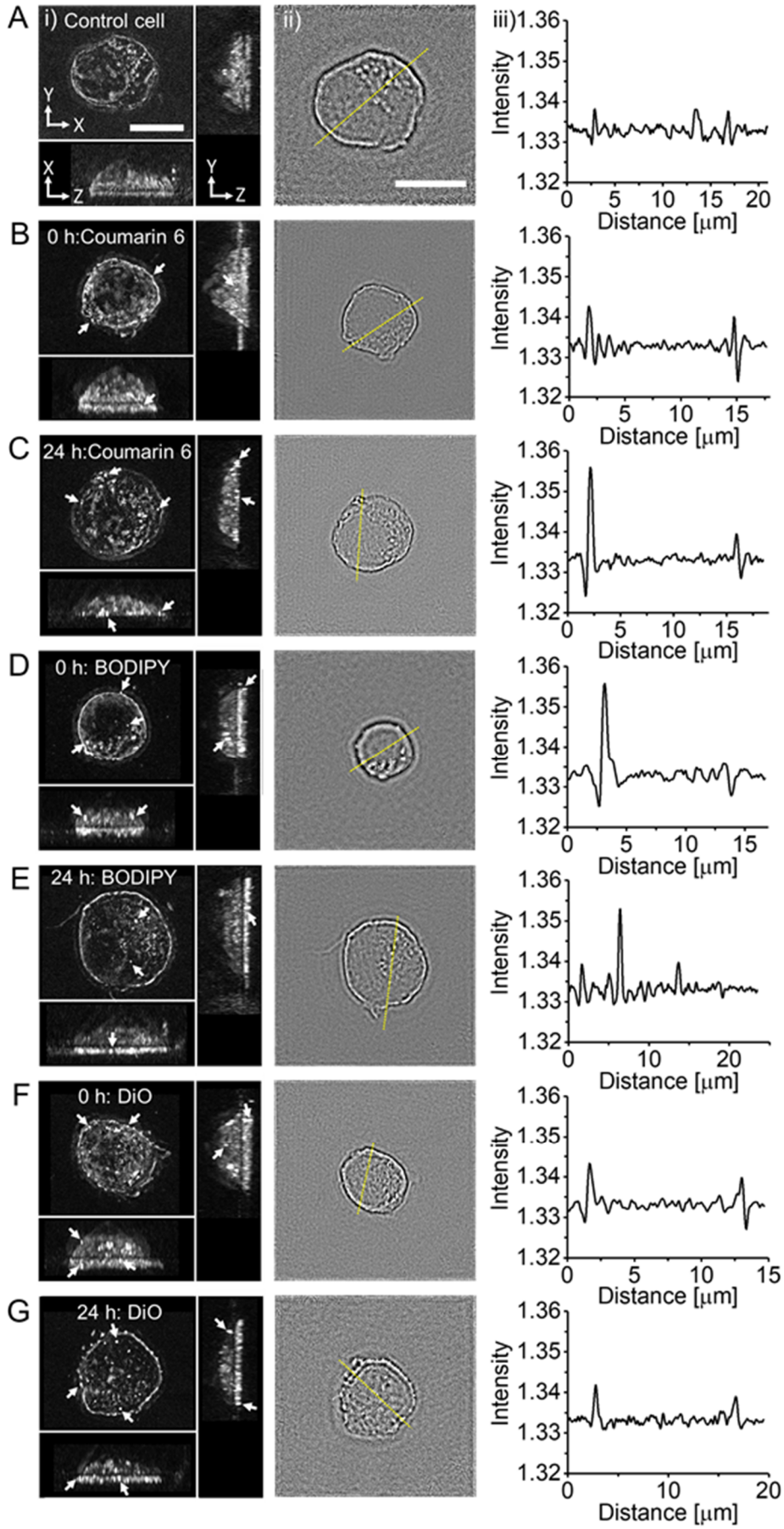
A
i) Control cell
ii)
iii)
B
0 h:Coumarin 6
C
24 h:Coumarin 6
D
0 h: BODIPY
E
24 h: BODIPY
F
0 h: DiO
G
24 h: DiO
Intensity
Distance [μm]

Figure 6: ODT analysis of (A) unmodified Jurkat cells as well as Jurkat cells modified with Coumarin 6 (B (t = 0) and E (t = 24 h)), BODIDY 493/503 (C (t = 0) and F (t = 24 h)) and DiO-loaded nanoparticles (D (t = 0) and G (t = 24 h)). Selected nanoparticles are indicated with arrows. (i) Amplitude based 3D ODT reconstructions (topleft: YX direction, right: YZ direction and bottom XZ direction); (ii): Optical YX slice and intensity profile (iii) through the cell shown on the left marked by the yellow line. The scale bar represents 10 µm.

To corroborate the hypothesis that it is leaching of the Coumarin 6 and BODIPY 493/503 dyes rather than loss of the surface attached payload, which is responsible for the FACS and confocal microcopy results that are presented in **Figure 2** and **Figure 3**, Jurkat cells were modified with double-labeled nanoparticles, which contained both a covalently attached as well as a physically entrapped fluorescent dye. These nanoparticles were obtained by coprecipitation of the carboxylic acid terminated PLA with Coumarin 6, BODIPY 493/503 or DiO as well as Cy5 endfunctionalized PLA using the same protocol that was also followed for the preparation of the other nanoparticles in this study. The characteristics of these double-labeled nanoparticles are summarized in **Supporting Information Table S1**. The particle size, polydispersity and zeta potential of the double-labeled nanoparticles were comparable to those of the nanoparticles shown in Table 1. Jurkat cells were modified with the double-labeled nanoparticles following the same protocol as described above and subsequently analyzed with flow cytometry, both directly after cell surface modification as well as after incubation for a period of 24 h in cell culture medium. **Figure 7** summarizes the results of the flow cytometry experiments. Analysis of the nanoparticle associated fluorescence that is related to the physically entrapped dye (Coumarin 6, BODIPY 493/503 and DiO) suggests complete or partial loss of the nanoparticle payload after 24 h, in agreement with the results presented in **Figure 2** and **Figure 3**. Monitoring the Cy5 fluorescence signal of the covalently tethered dye, in contrast, affords similar results for all three nanoparticles. The Cy5 mean fluorescence intensity decreases by a factor of 3.7 for Coumarin 6 nanoparticle decorated cells, by a factor of 3.3 for BODIPY 493/503 nanoparticle decorated cells and by a factor of 3.5 for DiO nanoparticle decorated cells. The reduction in the fluorescence signal of Cy5 is attributed to cell proliferation (dilution of the signal by a factor of ca. 2) as well as to a partial loss of nanoparticle payload.

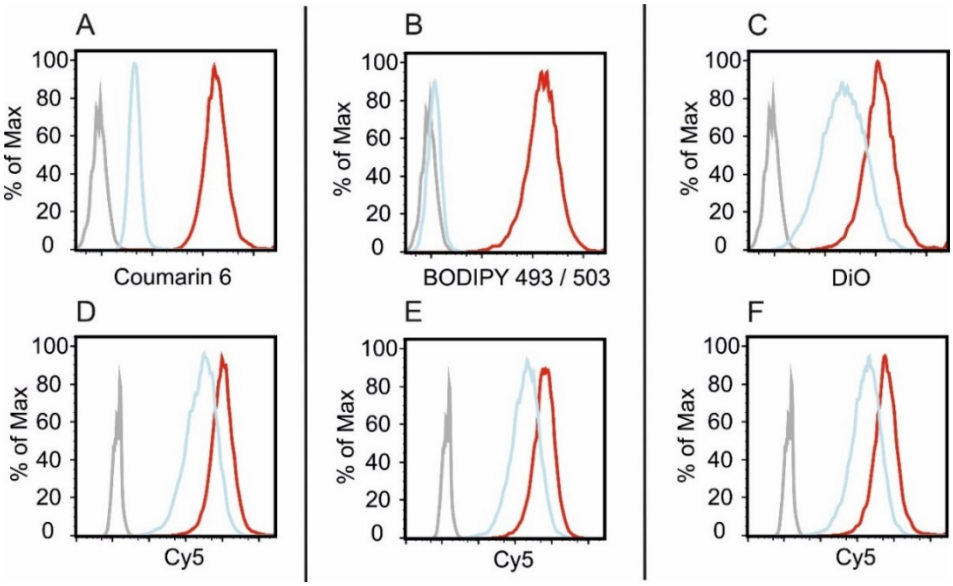

Figure 7: Flow cytometry histograms of Jurkat cells modified with nanoparticles that are covalently modified with Cy5 and which are loaded with either Coumarin 6, BODIPY 493/503 or DiO. Top row: Coumarin 6 (A), BODIPY 493/503 (B) and DiO (C) associated fluorescence at t = 0 h (red) and t = 24 (blue). Bottom row: Cy5-associated fluorescence of Jurkat cell modified with nanoparticles that contain Coumarin 6 (D), BODIPY 493/503 (E) and DiO (F) at t = 0 h (red), t = 24 h (blue). The autofluorescence of the unmodified control cells is shown in grey in each panel.

Figure 8 presents the results of confocal microscopy analysis of the double-labeled nanoparticle modified Jurkat cells. Directly after cell surface modification, for all three nanoparticles there is a clear overlap of the fluorescence signal due to the entrapped dye and that of the covalently bound Cy5 (**Figure 8A**). The overlapping fluorescence of the entrapped and bound dye is highlighted in white in the merged images. **Figure 8B** presents the images that were obtained after 24 h incubation. In agreement with the FACS analyses and confocal experiments on Jurkat cells modified with Coumarin 6 and BODIPY 493/503loaded nanoparticles that were presented earlier, essentially no Coumarin 6 or BODIPY 493/503-associated fluorescence can be discerned in the confocal images of cells decorated with the Coumarin 6/Cy5 and BODIPY 493/503/Cy5 double-labeled nanoparticles after 24 h. For the same cells, however, a clear Cy5-associated fluorescence can still be observed after 24 h. In agreement with the experiments described earlier, confocal images of Jurkat cells that were surface-modified with DiO/Cy5 double-labeled

nanoparticles, still reveal DiO-associated fluorescence after 24 h and also show the Cy5 signal of the covalently-attached dye. These results unambiguously confirm that the use of nanoparticles that contain physically entrapped dyes can lead to significant leaching of the dye and to false negative results when fluorescence-based techniques are used to characterize nanoparticle surface-modified cells.

Leaching of the dyes was confirmed in a control experiment in which dye-loaded nanoparticles were incubated in DPBS and the residual fluorescence measured after 24 h. The results that are included **Supporting Information Figure S9** reveal significant loss of fluorescence, even for DiO loaded nanoparticles. The observed leaching of DiO from the nanoparticles also indicates that a simple dye release assay may not necessarily be a good predictor for the behavior of the corresponding nanoparticle to monitor cell surface conjugation and underlines the value of the FACS analyses presented in **Figure 2**. The reduced loss of DiO from the nanoparticles as compared to Coumarin 6 and BODIPY 493/503 may be due to the higher lipophilicity of DiO (as indicated by the logP values listed in **Table 1**). Another factor could be the positively charged character of DiO, which may further help to reduce release from the negatively charged PLA nanoparticles. It is also important to note that the observations reported here are for a particular combination of nanoparticle (PLA) and dye (Coumarin 6, BODIPY 493/503 or DiO). The extent to which dye leaching occurs and obstructs analysis of surface-modified cells may be different for other combinations of dyes and nanoparticles and may also depend on the nature of the nanoparticle, e.g. solid nanoparticles versus polymer micelles or polymersomes.

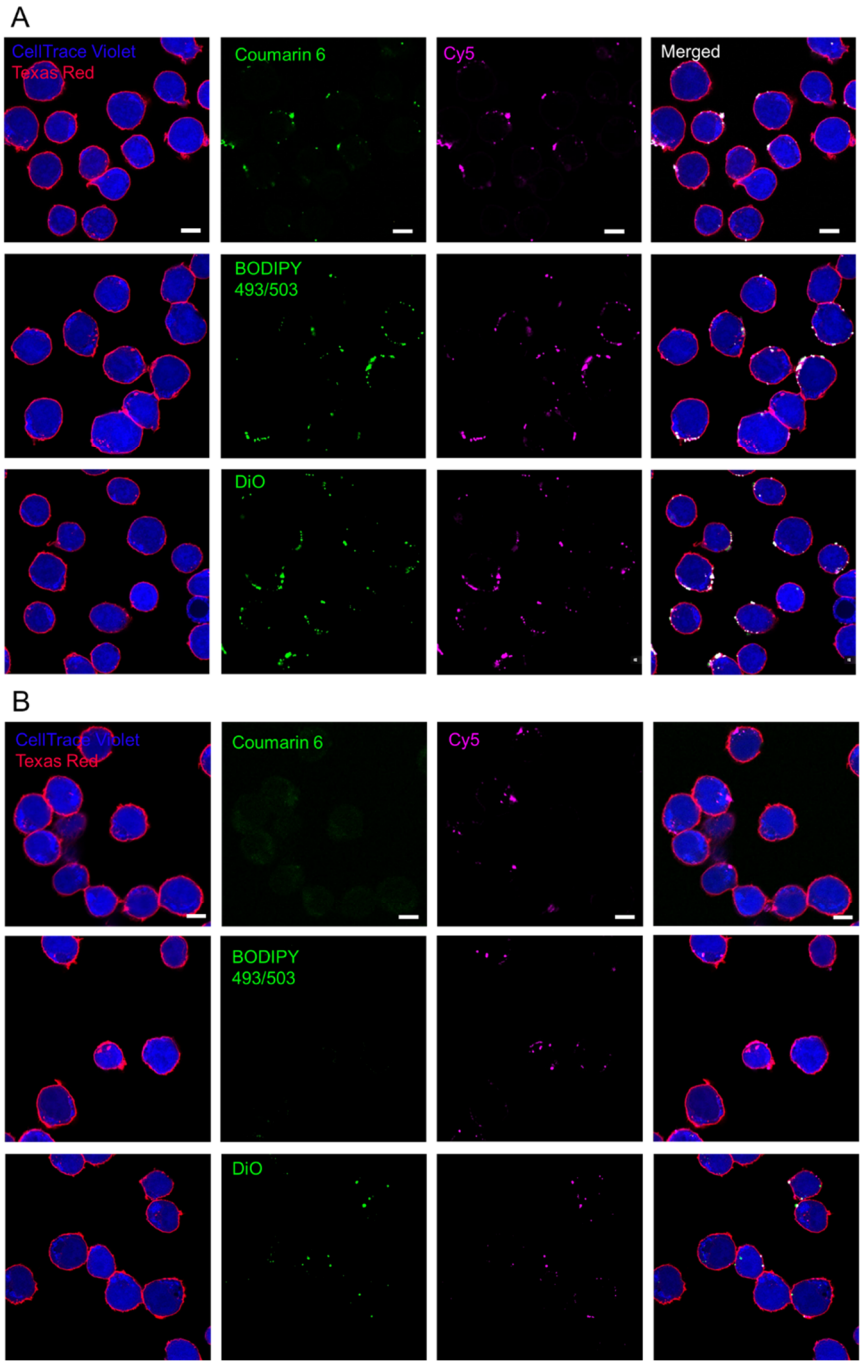

Figure 8: Confocal microscopy images of Jurkat cells decorated with double-labeled PLA nanoparticles, which entrap Coumarin 6, BODIPY 493/503 or DiO and a covalently bound Cy5. Panel A presents images of Jurkat cells modified with Coumarin-6, BODIPY or DiO-loaded, Cy5-conjugated nanoparticles directly after surface-modification. Panel B shows confocal images of Jurkat cells modified with Coumarin-6, BODIPY or DiO-loaded, Cy5-conjugated nanoparticles after an incubation time of 24 h (Scale bar = 5 µm).

2.4. Conclusions

Using poly(D,L-lactic acid) nanoparticles that are loaded with Coumarin 6, BODIPY 493/503 or DiO dyes as a model system, this study has investigated the use of fluorescent-based techniques, and in particular FACS and confocal microscopy, to monitor the modification of cell surfaces and to characterize the nanoparticle concentration and distribution on cells. For nanoparticles that were loaded with the less lipophilic fluorescent dyes (Coumarin 6 and BODIPY 493/503) leaching of dye from the nanoparticle within a period of 24 h prohibits characterization of the nanoparticle-modified cells and FACS and confocal microscopy experiments suggest an apparent, complete loss of the nanoparticle payload. For cells that were modified with nanoparticles loaded with the more lipophilic DiO, dye leaching was also observed, albeit to a lesser extent. The use of a covalently attached dye avoids dye leaching and provides a robust strategy that allows to monitor and characterize nanoparticle surface-modified cells for a period over up to 24 h. Finally, it was demonstrated that nanoparticle-decorated cells can also be characterized without the need for fluorescent labels using optical diffraction tomography as an alternative, label-free technique.

2.5. References

(1) Kamaly, N.; Yameen, B.; Wu, J.; Farokhzad, O. C., *Chem. Rev.* **2016**, *116* (4), 2602-2663.

(2) Duncan, R., *Nat. Rev. Cancer* **2006**, *6* (9), 688-701.

(3) Davis, M. E.; Chen, Z. G.; Shin, D. M., *Nat. Rev. Drug Discov.* **2008**, *7* (9), 771-82.

(4) Elsabahy, M.; Wooley, K. L., *Chem. Soc. Rev.* **2012**, *41* (7), 2545-61.

(5) Torchilin, V. P., *Adv. Drug Del. Rev.* **2012**, *64*, 302-315.

(6) Couvreur, P., *Adv. Drug Del. Rev.* **2013**, *65* (1), 581-596.

(7) Nicolas, J.; Mura, S.; Brambilla, D.; Mackiewicz, N.; Couvreur, P., *Chem. Soc. Rev.* **2013**, *42* (3), 1147-1235.

(8) Shi, J.; Kantoff, P. W.; Wooster, R.; Farokhzad, O. C., *Nat. Rev. Cancer* **2017**, *17* (1), 20-37.

(9) Wilhelm, S.; Tavares, A. J.; Dai, Q.; Ohta, S.; Audet, J.; Dvorak, H. F.; Chan, W. C. W., *Nat. Rev. Mater.* **2016**, *1* (5), 16014.

(10) Barua, S.; Mitragotri, S., *Nano today* **2014**, *9* (2), 223-243.

(11) Stephan, M. T.; Irvine, D. J., *Nano Today* **2011**, *6* (3), 309-325.

(12) Yoo, J.-W.; Irvine, D. J.; Discher, D. E.; Mitragotri, S., *Nat. Rev. Drug Discovery* **2011**, *10* (7), 521-535.

(13) Su, Y.; Xie, Z.; Kim, G. B.; Dong, C.; Yang, J., *ACS Biomater. Sci. Eng.* **2015**, *1* (4), 201-217.

(14) Fliervoet, L. A. L.; Mastrobattista, E., *Adv. Drug Del. Rev.* **2016**, *106*, 63-72.

(15) Villa, C. H.; Anselmo, A. C.; Mitragotri, S.; Muzykantov, V., *Adv. Drug Del. Rev.* **2016**, *106*, 88-103.

(16) Ayer, M.; Klok, H. A., *J. Controlled Release* **2017**, *259*, 92-104.

(17) Singh, B.; Mitragotri, S., *Biotechnol. Adv.* **2020**; *42*, 107339.

(18) Banskota, S.; Yousefpour, P.; Chilkoti, A., *Macromol. Biosci.* **2017**, *17* (1), 1600361.

(19) Pang, L.; Zhang, C.; Qin, J.; Han, L.; Li, R.; Hong, C.; He, H.; Wang, J., *Drug Deliv.* **2017**, *24* (1), 83-91.

(20) Zhao, Z.; Ukidve, A.; Kim, J.; Mitragotri, S., *Cell* **2020**, *181* (1), 151-167.

(21) Agrahari, V.; Agrahari, V.; Mitra, A. K., *Expert Opin. Drug Delivery* **2017**, *14* (3), 285-289.

(22) Chambers, E.; Mitragotri, S., *Exp. Biol. Med.* **2007**, *232* (7), 958-966.

(23) Holden, C. A.; Yuan, Q.; Yeudall, W. A.; Lebman, D. A.; Yang, H., *Int. J. Nanomed.* **2010**, *5*, 25-36.

(24) Stephan, M. T.; Moon, J. J.; Um, S. H.; Bershteyn, A.; Irvine, D. J., *Nat. Med.* **2010**, *16* (9), 1035-41.

(25) Tang, L.; Zheng, Y.; Melo, M. B.; Mabardi, L.; Castaño, A. P.; Xie, Y.-Q.; Li, N.; Kudchodkar, S. B.; Wong, H. C.; Jeng, E. K.; Maus, M. V.; Irvine, D. J., *Nat. Biotechnol.* **2018**, *36*, 707–716.

(26) Xie, Y.-Q.; Arik, H.; Wei, L.; Zheng, Y.; Suh, H.; Irvine, D. J.; Tang, L., *Biomater. Sci.* **2019**, *7*, 1345-1357.

(27) Xu, M.; Asghar, S.; Dai, S.; Wang, Y.; Feng, S.; Jin, L.; Shao, F.; Xiao, Y., *Int. J. Biol. Macromol.* **2019**, *134*, 1002-1012.

(28) Timin, A. S.; Litvak, M. M.; Gorin, D. A.; Atochina-Vasserman, E. N.; Atochin, D. N.; Sukhorukov, G. B., *Adv. Healthcare Mater.* **2018**, *7* (3), 1700818-1700837.

(29) Pan, D. C.; Myerson, J. W.; Brenner, J. S.; Patel, P. N.; Anselmo, A. C.; Mitragotri, S.; Muzykantov, V., *Sci. Rep.* **2018**, *8* (1), 1615.

(30) Swiston, A. J.; Cheng, C.; Um, S. H.; Irvine, D. J.; Cohen, R. E.; Rubner, M. F., *Nano Lett.* **2008**, *8* (12), 4446-4453.

(31) Doshi, N.; Swiston, A. J.; Gilbert, J. B.; Alcaraz, M. L.; Cohen, R. E.; Rubner, M. F.; Mitragotri, S., *Adv. Mater.* **2011**, *23* (12), H105-H109.

(32) Ahmed, K. K.; Geary, S. M.; Salem, A. K., *J. Controlled Release* **2017**, *248*, 1-9.

(33) Zheng, Y.; Tang, L.; Mabardi, L.; Kumari, S.; Irvine, D. J., *ACS Nano* **2017**, *11* (3), 3089-3100.

(34) Park, J.; Andrade, B.; Seo, Y.; Kim, M.-J.; Zimmerman, S. C.; Kong, H., *Chem. Rev.* **2018**, *118* (4), 1664-1690.

(35) Lee, D. Y.; Cha, B.-H.; Jung, M.; Kim, A. S.; Bull, D. A.; Won, Y.-W., *J. Biol. Eng.* **2018**, *12*, 28.

(36) Bi, X.; Yin, J.; Chen Guanbang, A.; Liu, C. F., *Chem. Eur. J.* **2018**, *24* (32), 8042 – 8050.

(37) Abbina, S.; Siren, E. M. J.; Moon, H.; Kizhakkedathu, J. N., *ACS Biomater. Sci. Eng.* **2018**, *4* (11), 3658-3677.

(38) Custódio, C. A.; Mano, J. F., *ChemNanoMat* **2016**, *2* (5), 376-384.

(39) Barbul, A.; Singh, K.; Horev-Azaria, L.; Dasgupta, S.; Auth, T.; Korenstein, R.; Gompper, G., *ACS Appl. Nano Mater.* **2018**, *1* (8), 3785-3799.

(40) Mooney, R., Weng, Y., Tirughana-Sambandan, R., Valenzuela, V., Aramburo, S., Garcia, E., Li, Z., Gutova, M., Annala, A. J., Berlin, J. M., Aboody, K. S. , *Future Oncol.* **2014**, *10* (3), 401-415.

(41) Sandin, P.; Fitzpatrick, L. W.; Simpson, J. C.; Dawson, K. A., *ACS Nano* **2012**, *6* (2), 1513-1521.

(42) Anselmo, A. C.; Gupta, V.; Zern, B. J.; Pan, D.; Zakrewsky, M.; Muzykantov, V.; Mitragotri, S., *ACS Nano* **2013**, *7* (12), 11129-11137.

(43) Brenner, J. S.; Pan, D. C.; Myerson, J. W.; Marcos-Contreras, O. A.; Villa, C. H.; Patel, P.; Hekierski, H.; Chatterjee, S.; Tao, J.-Q.; Parhiz, H.; Bhamidipati, K.; Uhler, T. G.; Hood, E. D.; Kiseleva, R. Y.; Shuvaev, V. S.; Shuvaeva, T.; Khoshnejad, M.; Johnston, I.; Gregory, J. V.; Lahann, J.; Wang, T.; Cantu, E.; Armstead, W. M.; Mitragotri, S.; Muzykantov, V., *Nat. Commun.* **2018**, *9* (1), 2684.

(44) Choi, M. R.; Bardhan, R.; Stanton-Maxey, K. J.; Badve, S.; Nakshatri, H.; Stantz, K. M.; Cao, N.; Halas, N. J.; Clare, S. E., *Cancer Nanotechnol.* **2012**, *3* (1-6), 47-54.

(45) Salvati, A.; Åberg, C.; dos Santos, T.; Varela, J.; Pinto, P.; Lynch, I.; Dawson, K. A., *Nanomed. Nanotechnol. Biol. Med.* **2011**, *7* (6), 818-826.

(46) Marquis, B. J.; Love, S. A.; Braun, K. L.; Haynes, C. L., *Analyst* **2009**, *134* (3), 425-439.

(47) Snipstad, S.; Hak, S.; Baghirov, H.; Sulheim, E.; Morch, Y.; Lelu, S.; von Haartman, E.; Back, M.; Nilsson, K. P. R.; Klymchenko, A. S.; de Lange Davies, C.; Aslund, A. K. O., *Cytometry, Part A* **2017**, *91* (8), 760-766.

(48) Thomsen, T.; Klok, H.-A.; Burri, O.; Seitz, A., (**2020**, August 25). *Zenodo*. http://doi.org/10.5281/zenodo.3999185

(49) Thakur, V., Thakur, M., *New York: Jenny Stanford Publishing* **2016**.

(50) Anselmo, A. C.; Kumar, S.; Gupta, V.; Pearce, A. M.; Ragusa, A.; Muzykantov, V.; Mitragotri, S., *Biomaterials* **2015**, *68*, 1-8.

(51) Wibroe, P. P.; Anselmo, A. C.; Nilsson, P. H.; Sarode, A.; Gupta, V.; Urbanics, R.; Szebeni, J.; Hunter, A. C.; Mitragotri, S.; Mollnes, T. E.; Moghimi, S. M., *Nat. Nanotechnol.* **2017**, *12* (6), 589-594.

(52) Wilhelm, C.; Billotey, C.; Roger, J.; Pons, J. N.; Bacri, J. C.; Gazeau, F., *Biomaterials* **2003**, *24* (6), 1001-1011.

(53) Nazarenus, M.; Zhang, Q.; Soliman, M. G.; Del Pino, P.; Pelaz, B.; Carregal-Romero, S.; Rejman, J.; Rothen-Rutishauser, B.; Clift, M. J. D.; Zellner, R.; Nienhaus, G. U.; Delehanty, J. B.; Medintz, I. L.; Parak, W. J., *Beilstein J. Nanotechnol.* **2014**, *5*, 1477-1490.

(54) Verma, A.; Stellacci, F., *Small* **2010**, *6* (1), 12-21.

(55) Tohver, V.; Smay, J. E.; Braem, A.; Braun, P. V.; Lewis, J. A., *Proc. Natl. Acad. Sci. U. S. A.* **2001**, *98* (16), 8950-8954.

(56) McKee, C. T.; Walz, J. Y., *J. Colloid Interface Sci.* **2012**, *365* (1), 72-80.

(57) Yang, B.; Gao, F.; Li, Z.; Li, M.; Chen, L.; Guan, Y.; Liu, G.; Yang, L., *J. Phys. Chem. Lett.* **2020**, *11* (8), 2788-2796.

(58) Leo, A. J., *Chem. Rev.* **1993**, *93* (4), 1281-1306.

(59) Wolf, E., *Opt. Commun.* **1969**, *1* (4), 153-156.

(60) Kim, K.; Yoon, J.; Shin, S.; Lee, S.; Yang, S.-A.; Park, Y., *J. Biomed. Photonics Eng.* **2016**, *2* (2).

2.6. Supporting Information

Table S1: Hydrodynamic diameter, PDIs and zeta potentials of double-labeled PLA nanoparticles.

Fluorophore	d_H [nm]	PDI	ζ-pot. [mV]
Coumarin 6/Cy5	238	0.3	-79 ± 8.5
BODIPY 493/503/Cy5	215	0.2	-74 ± 8.6
DiO/Cy5	205	0.2	-83 ± 8.7

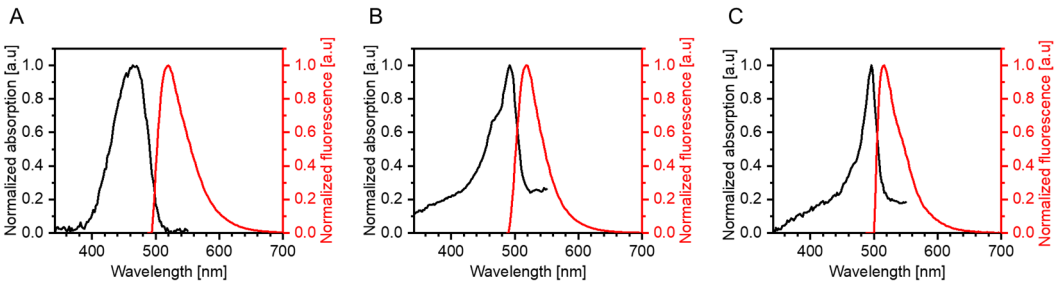

Figure S1: UV-Vis absorbance (left y-axis) and fluorescence emission spectra (right y-axis) (excitation at 488 nm) of (A) Coumarin 6, (B) BODIPY 493/503 and (C) DiO in DMSO at a concentration of 0.1 mg/mL.

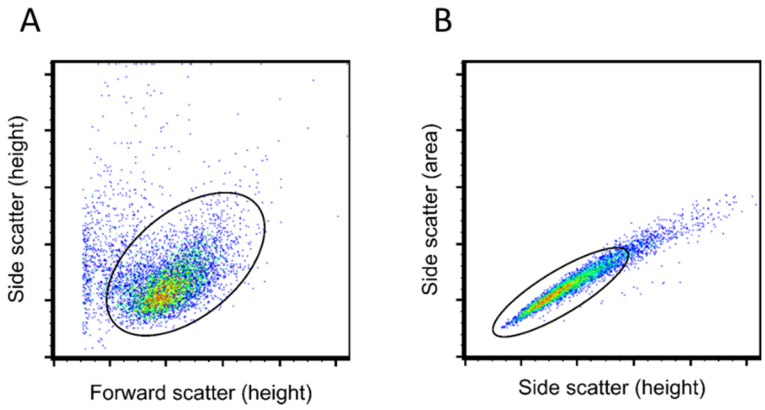

Figure S2: Flow cytometry scatter plots and gating strategy used for flow cytometry analysis. (A) The viable T cell population was selected by plotting height of the side scattered signal versus the height of the forward scattered signal; (B) Multiple cells were excluded from the analysis by plotting the area of the signal obtained from side scatter versus the height of the signal obtained from side scattering.

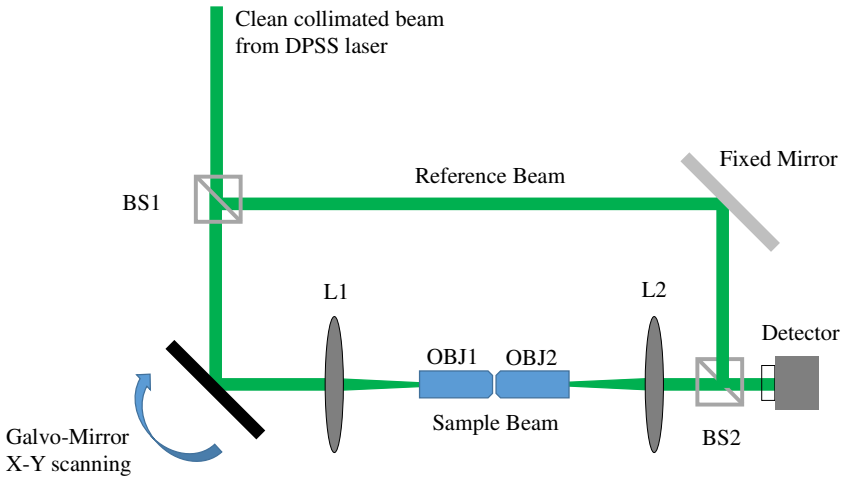

Figure S3: Schematic illustration of the optical diffraction tomography setup (L: Lens, OBJ: Objective lens, BS: Beam splitter). The optical system includes a diode pumped solid state (DPSS) 532 nm laser. The laser beam was first spatially filtered using a pinhole spatial filter. A beamsplitter (BS1) was used to split the input beam into a sample beam and a reference beam. The sample beam was directed onto the sample at different angles of incidence using Galvo-mirrors. Galvo-mirrors were rotated a full 360° with a resolution of 1 projection per degree for a total of 361 projections (including normal incidence) in a conical scenario. Using a 100X oil immersion objective lens with NA 1.4 (Olympus), the incident angle on the sample was 45°. The magnification of the illumination side was defined by the 4f system used before the sample (L1 and OBJ1). A second 4F system after the sample includes a 100X oil immersion objective lens with NA 1.45 (Olympus) and a lens (OBJ2 and L2). The sample and reference beams were collected on a second beamsplitter (BS2) and projected onto a scientific CMOS (sCMOS) camera (Neo, Andor) with a pixel size of 6.5 µm and resolution of 2150 x 2650 pixels.

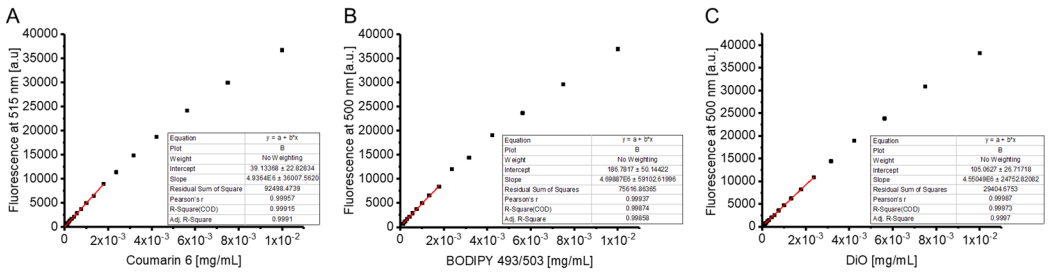

Figure S4: Fluorescence calibration curves of (A) Coumarin 6, (B) BODIPY 493/503 and (C) DiO recorded in DMSO.

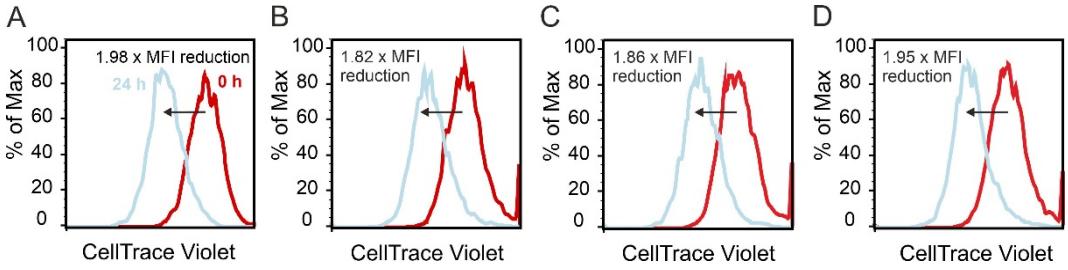

Figure S5: Flow cytometry histograms showing the CellTrace Violet signal at t = 0 h (red) and after 24 h incubation (blue). The proliferation rate was calculated by comparison of the mean fluorescence intensity (MFI) at t = 0 h and at t = 24 h and is indicated in each panel. (A) Control cells, (B) cells surface-modified with Coumarin 6 loaded nanoparticles, (C) cells surface-modified with BODIPY 493/503 loaded nanoparticles and (D) cells surface-modified with DiO loaded nanoparticles.

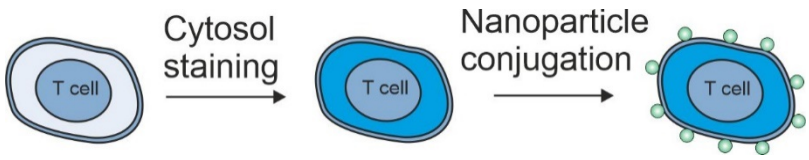

Figure S6: Illustration of the staining protocol that was used to allow simultaneous monitoring of cell surface modification and proliferation.

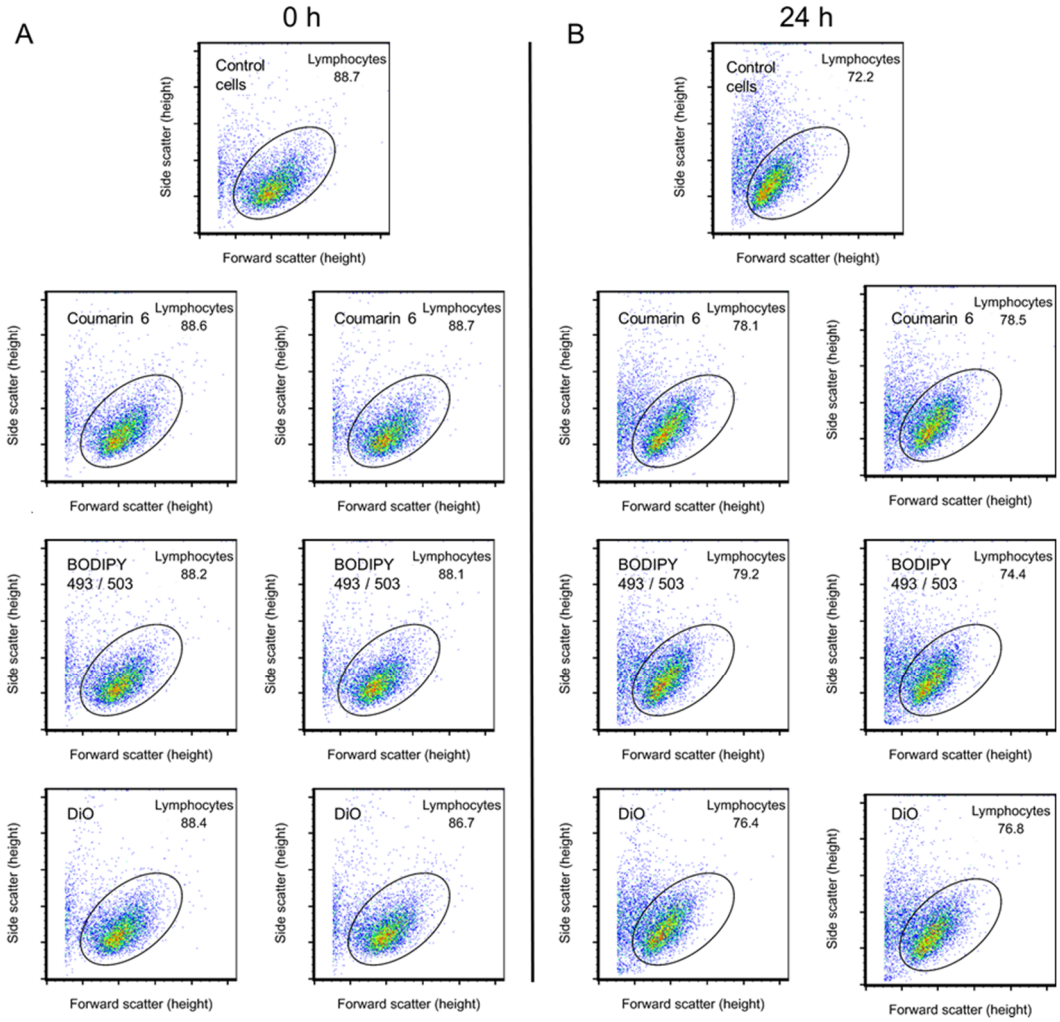

Figure S7: Flow cytometry scatter plots of control cells and nanoparticle decorated cells (A) directly after cell surface modification (t = 0 h) and (B) after an incubation period of 24 h (B). All cells are stained with CellTrace Violet at t = 0 h to analyze the cell proliferation during 24 h. The experiments were performed as duplicate for each dye.

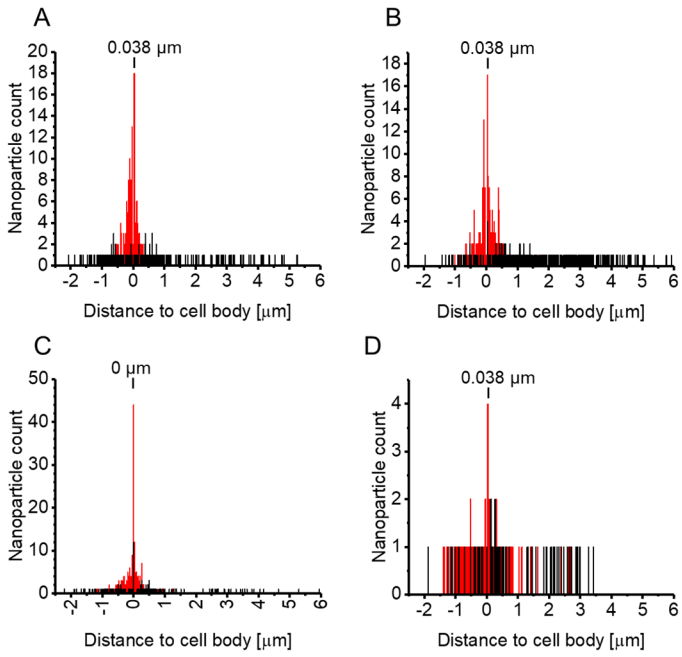

Figure S8: Histograms showing the nanoparticle count as a function of the nanoparticle distance to the cell body for WGA positive nanoparticles (red) and WGA negative nanoparticle (black). The most frequent distance for WGA positive nanoparticles is indicated in each panel. (A) Coumarin 6 loaded nanoparticles at t = 0 h, (B) BODIPY 493/503 loaded nanoparticles at t= 0 h, (C) DiO loaded nanoparticles at t = 0 h and D) DiO loaded nanoparticles at t = 24 h.

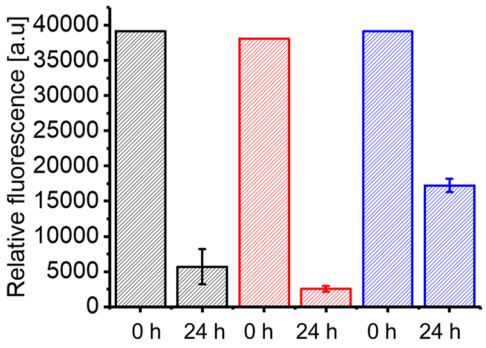

Figure S9: Fluorescence of lyophilized nanoparticles encapsulating Coumarin 6 (black), BODIPY 493/503 (red) and DiO (blue) directly after the preparation and after 24 h incubation in DPBS at 37 °C. Incubation was performed in triplicate and standard errors are reported.

3. Chemical Nanoparticle Conjugation to T lymphocytes and their Influence on Viability and functional Properties

3.1. Introduction

The treatment of diseases with low molecular weight drugs often suffers from unfavorable pharmacokinetics and pharmacodynamics i.e. low circulation time, fast excretion by the organs of mononuclear phagocyte system (MPS) and difficulties to overcome biological barriers, which restricts drug efficiency and can result in undesired side effects to patients. To some extent, these drawbacks can be mitigated by adding drugs in the form of nanosized particle formulations (micelles, polymersomes, solid core nanoparticles or another nanomedicine subclass as for example a polymer drug conjugate).[1-6] The use of polymers or polymer nanoparticle based carriers can improve control over biodistribution and also provide opportunity for targeted delivery. In many instances, especially in the context of cancer chemotherapy, only a minor fraction of these nanoformulations end up in the desired destination while the majority is delivered in off-target organs.[7-8] The use of cell-based carriers is a promising strategy to enhance control over the biodistribution of therapeutic nanoparticles, by relying on the inherent cellular properties.[9-19] For instance, non-covalent binding of polymer nanoparticles on the surface of red blood cells significantly increases their blood circulation time, allowing for enhanced accumulation in the lungs, while reducing uptake in liver and spleen.[20-24] Another class of cells for the transport of therapeutic nanoparticles are T cells. T cells, which are part of the adaptive immune system, possess tumor migratory properties and can penetrate tumor tissue making these cells attractive vectors for the delivery of nanoparticles loaded with cytotoxic agents or adjuvants.[25-27] For cells to be used for the transport of nanoparticles, the cargo must be either internalized by the cells, or attached to the cell surface. A plethora of covalent and noncovalent approaches have been used developed to attach nanoparticles to cell surfaces.[14,28,29,30] Non-covalent strategies include; electrostatic adsorption[23,31], lipophilic insertion[32,33] into the cell membrane, and receptor – ligand interactions (carbohydrate – lectin[34, 35] biotin – avidin[36, 37], receptor – antibody[38, 39, 40]). In addition to providing multiple opportunities for non-covalent attachment,

the cell membrane provides a wide range of functional groups including; -NH_2, -SH, -OH and -OH that can be targeted for covalent nanoparticle immobilization. Metabolic glycoengineering strategies allow for the introduction of bio-orthogonal functional groups such azido groups which further expand the chemical diversity for covalent nanoparticle attachment on cell membrane. These unnatural monosaccharides enable click reactions between the azido groups and strained cyclooctene modified nanoparticles[46] or triarylphosphines via a Staudinger ligation. These strategies have been used with polymer micelles to target cancer cells *in vivo*.[47] In addition, surface monosaccharides of cancer cells have been targeted with boronic acid modified nanoparticles[43]. Sialic acid has been used by oxidizing the terminal alcohol groups with sodium periodate to generate aldehyde groups on the cell surface for covalent nanoparticle immobilization. Further examples of covalent conjugation strategies for nanoparticle attachment include the reaction of dithiopyridyl and maleimide functionalized nanoparticles with free thiol groups on the cell surface.[25,41,42] Also amine functionalized nanoparticles can be reacted with the amines present on the cell surface to from a Schiff base linkages which can be further reduced to a stable secondary amine bond.[44] While there are plenty of examples of studies that demonstrate that cell-mediated delivery is a powerful strategy to enhance control over the biodistribution of nanoparticles, minimal effort has been made to explore and investigate the chemistry that underlies the surface modification of the cell-based carrier with the nanoparticle cargo. In spite of the many conjugation strategies, most studies resort to a single type of conjugation. Investigating and understanding the impact of different cell surface conjugation methods on the viability and functional properties could provide guidelines to improve the design of cell based drug delivery systems.

This article presents results of a comparative analysis that has evaluated seven different surface conjugation chemistries on the conjugation efficiency, viability and functional properties of T lymphocytes. The nanoparticles used in this study are based on PLA and were modified with a variety of cell surface reactive groups. The cells utilized in the study are $CD4^+$ T lymphocytes. These cells have blood-brain barrier (BBB) migratory properties and are attractive candidates for the delivery of cells based drug delivery systems to the central nervous system (CNS). The effect of conjugation chemistry and nanoparticle cell surface concentration on cell viability and T cell functionalities such as proliferation and ICAM-1 binding were investigated. Localization of the nanoparticles and quantification of nanoparticles/ cell was analyzed using colocalization in laser scanning confocal microscopy 3D reconstructions of the cell-nanoparticle conjugates. Furthermore, the influence of nanoparticle attachment to the cell membrane on the passage of the modified cells through

an endothelial cell layer was systematically probed. This work lays the foundation for robust cell-meditated drug delivery by providing critical insights into nanoparticles cell surface modification, cell viability and motility.

3.2. Experimental Section

3.2.1. Materials

All chemicals were used as received unless described otherwise. Methoxy terminated poly (D,L-lactic acid) (D,L mPLA-OH) (Mn: 10500 g/mol) and amino terminated poly (D,L-lactic acid) – poly(ethylene glycol) (Mn: PLA4.5k-PEG5.3-NH_2) were purchased from Advanced Polymer Materials Inc. Acid terminated poly (D,L-lactic acid) (Resomer R202H, Mw: 10000 – 18000 g/mol) (D,L-PLA-COOH), Coumarin 6 (3-(2-benzothiazolyl)-7-(diethylamino)coumarin), N-acetyl-D-galactosamine, BS3 (suberic acid bis(3-sulfo-N-hydroxysuccinimide ester) sodium salt), sulfo-SMCC (sulfosuccinimidyl 4-(N-maleimidomethyl)cyclohexane-1-carboxylate), dibenzocyclooctyne-sulfo-N-hydroxysuccinimidyl ester (DBCO-NHS), 1 mM staurosporine solution in DMSO (staurosporine solution from streptomyces, Albumin from bovine serum (lyophilized powder, ≥96% (agarose gel electrophoresis), dimethyl sulfoxide (Hybri-Max, sterile-filtered) and poly-L-lysine solution (0.1 % (w/v) in H2O, Mw: 150 000 – 300 000 g/mol) were purchased from Sigma Aldrich. DPBS (Dulbecco's phosphate-buffered saline, no calcium, no magnesium), HBSS (Hanks' balanced salt solution, no calcium, no magnesium), RPMI 1640 medium, GlutaMAX supplement, FBS (fetal bovine serum, qualified, E.U.-approved, south America origin), MEM non-essential amino acids solution, penicillin-streptomycin, 2-mercaptoethanol, HEPES (1 M), DMEM (Dulbecco's modified eagle medium), sodium pyruvate, TCEP-HCl (premium grade), NeutrAvidin protein, NeutrAvidin protein-DyLight 650, wheat germ agglutinin Texas Red X conjugate, ManNAz (N-azidoacetylmannosamine tetraacylated), biotin-XX, SSE (6-((6-((biotinoyl)amino)hexanoyl)amino)hexanoic acid, sulfosuccinimidyl ester, sodium salt), Annexin V, Alexa Fluor 647 conjugate, Annexin binding buffer, Click-IT Alexa Fluor 488 DBCO alkyne, Atto 647N-biotin, CellTrace Violet (Cell proliferation kit, for flow cytometry), NHS-fluorescein (5/6-carboxyfluorescein succinimidyl ester, mixed isomer), SAMSA Fluorescein (5-((2-(and-3)-S-(acetylmercapto) succinoyl) amino) Fluorescein, mixed isomers), Rhodamine Phalloidin and ProLong Gold Antifade mountant were purchased at Fisher Scientific AG. Precision cover slips (diameter

12 mm) were purchased at Roth. Wheat germ agglutinin (WGA) was purchased from Reactolab. DSPE-PEG2000-biotin (1,2-distearoyl-sn-glycero-3-phosphoethanolamine-N-[biotinyl(polyethylene glycol)-2000] (ammonium salt)) was obtained from Avanti Polar Lipids, Inc. Protein A was obtained from BioVision. Mouse ICAM-1-Fc chimera and DNER-Fc was chimera obtained from R&D Systems. Biotin anti-mouse CD45 was purchased from BioLegend. Cy5-conjugated Streptavidin was obtained from Jackson ImmunoResearch Laboratories, Inc. Jurkat cells, clone E6-1(cat. no. TIB-152) (a lymphocyte line derived from human acute T cell leukemia) were obtained from ATCC. Encephalitogenic $CD4^+$ effector/memory proteolipid protein (PLP) peptide aa139-153specific T cells (line SJL-PLP7) were provided by the Theodor Kocher Institute in Berne.

3.2.2. Methods

Particle sizes and zeta-potentials. Particle sizes and zeta-potentials were measured by dynamic light scattering (DLS) using a Zetasizer Nano Zs instrument (Malvern). Size measurements were performed at a concentration of 0.02 mg nanoparticles/ mL in DPBS at room temperature. Zeta-potential measurements were performed using a nanoparticle concentration of 0.06 mg / mL in 1 mM NaCl solution.

Transmission electron microscopy. A 5 µl drop of the PEG-PLA nanoparticle solution at a concentration of 4 mg/mL was adsorbed to a glow-discharged carbon-coated copper grid 400 mesh (Canemco & Marivac, Canada), washed with deionized water, and stained with 5 µl of uranyl acetate 2%. Observation was made using an F20 electron microscope (Thermo Fisher, Hillsboro, USA) operated at 200 kV. Digital images were collected using an Eagle CCD camera (Thermo Fisher, Hillsboro, USA) at 4098 x 4098 pixels, using a defocus range of -2 µm to -5 µm.

Flow cytometry. Flow cytometry was performed using a Beckman Coulter Gallios cytometer with violet (405 nm), blue (488 nm), green (561nm) and red (640 nm) lasers. For FACS analysis, the cells were resuspended in FACS buffer (DPBS containing 2.5% FBS and 0.1% sodium azide) at a concentration of 1 mio cells/mL. Ten thousand events were analyzed per experiment. The gating strategy that was applied for the analysis of the cells is shown in **Supporting Information Figure S1**. The data were analyzed using FlowJo software.

Laser scanning confocal microscopy. Confocal microscopy images were acquired on a Zeiss LSM700 microscope with a Plan-Apochromat 63×/1.40 oil objective. Z-stacks were taken with a distance of 130 nm between each focal plane. The resolution of the images are 26.2 pixel per µm and the voxel size 38.2 x 38.2 x 130 nm^3. Images were acquired sequentially (Channel 1 and channel 2 together and channel 3 separately) in order to avoid excitation and emission bleed-through with the following settings for the individual channels. Channel 1 excitation: 405 nm, recording: 405–490 nm, channel 2 excitation: 555 nm, recording: 555–588 nm and channel 3 excitation: 488 nm, recording: 488–555 nm. The pinhole was set to 0.27 Airy Units (AU) for channel 3 corresponding to an optical thickness of 0.4 µm. For channels 1 and 2, the pinhole was set in order to obtain the same optical slice thickness as in channel 3 as 0.33 AU. The zoom was adjusted to 1.3.

Confocal microscopy image analysis. Microscopy images were deconvolved using Huygens Remote manager and processed using Image J 1.52p and Imaris. Nanoparticle localization with respect to the cell membrane and cell body was analyzed with the help of the Imaris spot detection and a distance transform operation. Nanoparticles are detected as spots based on the fluorescence signal above the threshold and their size using Imaris' built-in spots detector (smoothing: 0.15, quality: 20, spot XY: 0.2 µm, spot Z: 0.4 µm (detect ellipsoid), perform region growing, threshold: 2). Bigger spots were fit with multiple nanoparticles based on the size. Surfaces are detected using Imaris' built-in surface detector (smoothing: 0.25, surface threshold: 200 (auto), largest sphere: 0.5 µm, min. volume 80 µm3). Cell bodies are detected using Imaris' built-in surface detector (smoothing: 0.2, surface threshold: 500 (auto), largest sphere 10 µm, min. volume 100 $µm^3$). For each detected surface, a Euclidean distance map is computed. In the distance map, each pixel contains its distance to the nearest surface edge. Then, the average distance to the surface edge for each spot by measuring the mean intensity around the spot in the Euclidean distance map was computed. Negative values represent objects inside the surface and positive values outside the surface. Nanoparticle agglomerates were fitted with several nanoparticles based on the nanoparticle size.

3.2.1. Procedures

Preparation of dye-loaded amino-functionalized PEG-PLA nanoparticles. Nanoparticles were prepared by slowly precipitating 1 mL of an acetone solution containing 10 mg methoxy-terminated poly(D,L-lactid acid), 10 mg PLA-PEG-NH_2 together as well as 10 µL of a 1 mg/ mL DiO solution in acetone into 2 mL DPBS. The nanoparticle suspension was stirred for 5 min and the organic solvent was removed by evaporation under reduced pressure at room temperature. Nanoparticles were washed 2 x (centrifugation 30000 g, 5 min) with 2 mL DPBS and resuspended in DPBS at a concentration of 1 mg/mL. The number of nanoparticles per volume was estimated using the nanoparticle diameter as determined by DLS and the bulk density of PLA. (ρ_{PLA}: 1.25 g/cm^3).[48]

Preparation of amino-reactive PEG-PLA nanoparticles. To a 1 mg/ mL suspension of nanoparticles 20 µL of a 25 mM solution in DPBS BS3 (500 nmol) was added. The nanoparticles were shaken for 20 min and the excess linker was removed by washing with DPBS. The nanoparticles were directly used for the cell surface conjugation to avoid hydrolysis reactions of the NHS-ester.

Preparation of thiol-reactive PEG-PLA nanoparticles. To a 1 mg/ mL suspension of nanoparticles 20 µL of a 25 mM solution in milliQ-water Sulfo-SMCC (500 nmol) was added. The nanoparticles were shaken for 45 min and the excess linker was removed by 2 x washing with DPBS.

Preparation of lectin functionalized PEG-PLA nanoparticles. To a 1 mg/ mL suspension of nanoparticles 20 µL of a 25 mM BS3 solution in DPBS (500 nmol) was added. The nanoparticles were shaken for 20 min and the excess linker was removed by washing with DPBS. Subsequently, 0.22 mg WGA (600 nmol) were added. The nanoparticle suspension was shaken for 60 min and washed 2 x with DPBS.

Preparation of biotin functionalized PEG-PLA nanoparticles. To a 1 mg/ mL suspension of nanoparticles 66 µL of 5 mg/mL solution (7.5 mM) solution biotin XX, SSE in DPBS was added. The nanoparticles were shaken for 45 min and the excess linker was removed by 2 x washing with DPBS.

Preparation of NeutrAvidin functionalized PEG-PLA nanoparticles. To a 1 mg/mL suspension of biotin PEG-PLA nanoparticles 0.3 mg NeutrAvidin in DPBS (500 nmol) were added. The nanoparticle suspension was shaken for 60 min and washed 2 x with DPBS.

Preparation of DBCO functionalized PEG-PLA nanoparticles. To a 1 mg/mL suspension of biotin PEG-PLA nanoparticles 0.27 mg in 27 µL DMSO DBCO-NHS (500 nmol) was added. The nanoparticles were shaken for 45 min and the excess linker was removed by 2 x washing with DPBS.

Amino group surface concentration. PEG-PLA nanoparticles were prepared without the addition of a dye as described above. To a nanoparticle suspension of 1 mg/ mL 7.5 µmol NHS-fluorescein was added for 45 min. The free dye was removed from the nanoparticle suspension by centrifugation (3 x, 5 min, 30000 g) and washing with 1 mL DPBS. Subsequently, the nanoparticles were lyophilized and a known amount dissolved in DMF. The fluorescence of the fluorescein nanoparticles were recorded using a Tecan plate reader (Excitation wavelength: 494 nm and emission wavelength: 518 nm). A calibration curve of NHS fluorescein in DMF was recorded and by plotting a linear regression the concentration of the unknown fluorescence of the polymer samples was calculated. The amino surface concentration is 1.2 nmol/mg polymer nanoparticles. (**Supporting Information S3 A**).

Maleimide group surface concentration. PEG-PLA maleimide functionalized nanoparticles were prepared without the addition of a dye as described above. SAMSA Fluorescein (5-((2-(and-3)-S-(acetylmercapto) succinoyl) amino) Fluorescein) was first activated to remove the acteyl protecting group and thereby generate a thiol containing fluorescein. 2.0 mg SAMSA Fluorescein were dissolved in 0.2 mL 0.1 mM NaOH and incubated for 15 min before the solution was neutralized with 10 mM HCl (0.6 mL) and buffered with PBS (0.4 mL) to obtain a solution with neutral pH. To a nanoparticle suspension of 1 mg/ mL 6.4 µmol mmol SAMSA Fluorescein was added for 45 min. The free dye was removed from the nanoparticle suspension by centrifugation (3 x, 5 min, 30000 g) and washing with 1 mL DPBS. The fluorescence of the fluorescein nanoparticles in water was recorded using a Tecan plate reader (Excitation wavelength: 495 nm and emission wavelength: 520 nm). A calibration curve of SAMSA Fluorescein in water was recorded and by fitting a linear regression the concentration of the unknown fluorescence of the polymer

samples was calculated. The maleimide surface concentration is 1.1 nmol/mg polymer nanoparticles. (**Supporting Information S3 B**).

Preparation of dye-loaded carboxylic PLA nanoparticles. Nanoparticles were prepared by slowly precipitating 1 mL of an acetone solution containing 10 mg of acid terminated polymer poly(D,L-lactid acid) together with 5 µl of a 1 mg/mL DiO solution in acetone into 2 mL DPBS. The organic solvent was removed by evaporation under reduced pressure at room temperature. Nanoparticles were washed 2 x with 2 mL DPBS and suspended in DPBS at a concentration of 1 mg/mL.

Dye encapsulation efficiency. To determine the dye encapsulation efficacy, PEG-PLA and PLA-COOH nanoparticles were washed twice with MiliQ-water, lyophilized and dissolved in DMSO at a concentration of 1 mg/mL. The fluorescence of the DMSO solution was determined using a plate reader (Tecan Infinite M200Pro). Standard fluorescence curves for and DiO: (excitation wavelength: 480 nm, emission wavelength: 520 nm) in DMSO were recorded. The unknown dye concentration of the nanoparticles dissolved in DMSO was calculated using the y-intercepts and slopes of the dye standard curves obtained by linear regression. The encapsulation efficiency was calculated by comparing the input dye concentration (500 ng dye/mg polymer) with the experimentally determined dye concentrations. The encapsulation efficiency was calculated 95 % (0.0475 weight % DiO/ mg polymer) for DiO loaded carboxylic PLA nanoparticles and 30 % for PEG-PLA nanoparticles (0.015 weight % DiO/ mg polymer). (**Supporting Information Figure S2**).

Cell culture. Jurkat cells were cultured in RPMI 1640 Medium supplemented with 10% fetal bovine serum (FBS) and 1% penicillin/streptomycin. Cells were maintained in a humidified atmosphere containing 5% (v/v) of CO_2 at 37 °C and split every 3-4 days until they reached a concentration of maximal 1 mio cells/mL in complete cell culture medium. The cells were used up to the 5th passage for the experiments described here. Encephalitogenic CD4$^+$ effector/memory proteolipid protein (PLP) peptide aa139-153 specific T cells (line SJL-PLP7) (described before [49]) were cultured in RPMI 1640 Medium supplemented with 10% fetal bovine serum (FBS), 1% non-essential amino acid, 1% Na-pyruvate, 0.4% β-mercaptoethanol and 1% IL-2 supernatant (self-made) and maintained in a

humidified atmosphere containing 5% (v/v) of CO_2 at 37 °C. Cells were used for modification and in functional assays at day 3 after restimulation (3. or 4. restimulation).

Reduction of cell surface- disulfide groups. Cells (Jurkat cells and SJL-PLP7 cells) were washed 2 x with DPBS and resuspended at a cell concentration of 15 mio/ mL in a DPBS solution containing TCEP-HCl (10 mM, pH = 7.4) and incubated for 30 min at 37 °C. After that, the cells were again washed 2 x with DPBS in order to remove the reducing agent. To monitor the reduction of the disulfide surface groups, 0.5 mio cells at a concentration of 5 mio cells/ mL were stained with 20 µM sulfo-cyanine 5 maleimide for 20 min at 4 °C, washed 2 x with DPBS and then analyzed by flow cytometry and confocal microscopy (**Supporting Information Figure S4**).

Quantification of thiol cell surface concentration. Jurkat cells were washed 2 x with DPBS and 30 mio cells at a cell concentration of 15 mio cells/ mL were incubated with 0, 0.5, 1.0, 2.5, 5.0 and 10 mM TCEP at 37 °C for 30 min. Then, the cells were washed 2 x with DPBS, resuspended in 200 µM Ellman's reagent (5,5'-dithiobis-(2-nitrobenzoic acid) (DTNB)) in DPBS and incubated for 30 min at room temperature. Subsequently, the cells were centrifuged to form a cell pellet and the absorption of the cells supernatant was measured at 412 nm. A calibration curve of the reaction of 1 mM L-cysteine with Ellman's reagent for 20 min at room temperature was recorded and the unknown cell surface thiol concentration was calculated using a linear regression curve (**Supporting Information Figure S5**).

Biotinylation of the cell surface. Cells (Jurkat cells and SJL-PLP7 cells) were washed 2 x with DPBS and resuspended at a cell concentration of 15 mio/mL in DPBS and cooled to 4 °C for 5 min. Then, 3 µL of a 5 mg/mL (10 µM) solution Biotin, XX, SSE in DPBS was added to 1 Mio cells and incubated at 4 °C for 20 min. After that cells were washed 2 x. To monitor successful cell surface modification, 0.5 mio cells at a concentration of 5 mio cells / mL were stained with 2 µM NeutrAvidin – Oregon Green 488 at 4 °C for 20 min, washed 2 x with DPBS and then analyzed by flow cytometry and confocal microscopy (**Supporting Information Figure S6**).

Cell surface immobilization of NeutrAvidin. 1 mio biotinylated cells (Jurkat cells and SJL-PLP7 cells) at a concentration of 5 mio/mL were incubated with NeutrAvidin (1.35 mg, 10 µM) in 135 µL DPBS at room temperature for 20 min and then washed twice to remove the excess protein. To monitor successful cell surface modification, 0.5 mio cells at a concentration of 5 mio cells/mL were stained with 20 µM Atto 647N-Biotin for 20 min at 4 °C, washed 2 x with DPBS and then analyzed by flow cytometry and confocal microscopy (**Supporting Information Figure S7**).

Introduction of cell surface N_3- groups by metabolic incorporation of tetraacylated N-azidoacetylmannosamine. To 25 mL of cell growth medium containing 2.5 mio cells 25 µL of a 10 mM ManNAz (N-azidoacetylmannosamine tetraacylated) solution in DMSO was added. The cells were incubated for 72 h. To confirm the successful introduction of the azido mannose, 0.5 mio cells at a concentration of 5 mio cells/mL were incubated with 20 µM Alexa Fluor 488 DBCO in DPBS for 20 min at 4 °C, washed 2 x with DPBS and then analyzed by flow cytometry and confocal microscopy (**Supporting Information Figure S8**).

Lipid insertion of DSPE-PEG2000-biotin. Cell were washed 2 x with DPBS and resuspended at a cell concentration of 15 mio cells/ mL in DPBS and incubated with DSPE-PEG200-biotin (3.3 µM/ 1 mio cells) for 20 min. The cells were washed 2 x with DPBS before nanoparticles conjugation. To monitor successful cell surface modification, 0.5 mio cells at a concentration of 5 mio cells/mL were incubated with 2 µM NeutrAvidin, Oregon Green 488 conjugate for 20 min at 4 °C, washed 2 x with DPBS and then analyzed by flow cytometry and confocal microscopy (**Supporting Information Figure S9**).

Cell surface immobilization of nanoparticles. Cells (Jurkat cells and SJL-PLP7 cells) were washed 2 x with DPBS and then suspended in DPBS at a concentration of 5 mio/mL. Modified PEG-PLA or PLA-COOH nanoparticles in DPBS (1 mg/ mL) were added to this cell suspension at the desired nanoparticles/cell ratio and incubated for 30 min at 37 °C. The nanoparticle cell mixture was mixed every 10 min to ensure a homogenous distribution of the nanoparticles. After immobilization of the nanoparticles on the cell membrane, the cells were washed 3 x with 10 mL DPBS to remove unbound nanoparticles.

Screening of conjugation chemistries. For this experiment the cell surface immobilization was performed according to the protocol above. Nanoparticles were added at an initial nanoparticle/ cell ratio of 100, 500, 1000, 2500, 5000, 10000, 25000 or 50000 to the cell suspension. Then, the cell surface decorated were prepared for apoptosis/ necrosis (cytotoxicity assay (DAPI / Annexin V viability assay) and directly analyzed with flow cytometry. Cell viabilities of nanoparticle decorated cells were determined and normalized by the viability control cell viabilities. The mean fluorescent intensities were calculated by subtracting the MFI of the unmodified control cells from the nanoparticle decorated cell MFI.

Cell viability. Viability assays were performed using Annexin V – Alexa Fluor 647 and DAPI as a dead cell stain. Briefly, unmodified or surface-modified T cells (Jurkat cells and SJL-PLP7 cells) were washed once with DPBS and 0.3 Mio cells were resuspended in Annexin buffer containing 1µg/mL DAPI at a concentration of 1 mio cells/ mL. Then, 15 µL Annexin V - Alexa Fluor 647 conjugate were added to the cell suspension and cells were incubated at room temperature for 15 minutes in the dark. Subsequently, 400 µL Annexin binding buffer was added and cells were directly analyzed by flow cytometry. As a positive control for apoptosis, T cells were incubated overnight in complete growth medium supplemented with 1 µM staurosporine. Control cells and staurosporine treated cells were used to gate cell population as follows: viable cells were gated as quadrant Q4, early apoptotic cells as quadrant Q1, late apoptotic quadrant Q2 and necrotic cells as quadrant Q3 (**Supporting Information Figure S10**).

CellTrace Violet staining. Cells (Jurkat cells and SJL-PLP7 cells) were washed 2 x with DPBS and resuspended at a concentration of 1 mio/ mL cells. Then, CellTrace violet (5 µM, 1 mg/mL in DMSO) was added to the cell suspension and incubated for 20 min. Subsequently, 30 mL cell culture medium was added for 5 min followed by a resuspension in cell culture medium and additional incubation of at least 30 min.

WGA Texas Red staining and microscopy slide preparation. To a suspension containing 0.5 million CellTrace Violet stained cells (Jurkat cells and SJL-PLP7 cells) at a concentration of 1 mio cells/ mL, 25 µL of a 1 mg /mL solution of WGA Texas red in DPBS (1.4 mM) was added. After incubation for 30 min on ice, cells were washed twice with DPBS and fixed with 4 % PFA solution in DPBS at room temperature for 20 min. After two washing

steps, the cells were resuspended at 1 mio cells/ mL in DPBS and sedimented on a poly(L-lysine) coated cover slip (diameter 12 mm) by centrifugation (200 g, 3 min). The supernatant was discarded and the cover slip mounted with mounting media (ProLong Gold Antifade Mountant) on a microscopy slide. The slides were cured for 24 h and sealed.

Flow cytometry proliferation assay. Surface decorated, CellTrace Violet-stained cells were resuspended in cell culture medium at a concentration of 0.5 mio cells / mL and incubated for 24 h. Cells were analyzed by FACS analysis both t = 0 h and after 24 h. Cell proliferation was assessed by comparison of the CellTrace violet mean fluorescence intensity at t = 0 h and after 24 h.

ICAM-1 binding assay. Standard 12 well diagnostic slides (ER-202W-CE24, ThermoFisher Scientific) were coated with a protein A solution at a concentration of 20 mg/ mL in PBS (pH 9) for 1 h at 37°C. The incubation was followed by three PBS washes and subsequently a blocking step using with 1.5% bovine serum albumin (BSA) in PBS overnight at 4°C. Wells were then washed once with PBS pH 7.4 and protein A was exposed to recombinant purified cell-adhesion molecule (100 mM) mouse ICAM-1-Fc chimera for 2 hours at 37°C and finally the wells blocked with 1.5% BSA in PBS for 30 min at room temperature and washed once with PBS before used in a binding assay. As a control DNER-Fc chimera was used instead of mouse ICAM-1-Fc chimera. For the binding assay, T cells were collected at 10 mio cells/mL in migration assay medium (MAM: DMEM, 25 mM HEPES, 5% FBS, 2% L-glutamine) and $1x10^5$ cells were added to each well and the slide was incubated for 30 minutes at room temperature on a rotating platform. The slides were finally washed twice by dipping them into PBS and fixed for 2 h in 2.5% v/v glutaraldehyde in PBS. The number of adherent cells was evaluated by counting the number of bound cells per field of view using a 20x objective mounted on an Olympus CKX41 inverted microscope equipped with a 10 mm x 10 mm /10 divisions counting reticle. Each dot in **Figure 8** represents a single cell count from the diagonal of the reticle. 3 counts per well were recorded.

Transendothelial migration (TEM) assay. Primary mouse brain microvascular endothelial cells (pMBMECs) from B6 WT mice were seeded on a 6.5 mm transwell filter (5 µm pore size) previously coated with laminin and matrigel. The cells were grown for 7 days, 2 days with puromycin. In order to prevent the pMBMECs from sprouting through the pores of the filter, they were grown to confluency without medium in the lower compartment. Prior to the experiment, pMBMECs were stimulated with the cytokine protein Interleukin 1

beta (IL-1β) (20 ng/ mL) for 12 h. At the beginning of the transmigration assay, pMBMEC inserts were washed twice with migration assay medium (MAM: DMEM, 2 % L-Glutamine, 25 mM HEPES 5 % FBS) before being transferred into a new 24-well Costar plate well containing 600 µL MAM. Then, 100 µL MAM containing 100000 nanoparticle- decorated SJL-PLP7 T cells were added per insert and T cells were allowed to transmigrate for 6 h at 37 °C. Additionally, aliquots of $1x10^5$ T cells were kept in MAM and used as representative for the input. The number of transmigrated T cells and the number of the cells in the input samples were assessed by flow cytometry. The percentage of migrated T cells was calculated referring to the input as 100 %. Finally, the inserts were washed twice in PBS and fixed in 37 % PFA for 2 h. Fixed inserts were blocked 20 min in blocking buffer, stained for 1 h at room temperature with Rhodamine Phalloidin (stock solution in 1.5 mL methanol, 1 : 200) and CD45 biotin (1:50, 10 µg/mL). After 3 washing steps with PBS, Streptavidin-Cy 5 (1: 100, 15 µg/mL) was added for 1 h at RT. Then the filters were washed again with PBS and the cell nuclei were stained with DAPI in blocking buffer (1: 2000, 0.5 ng/mL). The inserts were mounted with Mowiol on glass slides and the confluency of the endothelial monolayer was confirmed with immunofluorescence microscopy imaging of each filter after each assay.

3.3. Results and Discussion

As a model system to illustrate the impact of various surface conjugation chemistries on the viability and functional properties of cell based carrier, this study uses blood-brain barrier migratory T cells that will be modified with PLA nanoparticles displaying a range of cell surface reactive chemistries. Jurkat cells are an immortalized cell line that is used as model T lymphocytes. T lymphocytes are non-phagocytic cells with minimal risk of particle internalization making them ideal candidates to study cell surface modification with nanoparticles. SJL-PLP 7 is a PLP- (proteolipid protein) specific cell line which is used to study inflammatory T cell infiltration of the central nervous system. In this work, mice SJL-PLP 7 cells serve as proof of concept study of cell-mediated nanoparticle delivery across an endothelial cell barrier. **Figure 1** provides an overview of the different surface functionalities present on the nanoparticles and subsequent cell surface conjugation chemistries that will be explored. Nanoparticles will be immobilized using both covalent and non-covalent strategies. Three covalent cell surface conjugation chemistries that will be assessed. First, active ester functionalized PLA nanoparticles which react with cell surface amino groups (**Figure 1 A**).

Second, maleimide functionalized PLA nanoparticles that can modify thiol groups present on the cell surface (**Figure 1 B**). Third, bioorthogonal strain promoted azide alkyne cycloaddition of alkyne functionalized nanoparticles which can react with cell surfaces that present azido groups (**Figure 1 C**). In addition to the three covalent strategies, four non-covalent cell surface conjugation chemistries that will be examined. First, the binding of WGA modified nanoparticles to N-acetylglucosamine and sialic acid present on the cell surface (**Figure 1 D**). Second, the electrostatic association of negatively charged PLA nanoparticles (**Figure 1 E**). Fourth, the immobilization of PLA nanoparticles using biotin – NeutrAvidin interactions, by either using biotin molecules that are covalently coupled to the cell surface amino groups (**Figure 1 F**) or by non-covalent insertion of biotin- functionalized PEGylated lipids (**Figure 1 G**). The binding of negatively charged nanoparticles to cell surfaces can be driven by two mechanisms. First, nanoparticle attachment to the cell membrane can result from electrostatic interactions between the negatively charged nanoparticles and cationic sites on the cell membrane.[50-52] A second mechanism that may help to drive the adsorption of negatively charged nanoparticles onto the cell membrane is entropy gain-driven depletion.[53-55]

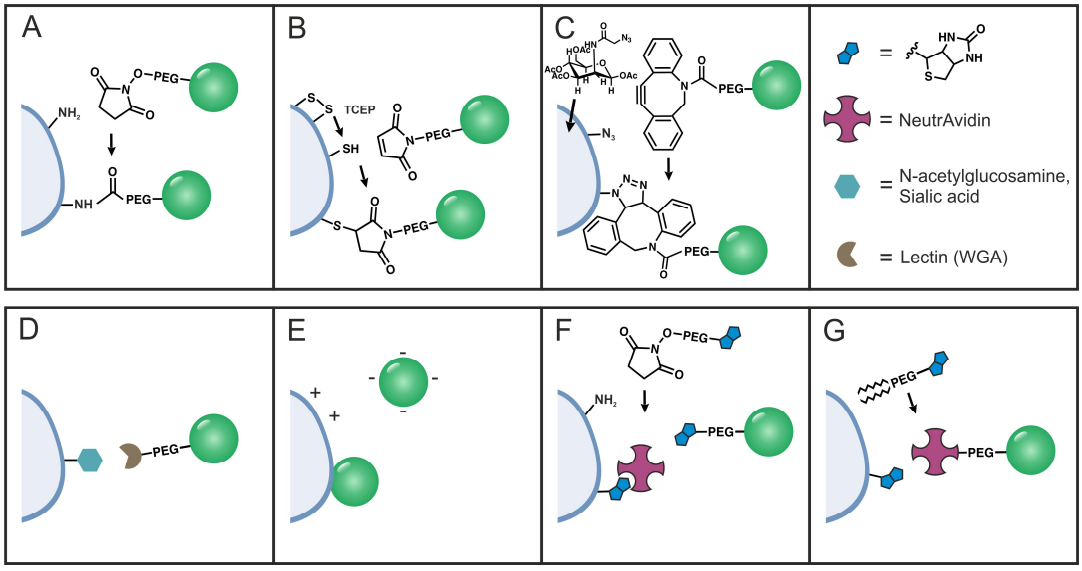

Figure 1: Nanoparticles can be immobilized on cell surfaces using various covalent and non-covalent conjugation chemistries. Direct covalent bonds in between the cell membrane and the nanoparticle can be created by the reaction of an active ester with surface amino-groups (A), the coupling of maleimide nanoparticles with thiol groups (B) or the click reaction between a non-native azido group and ring-strained cyclooctene modified nanoparticles (C).

Direct non-covalent NP immobilization strategies include the binding of lectin nanoparticles to carbohydrates in the glycocalyx (D) and the electrostatic adsorption of negatively charged nanoparticles (E). Furthermore, the cell surface can be covalently modified with a biotin reagent by e.g. an activated ester prior to receptor –ligand conjugation of NeutrAvidin nanoparticles to the cell surface (F). The cell surface can also be modified non-covalently by insertion of a lipid linked biotin moiety before binding of NeutrAvidin nanoparticles to the cell surface (G).

3.3.1. Nanoparticle preparation and modification

All PLA nanoparticles were prepared via nanoprecipitation. NHS ester (**Scheme 1, (1)**), maleimide (**Scheme 1, (3)**), DBCO (**Scheme 1, (4)**), WGA (**Scheme 1, (2)**), biotin (**Scheme 1, (5)**) and NeutrAvidin (**Scheme 1, (6)**) functionalized PLA nanoparticles were obtained via modification of amino- functionalized nanoparticles. Amino functionalized nanoparticles were obtained by co-precipitation with equal amounts of PLA and PLA-PEG-NH_2 and loaded (if needed) with green fluorescent DiO to facilitate analysis by flow cytometry and confocal microscopy. Nanoparticle hydrodynamic diameter, zeta-potential and morphology was analyzed by dynamic light scattering (DLS) and transmission electron microscopy (TEM) (**Figure 2**). TEM illustrates the spherical morphology of the PEG-PLA nanoparticle showing a heterogeneous size distribution with an average diameter of 130 ± 36 nm based on analyzing 183 nanoparticles in total (**Figure 2 A and B**). The hydrodynamic diameter of 185.7 ± 3.5 nm and a PDI of 0.1 was obtained by DLS for PEG-PLA nanoparticles. Loading of the nanoparticles with 0.015 weight % DiO/ mg polymer (encapsulation efficiency 30 %) led to minor changes in the hydrodynamic radius and the PDI increasing from 0.6 to 0.8 (**Supporting Information Figure S11**). The composition of lyophilized PEG-PLA nanoparticles was determined by ^{1}H-NMR spectroscopy. The methyl peak present at ~5.3 ppm from the protons of PLA and PLA-PEG was normalized and compared with signal of the four methylene protons of PLA-PEG at ~3.7 ppm (**Supporting Information Figure S2 A**). Considering the ratio of repeating units of PEG to PLA, the relative amount of PLA-PEG in the blend of PLA homopolymer and PLA-PEG copolymer was estimated. The nanoparticles contain 7.5 mol % PLA-PEG which represents only a small fraction of the copolymer used in the preparation. The surface concentration of NH_2 groups of these PLA nanoparticles was determined by reacting the nanoparticles with NHS-

Fluorescein (5- (and 6-) carboxyfluorescein succinimidyl ester) and estimated to 1.2 nmol/ mg (**Supporting Information Figure S3 B**). Negatively charged PLA nanoparticles (**Figure 1 E**) were obtained by precipitation of an acetone solution containing PLA-COOH in DPBS. A hydrodynamic diameter of 205.3 ± 1.3, a PDI of 1.7 and a zeta-potential of -30.4 mV was measured with DLS. The encapsulation of 0.0475 weight % DiO/mg polymer (encapsulation efficiency 95 %) did not alter the nanoparticle size or size distribution (**Figure 2 C**). Nanoparticles that were used in the experiments that involve flow cytometry/confocal microcopy were loaded with DiO.

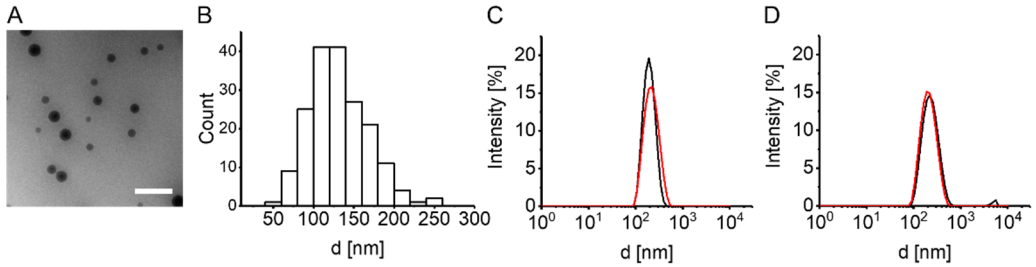

Figure 2: Characterization of amine functionalized PEG-PLA and carboxylic PLA nanoparticles. A: TEM image of PEG-PLA nanoparticles. B: Histogram of size distribution determined by the evaluation of 183 nanoparticles from TEM images. The scale bar represents 500 nm. C and D: Nanoparticle characterization using intensity-weighted distribution of hydrodynamic nanoparticle diameters of PEG-PLA nanoparticles (C) and PLA-COOH nanoparticles (D). In black the distribution of plain nanoparticles are shown and in red nanoparticles encapsulating DiO. The data is expressed as average of 3 measurements (C and D).

To introduce cell surface reactive NHS (**Figure 1 A**), maleimide (**Figure 1 B**), DBCO (**Figure 1 C**), WGA (**Figure 1 D**), biotin (**Figure 1 F**) or NeutrAvidin (**Figure 1 G**), the NH_2 functionalized nanoparticles were modified as shown in **Scheme 1**. Therefore nanoparticle surface reactions were performed by treatment of the NH_2 nanoparticles with the representative (sulfo) NHS reagent, eventually followed by supplemental coupling of WGA or NeutrAvidin, if needed. The surface modified nanoparticles were analyzed by DLS and zeta-potential (**Supporting Information Figure S11**). These analyses demonstrated that the variety of nanoparticles surface modification or DiO loading did not significantly change nanoparticle size, PDIs or zeta-potentials. Only DBCO and NeutrAvidin modified nanoparticles showed a slight increase in hydrodynamic diameter and PDI. However, this small change could be due to an increase in surface hydrophobicity of the nanoparticles.

Maleimide functionalized nanoparticles were further analyzed by the addition of a thiol modified fluorescein (SAMSA Fluorescein) to the nanoparticle suspension in water. The unknown fluorescein concentration was determined by comparison with a calibration curve of SAMSA fluorescein in water and a maleimide concentration of 1.1 nmol/mg nanoparticles was determined. The conversion of the reaction with Sulfo-SMCC can be considered as quantitative (**Supporting Information Figure S3 B**).

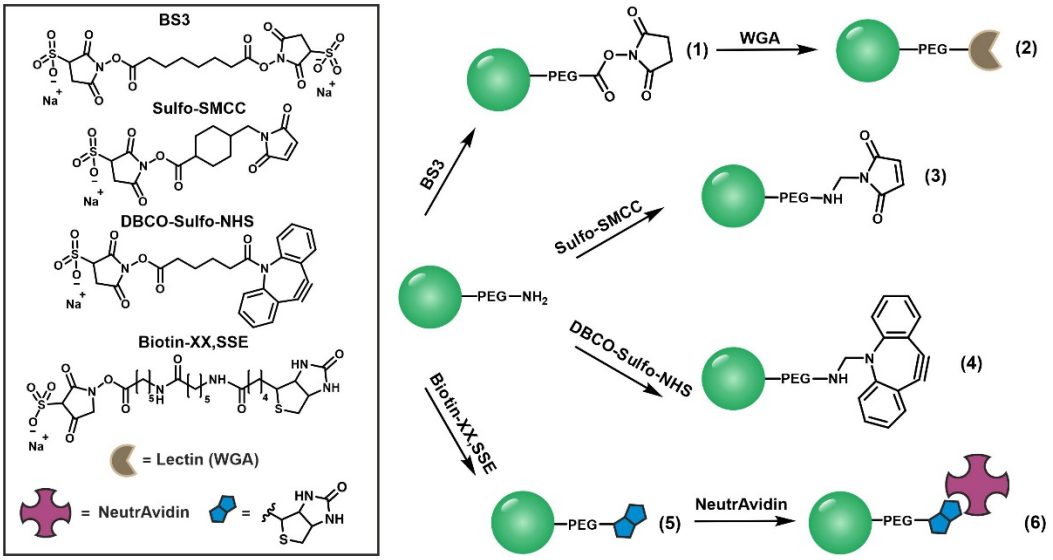

Scheme 1: Surface modification of PEGylated amine functionalized PLA nanoparticles with active ester containing ligands. NHS ester functionalization (1) and if needed WGA modification (2). Introduction of maleimide (3), DBCO (4), biotin (5) or NeutrAvidin (6) functionalities.

3.3.2. Nanoparticle conjugation to the cell surface

A number of the nanoparticle immobilization strategies summarized in **Figure 1** require pre-activation or pre-modification of the cell surface. To increase the number of free surface thiol groups, cells to be reacted with maleimide nanoparticles were activated with TCEP. With increasing TCEP concentration the concentration of surface thiols increases, up to a two-fold increase for cells treated with 10 mM TCEP compared to control cells (**Supporting Information Figure S5**). Higher concentrations of TCEP were not tested due to cellular toxicity.[56] The strain- promoted cycloaddition of alkyne nanoparticles to the cell surface requires cell surface bound N_3 groups, which were introduced via metabolic glycoengineering. Finally, biotin was introduced to the cell surface either by NHS coupling

or non-covalent insertion of biotin functionalized PEG lipids. Cell surface modification was analyzed qualitatively via flow cytometry and confocal microscopy (**Supporting Information S4, S6 - S9**). The surfaces of modified cells were stained with a reactive dye whereas, the control cells didn't show any fluorescence. The dye is located in the cell membrane and not internalized as shown by intensity profiles. Only NeutrAvidin modified cells show slight internalization of the fluorescent dye (**Supporting Information Figure S7**). In a final series of experiments, the variety of covalent and non-covalent conjugation chemistries that are illustrated in **Figure 1** were compared using flow cytometry. Cells were incubated with differently functionalized nanoparticles at a variety of nanoparticle/cell ratios ranging from 100 to 50000. The resulting modified cells were subsequently analyzed by flow cytometry. By monitoring the nanoparticle associated fluorescence, the extent of the nanoparticle conjugation on the cell surface could be quantified. In these fluorescence screening experiments the nanoparticle associated fluorescence observed in flow cytometry was taken as an indirect measure of the nanoparticle cell surface concentration. The viability of the nanoparticle decorated cells was analyzed by an apoptosis/necrosis (cytotoxicity assay (DAPI / Annexin V viability assay). In order to analyze the cell viability at the same time using flow cytometry, nanoparticle- modified cells were incubated with DAPI and Annexin V – Alexa Fluor 647 directly after the nanoparticle immobilization. These experiments were performed both with Jurkat as well as SJL-PLP7 cells. **Figure 3 A and 3 B** summarize the results for the Jurkat cell. At a given nanoparticle/cell ratio, non-covalent nanoparticle coupling strategies result in more pronounced shifts in nanoparticle- associated fluorescence as compared to the covalent chemistries (**Figure 3 A**). NHS ester modified nanoparticles shows the least prominent binding to cell surfaces, followed by maleimide nanoparticles and DBCO nanoparticles. Conjugation of maleimide functionalized nanoparticles could be significantly enhanced by pretreating the Jurkat cells with TCEP, which reduces surface disulfides and increases the concentration of available surface thiol groups. For all conjugation chemistries, increased nanoparticle/cell ratios led to increased nanoparticle-associated fluorescence, indicating that the nanoparticle cell surface concentration can be tuned simply by adjusting the nanoparticle/cell ratio. The most efficient surface decoration of cells, especially in the case of Jurkat cells, was non-covalent immobilization of nanoparticles via lectin modified WGA PEG-PLA nanoparticles. WGA interacts with the carbohydrates N-acetylglucosamine and sialic acid which are abundant in the cell's glycocalyx. NeutrAvidin nanoparticles can be immobilized on cells which were pretreated with a biotinylation agent. A biotin moiety can be introduced by lipid insertion of a biotin modified DSPE (**Figure 3 A, c (green)**) or by the covalent conjugation of activated ester

biotin (**Figure 3 A, d (blue)**). By comparison, the highest number of nanoparticles/ cell in d is reached with the highest initial ratio of 50000 nanoparticles/cell, whereas for c the maximum is reached with an initial ratio of 10000 nanoparticles/cell and decreases with increasing nanoparticle concentration.

Most nanoparticle conjugation chemistries did not significantly affect the viability of the Jurkat cells, including the highest nanoparticle/cell ratios (**Figure 3 B**). Exceptions are when NeutrAvidin and WGA nanoparticles were used and the cell viability decreased to 50 % at very high nanoparticle/ cell ratio. A too high nanoparticle coverage is toxic for the cells. The precise mechanism that impairs cell viability is unknown however, it is possible the nanoparticles are covering to great of cell surface area, preventing critical functions.

The results obtained with the SJL-PLP7 cells are summarized in **Figure 3 C and 3 D**. Since the coupling of NHS ester and DBCO modified nanoparticles did not present to be effective on Jurkat cells, this approach was not assessed on SJL-PLP 7 cells. The conjugation of biotin nanoparticles to NeutrAvidin modified cells was chosen as example for the biotin-NeutrAvidin interaction. The results of the surface modification experiments with SJL-PLP 7 cells confirm the results obtained with the Jurkat cells, further illustrating nanoparticle surface concentration can be controlled by tuning the initial nanoparticle/cell ratio. For the SJL-PLP 7 cells, pretreating cells with TCEP is an important to enhance the coupling of the maleimide nanoparticles. In comparison to Jurkat cells, viability assays indicate SJL-PLP 7 cells are more sensitive to nanoparticle conjugation, results in lower overall viability. For most immobilization strategies a decrease in the cell viability of the SJL-PLP 7 cells was observed at nanoparticle/cell ratio over 5000 nanoparticles/cell. Especially NeutrAvidin modified nanoparticles have a negative impact on cell viability. The cell viabilities decrease to ~ 20 % at high nanoparticle/cell feed ratios.

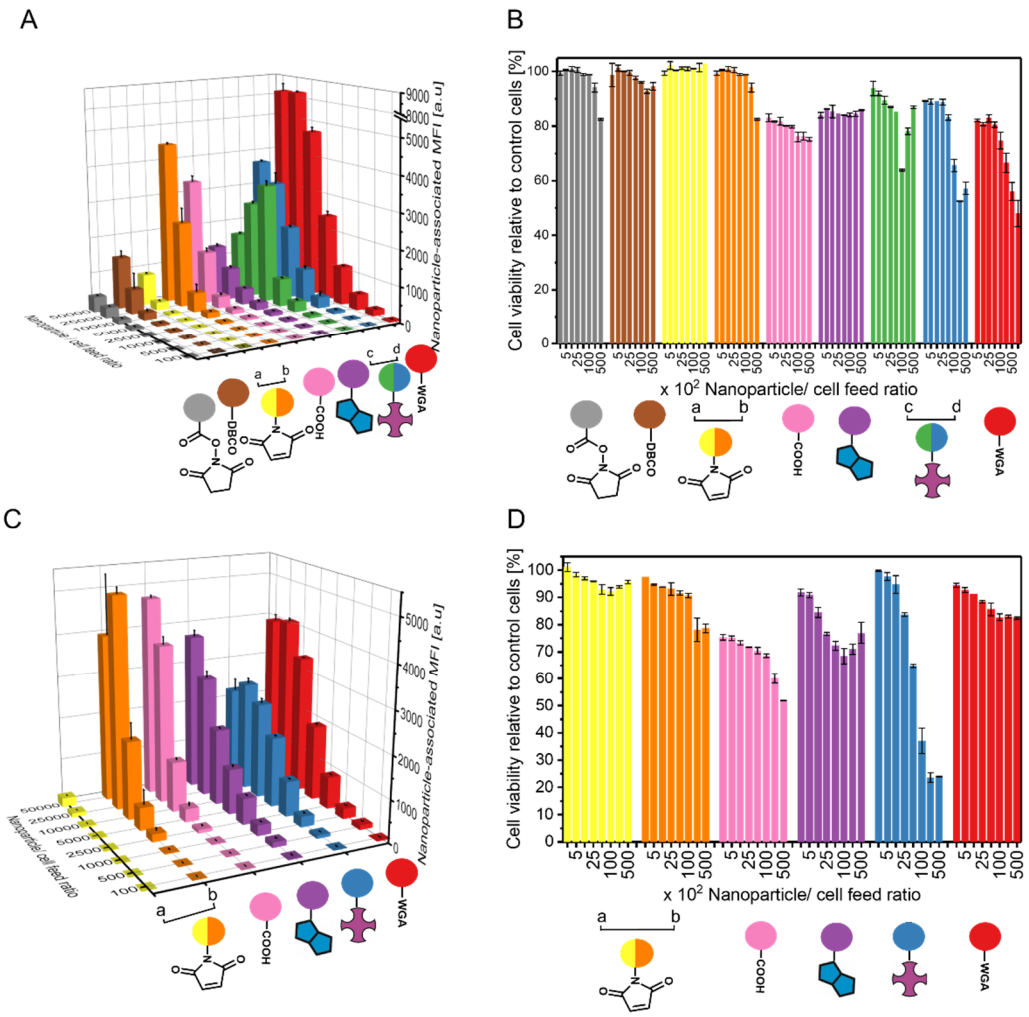

Figure 3: Nanoparticle-associated fluorescence and cell viabilities of nanoparticle decorated Jurkat cells (A and B) and SJL-PLP7 cells (C and D) obtained by flow cytometry. The cells were incubated with an initial nanoparticle/cell feed ratio of 100, 500, 1000, 2500, 5000, 10000, 25000 and 50000 nanoparticles with various functionalities. NHS ester PEG-PLA functionalized nanoparticles are shown in grey, DBCO PEG-PLA nanoparticles in brown, maleimide PEG-PLA nanoparticles in yellow/ orange, PLA-COOH nanoparticles in pink, biotin PEG-PLA nanoparticles in violet, NeutrAvidin modified PEG-PLA nanoparticles in blue / green and WGA functionalized PEG-PLA nanoparticles are shown in red. Data are expressed as mean ± SD (n = 2).

From the different nanoparticles immobilization chemistries that were screened in the initial experiments, 4 were selected and investigated in more detail. This second series of experiments was carried with maleimide, biotin, WGA and COOH nanoparticles. The aim of these experiments was to quantitatively study the conjugation and localization of the nanoparticles on the cell surface and to compare the proliferation and functional properties of T-cell decoration with nanoparticles using those different chemistries.

3.3.3. Detailed analysis of nanoparticle-modified cells

From the different nanoparticles immobilization chemistries that were screened in the initial experiments, 4 were selected and investigated in more detail. This second series of experiments was carried with maleimide, biotin, WGA and COOH nanoparticles. The aim of these experiments was to quantitatively study the conjugation and localization of the nanoparticles on the cell surface and to compare the proliferation and functional properties of T-cell decoration with nanoparticles using those different chemistries.

The conjugation and localization of the nanoparticles at the cell surface was investigated with confocal microscopy. These experiments were carried out with Jurkat T cells that were modified with DiO labeled nanoparticles at an initial nanoparticle/ cell ratio of 500, 2500 and 5000. For confocal microscopy analysis, cells were stained with CellTrace Violet to visualize the cell cytosol and with WGA Texas Red to label the cell membrane. Z-stacks of single cells were recorded and the individual images were compiled to generate a 3D reconstruction. The results of this analysis are shown in **Figure 4** and **Figure 5**. **Figure 4** shows representative confocal images of Jurkat cells modified with the 4 different nanoparticles at nanoparticles/cell ratios of 500, 2500 and 5000. In those images the nanoparticles can be clearly identified as green fluorescent spots. The number of nanoparticles per cells was analyzed using the spot identification tool of Imaris. For each of the nanoparticle immobilization chemistries investigated, the nanoparticle cell surface coverage was found to increase with increasing the initial nanoparticle/cell ratio, confirming the flow cytometry results. Nanoparticle cell surface concentration was relatively high for biotin and WGA nanoparticles (154 ± 45) respectively (76 ± 44) at 5000. Maleimide modified nanoparticle couple results in fewer particles being attached to the cells approximately (76 ± 37) for untreated cells and (104 ± 65) cells pretreated with TCEP. Although the pretreatment of cells with a reducing agent such as TCEP increases the number of available thiol groups by a factor of 2 and enhances the nanoparticle-associated mean fluorescent intensity 7 fold

(at a NP/ cell ratio of 5000), the determined average number of nanoparticles represents only a slight increase. The source of this discrepancy is unknown. The immobilization of COOH nanoparticles leads to a comparable nanoparticle surface coverage for maleimide nanoparticles. At a nanoparticle/cell feed ratio of 5000 the nanoparticle surface concentration of biotin nanoparticles is comparable to the nanoparticles surface concentration of WGA nanoparticles. The affinity of WGA to cell surface carbohydrates is weaker than biotin/streptavidin. Thus, higher nanoparticle excesses are required to achieve comparable nanoparticle loading. The interaction of biotin nanoparticles with NeutrAvidin modified cells is characterized by a high affinity which leads to an efficient nanoparticle immobilization. In addition to the quantitative determination of the surface concentration of the nanoparticles, the images were analyzed with Imaris and distance maps were created. The distance maps provide the localization of nanoparticles with respect to the cell body and cell membrane. The results of these analyses are summarized in **Figure 5**. For all nanoparticle modified cells the increase of nanoparticles/cell in the feed resulted in increased number of nanoparticles located further from the cell body (WGA negative nanoparticles, black spots). This is possibly due to nanoparticles interacting with each other. Maleimide nanoparticles modified cells (**Figure 5 A**) show only negligible amounts of nanoparticle internalization, whereas after the surface pretreatment with TCEP more nanoparticles are internalized by the cells (**Figure 5 B**). The fraction nanoparticles colocalizing with WGA Texas Red decreases with increased nanoparticle/ cell ratio for maleimide nanoparticles (**Supporting Information Figure S12**). The colocalization of maleimide nanoparticles with the cell membrane of TCEP treated cells is decreasing with higher increasing nanoparticles/ cell feed ratios; at an initial nanoparticle/ cell ratio of 500 90 % of all nanoparticles are positive for the membrane stain, at 2500 it reduces to 71 % and further to 60 % at 5000 nanoparticles/ cell. Also for COOH nanoparticle modified cells, nanoparticles internalization was observed. In contrast to maleimide nanoparticles, the fraction of WGA Texas Red positive cells increased with increasing nanoparticle/ cell feed ratios. Biotin and WGA nanoparticles are located mostly in the cell membrane with WGA Texas Red colocalization of more than 90 % for both chemistries and all ratios (**Supporting Information Figure S12**) indicating a high specificity of the nanoparticle binding to the cell membrane.

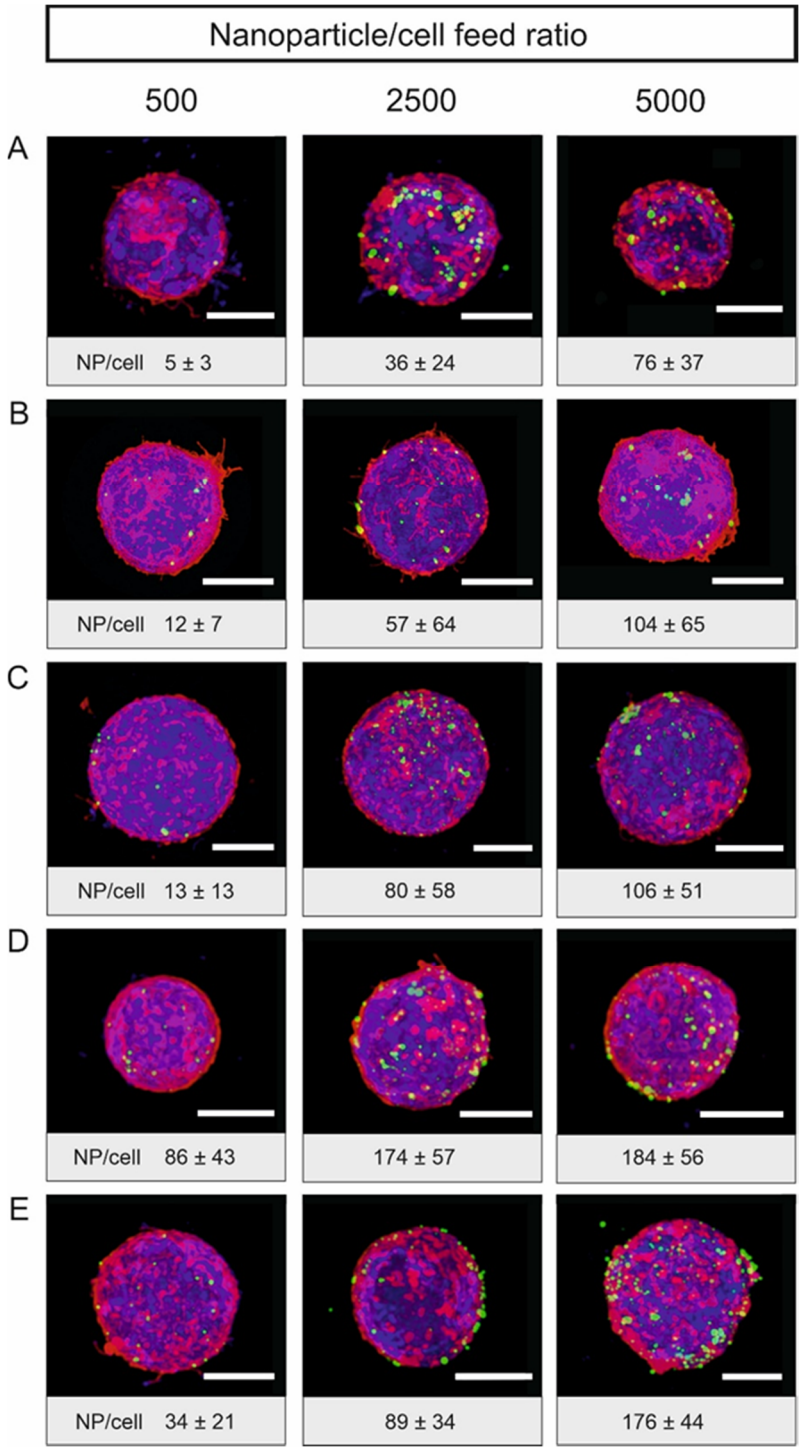

Figure 4: Confocal laser scanning microscopy images of surface engineered Jurkat T cells which were incubated with an increasing NP/cell ratio, i.e. 500, 2500 and 5000 NP / cell feed ratio. A) Unmodified cell surface and maleimide PEG-PLA nanoparticles, B) TCEP- treated cells and maleimide PEG-PLA nanoparticles, C) PLA-COOH nanoparticles, D) biotin PEG-PLA nanoparticles and E) WGA PEG-PLA nanoparticles. The cell cytosol shown in blue was stained with CellTrace violet and the membrane which is shown in red was stained with

WGA Texas Red. Nanoparticles encapsulate the green dye DiO. The average number of nanoparticles per condition were calculated over at least 10 different cells. The scale bars represent 5 µm.

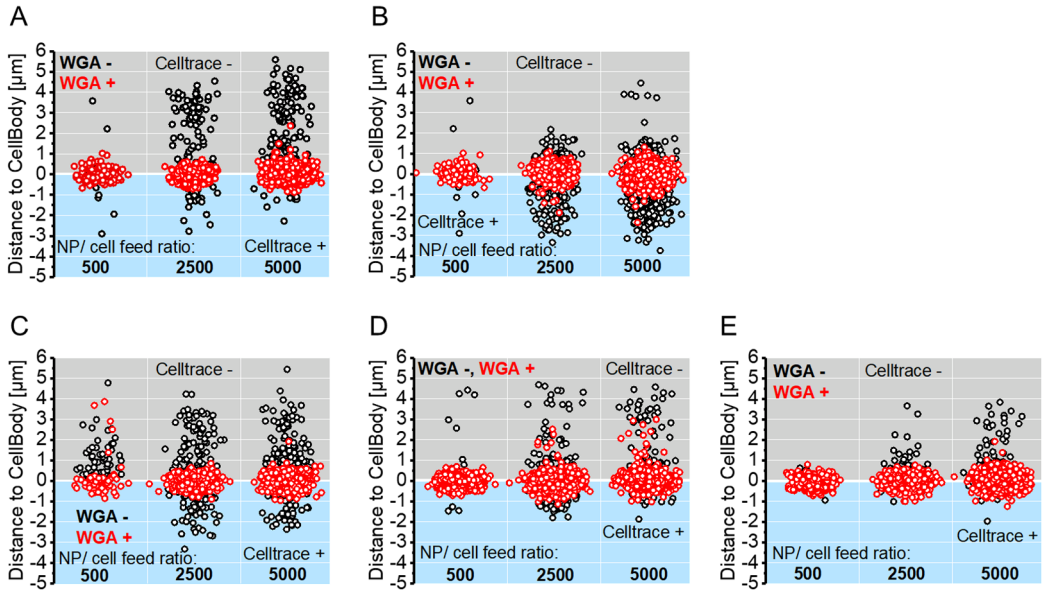

Figure 5: Distance analysis of nanoparticle distribution from the CellBody. Statistical distribution of nanoparticles on at least 10 cells with respect to their distance to the whole cell edge (CellTrace Violet). Each dot represents a single nanoparticle. Red dots represent nanoparticles which are found between the inner and outer boundaries outlined by the membrane staining (WGA Texas Red X) and black dots those which are not. Cells decorated maleimide PEG-PLA nanoparticles without pretreatment (A) and pretreatment with TCEP (B), carboxylic PLA nanoparticles (C), biotin PEG-PLA nanoparticles (D) or PEG-PLA lectin nanoparticles (E) initial nanoparticle/ cell feed ratio of 500, 2500 and 5000.

In a next series of experiments, the proliferation of Jurkat T cells decorated with maleimide functionalized, COOH, biotin and WGA functionalized nanoparticles was compared with that of unmodified Jurkat cells. These experiments were carried out with cell that were modified with nanoparticles at initial nanoparticle/ cell ratio of 500, 2500 and 5000. Proliferation was analyzed by flow cytometry by staining cells with CellTrace Violet and compare the CellTrace Violet associated fluoresce directly after cell surface modification and after 24 h. **Figure 6** compares the proliferation of unmodified cells with that of the modified cells. Control cells have a proliferation rate of ~ 2 over 24 h. TCEP treated and maleimide

nanoparticle modified cells show a slight increase in proliferation and NeutrAvidin modified and biotin nanoparticles decorated cells show a slight decrease in proliferation. This effects might be caused by the cell pretreatment because no change in proliferation can be observed with increasing number of nanoparticles per cell.

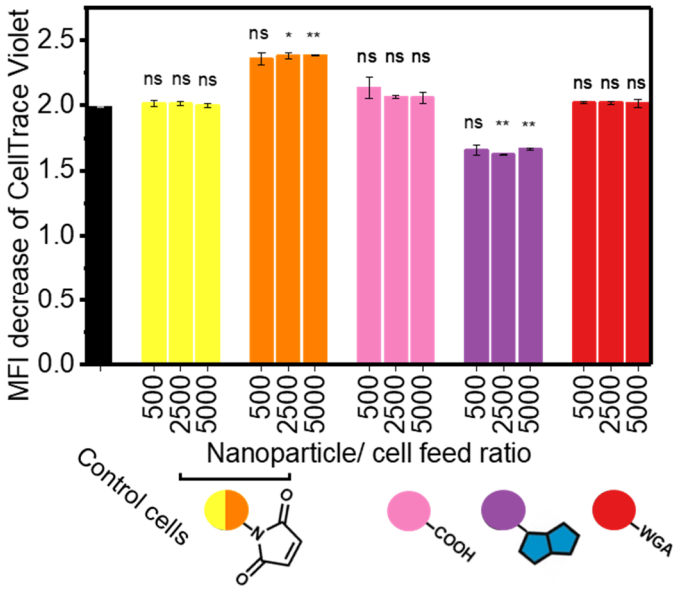

Figure 6: Mean fluorescence intensity (MFI) decrease of CellTrace violet stained Jurkat T cells to obtain the cell proliferation. Control cells are illustrated in black, maleimide nanoparticle decorated cells in yellow, maleimide nanoparticle decorated cells with TCEP pretreatment in orange, COOH nanoparticle decorated cells in pink, biotin nanoparticles decorated cells in violet and WGA nanoparticle decorated cells in red. The cells were decorated with functionalized nanoparticles using a nanoparticle/ cell feed ratio of 500, 2500 and 5000 nanoparticles/cell. P-values were determined by a two-tailed t- test: ns= not significant, *= $P \leq 0.05$ and **= $P \leq 0.01$. Data are expressed as mean ± SD (n = 2).

Figure 7 A and B shows the analysis of biotin nanoparticle modified cells at an initial ratio of 5000 nanoparticles/cell using SJL-PLP 7 cells. The average number of nanoparticles/cell and nanoparticles distributions indicates that SJL-PLP7 cells can be decorated with nanoparticles similar to Jurkat cells shown above. Only 48 % of all nanoparticle colocalize with the membrane stain WGA Texas Red and more internalization than for Jurkat cell has been observed. The decrease of the CellTrace Violet mean fluorescent intensity of biotin, COOH and WGA nanoparticle modified SJL-PLP 7 cells suggest a

proliferation rate of 1.6 compared to the proliferation rate of 1.7 for control cells and suggest no impairment of cell proliferation in a time period of 24 h.

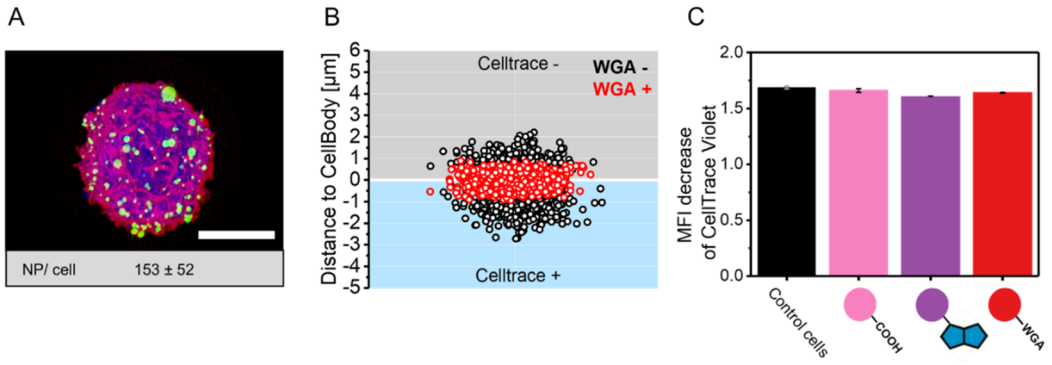

Figure 7: Analysis of SJL-PLP 7 surface decorated cells. A and B: SJL-PLP 7 cells which were modified with NeutrAvidin and decorated with biotin nanoparticles at an initial feed ratio of 5000 nanoparticles/ cell. A: Representative confocal microscopy image. The cell cytosol shown in blue was stained with CellTrace violet and the membrane which is shown in red was stained with WGA Texas Red, the green nanoparticles are loaded with DiO. An average nanoparticles decoration of 153 ± 52 nanoparticle/cell was calculated over 11 z-stacks. The scale bar represents 5 µm. B: Nanoparticles localization with reference to the cell body and the cell membrane. Nanoparticles which colocalize with the cell membrane are shown as red dots (WGA +) and nanoparticles which do not colocalize with the cell membrane stain are shown as black spheres (WGA -). C: Cell proliferation during 24 h of control SJL-PLP 7 cells (black), COOH nanoparticle decorated cells (rose), biotin nanoparticles decorated cells (violet) and WGA nanoparticle modified cells (red) analyzed by a CellTrace Violet proliferation assay.

To study the influence of nanoparticle cell surface modification on the functional properties of cells, SJL-PLP 7 cells were used. This subset of T cell was chosen as it possesses blood-brain barrier migratory properties, which makes these cells of potential interest for the cell mediated delivery of nanomedicines to the central nervous system. The blood-brain barrier migratory properties of the SJL-PLP 7 cells were evaluated in 2 experiments. In a first experiment, the binding of unmodified SJL-PLP 7 cells and SJL-PLP 7 cells that were modified with maleimide, COOH, biotin and WGA nanoparticles at an initial nanoparticle/cell ratio of 5000 to the protein ICAM-1 was evaluated. ICAM-1 was selected as it has been identified as a critical adhesion molecule that mediates T cell polarization and crawling in the extravasation of $CD4^+$ T cells across the blood-brain barrier.[57, 58] T cell

binding to ICAM-1 was assessed by immobilization the protein on glass substrate and comparing the number of adhered cells. As a control experiment to validate that the binding is ICAM-1 specific, cells were also presented to substrates that were modified with DNER. The ICAM-1 binding properties of the nanoparticle decorated cells are summarized in **Figure 8**. The data in **Figure 8** show that ICAM-1 binding is not impaired by the presence of the nanoparticle payload on the cell surfaces, irrespective of the immobilization chemistry used. Some cells, most notably these that were modified with biotin or WGA nanoparticles even show an increased ICAM-1 biding as compared to the unmodified control cells. All cells, however, both unmodified control and nanoparticle decorated cells show negligible binding to DNER coated substrates, illustrating that binding of the cells is ICAM-1 selective.

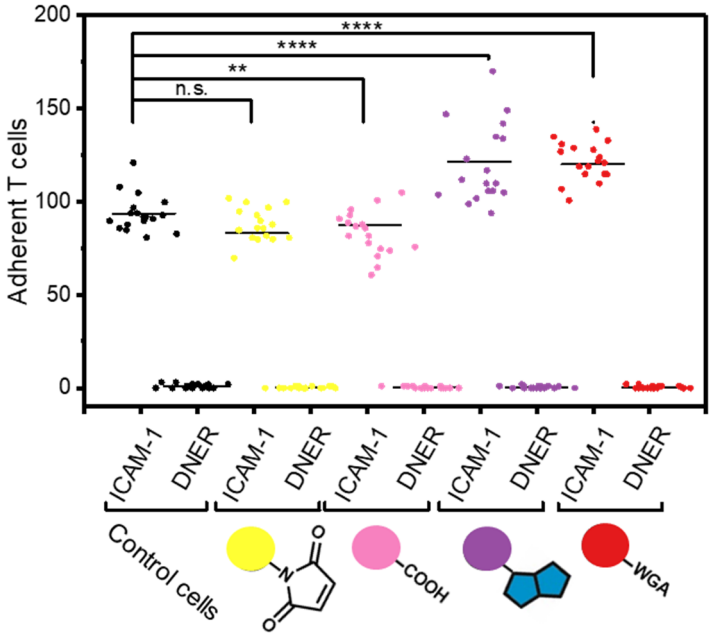

Figure 8: SJL-PLP 7 T-Cell binding to ICAM-1. Cell count of a binding assay on ICAM-1 coated wells and DNER coated wells for unmodified control cells and nanoparticle decorated T cells (using 5000 NP / cell) immobilized with different chemistries performed at room temperature for 30 minutes under moderate shear conditions. Each dot represents one cell count from the diagonal of a 10 nm x 10 nm/10 divisions counting reticle using a 20x objective. The figures represent the results of two independent assays performed in triplicate. Each well was counted at 3 different positions. The horizontal bar represents the mean over all counts. P-values were determined by a t test: COOH: $P < 0.01$, Mal: $P > 0.05$, WGA: $P < 0.001$ and Biotin: $P < 0.001$.

Next, the blood-brain barrier migratory behavior of the nanoparticle modified cells was studied *in vitro* with a TEM assay (**Figure 9 A**). The TEM assay investigates migration of the T cells under static conditions across a monolayer of pMBMEC cells (primary mouse brain microvascular endothelial cells) that have been grown onto a porous substrate. This model was used because it retains some BBB characteristics such as complex tight junctions and low permeability. To imitate an inflammation and to increase the number of cells transmigrating, the endothelial cell layer was stimulated 16 h prior to the experiment. The addition of Il-1 beta increases the level of adhesion molecules such as ICAM-1 and mimics an inflamed BBB. These experiments were carried out with SJL-PLP 7 cells T cells that were modified with maleimide (T cells were pretreated with TCEP), COOH, biotin and WGA nanoparticles at a nanoparticle/ cell ratio of 5000. As a control non-modified SJL-PLP 7 cells were used. **Figure 9 B** shows the % of transmigrated cells/ relative to the input as determined by flow cytometry. Each symbol represents a single condition of a set of triplicates showing that the ratio of transmigrated within one experiment is relatively consistent but can spread in between different experiments. A transmigration rate between 2 % and 60 % has been observed. A non-confluent pMBMEC monolayer could be a reason for the big transmigration variance. However, when comparing the ratio of modified T cells with unmodified control T cells of the same experiment, it shows that cell surface modification with COOH, biotin and WGA nanoparticles does not have a big impact on the fraction of T cells transmigrating across the pMBMEC monolayer. The treatment of T cells with TCEP and surface conjugation of maleimide nanoparticles leads to a significant decrease of T cell migration in comparison to the control cells.

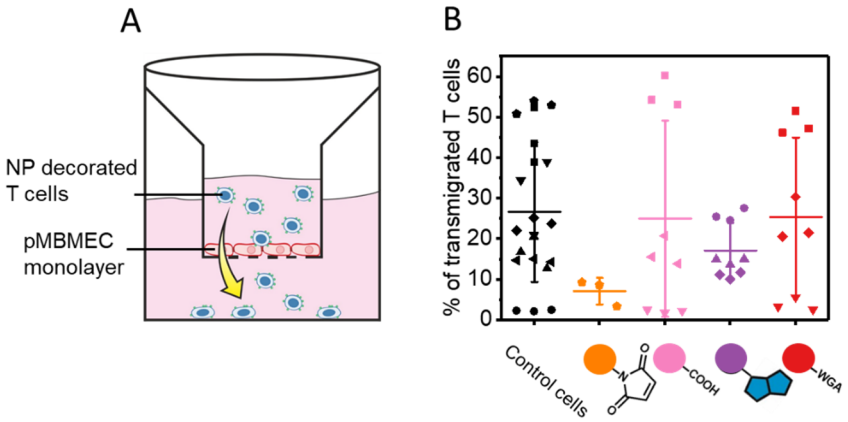

Figure 9: A) Scheme of transendothelial migration assay (TEM) set-up. The cell layer is made of stimulated primary mouse brain microvascular endothelial cells (pMBMECs) on porous filter inserts. 100 000 cells decorated with nanoparticles (NP / cell feed ratio of 5000)

were added for a transmigration time of 6 h. B) FACS analysis of % of T cells transmigrated for control cells and cell modified with biotin, WGA, COOH or maleimide nanoparticles. The plot present the results of three independent experiments performed in triplicate and the error bars are standard deviations.

In addition to quantify the total number of cells that migrate across the pMBMEC monolayer, flow cytometry analysis also allows to determine the fraction of transmigrated cells that carry a nanoparticle payload and to assess a possible loss of nanoparticles. For the biotin, WGA, COOH and maleimide nanoparticle functionalized cells that were studied in the TEM experiments. **Supplementary Figure S13** compares for the different immobilization chemistries, the nanoparticle associated fluorescence of the transmigrated cells with the one of the input cells, which is taken as a measure for the extend of nanoparticle loss from the cell surface during migration. Flow cytometry histograms illustrate that cells which were modified with maleimide, COOH or WGA nanoparticles lose most of the nanoparticles during diapedesis, indicated by the partial overlap of the nanoparticle associated flow cytometry histogram of the nanoparticle modified cells and of the control cells. While on the contrary, the fluorescence signal of biotin nanoparticle modified cells only shows a shift with a small overlap of the fluorescence signal of the control cells (**Supporting Information Figure S13**). **Figure 10 A** shows the fraction of the total population of migrated cells that still display nanoparticle associated fluorescence (i.e. that still carry a payload) and reveals that 61 ± 7 % of all transmigrated maleimide nanoparticle modified cells, 34 ± 7 % of transmigrated COOH nanoparticle modified cells, 80 ± 7 % of all transmigrated biotin nanoparticle modified cells and 43 ± 14 % of all transmigrated WGA nanoparticle modified cells still carry nanoparticles. Although maleimide- thiol coupling is anticipated as strongest attachment to the cell surface the non-covalent immobilization of biotin nanoparticles to NeutrAvidin modified cells was observed to retain the most nanoparticles on the cell surface during diapedesis. To further investigate the numbers of nanoparticles which detached from the cell surface during transmigration the mean fluorescent intensity of the subpopulation which still carried nanoparticles post migration was compared with the mean fluorescent intensity of the cells directly after the nanoparticle modification (**Figure 10, B**).

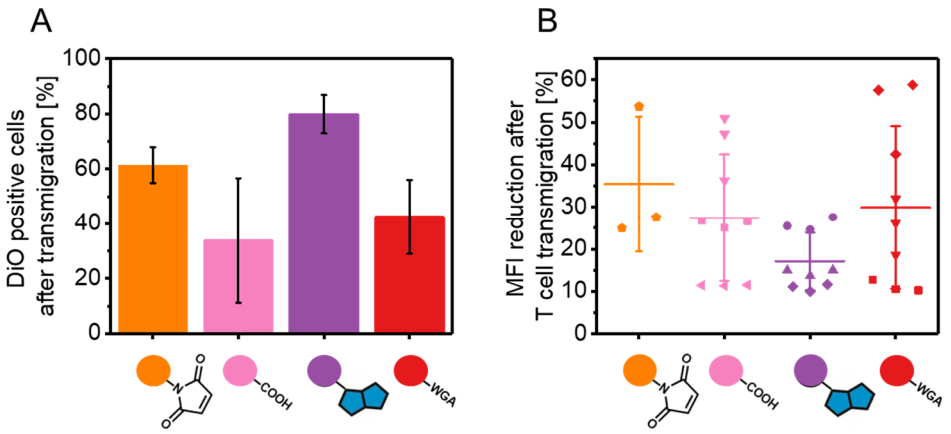

Figure 10: Flow cytometry analysis of transmigrated T cells based on the comparison of the DiO MFI. A: % of transmigrated T cells which still carry nanoparticles (DiO positive). B: The subpopulation of T cells which is still carrying nanoparticles was selected and the MFI compared to the MFI directly after modification to estimate how many nanoparticles were lost in the process of T cell diapedesis. The histogram presents the results of three independent experiments performed in triplicate and the error bars are standard deviations. The results obtained with the maleimide nanoparticles were performed as one experiment in triplicate.

Figure 11 shows fluorescent images taken from the luminal side of pMBMEC monolayer after the transmigration assay. The free nanoparticles and nanoparticle cluster on the cell monolayer confirm the above observed behavior that the T cells lose nanoparticles during the transmigration (**Figure 11 A**). However, also polarized T cells which are currently undergoing the process of diapedesis are visible. Activated T cells can be recognized by their elongated shape due to the morphological remodeling due to the interaction of the T cells and its ligands on the endothelial cell monolayer.[59] This process leads to the rearrangement of the nanoparticles to the uropod (**Figure 11 B**).

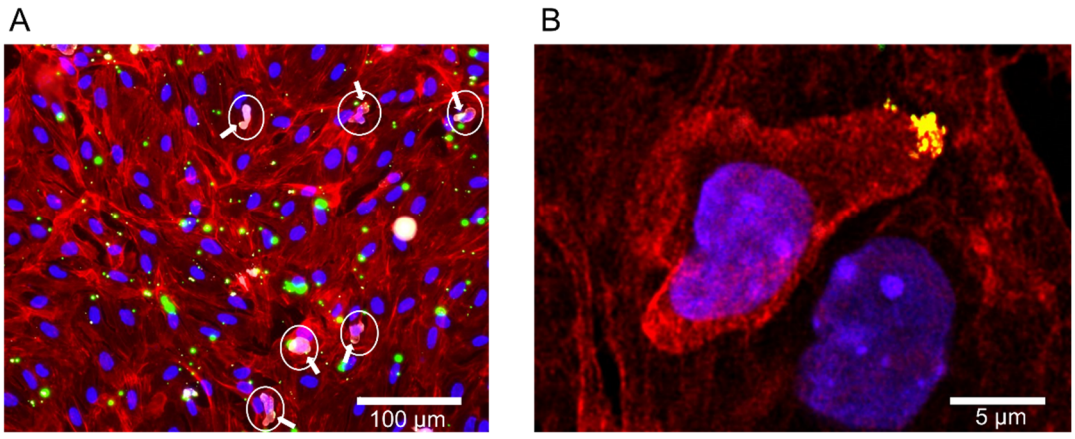

Figure 11: Fluorescent images of the pMBMEC monolayer after the transmigration assay. The actin filaments are shown in red (Rhodamine Phalloidin), the cell nuclei in blue (DAPI), biotin nanoparticles in green (DiO) and T cells in white (CD45-biotin, SA-Cy5). A: Widefield fluorescent image (20 x magnification) of the luminal pMBMEC monolayer. Exemplary nanoparticle conjugated SJL-PLP 7 are highlighted with white circles and nanoparticle localization is indicated with white arrows. B: Confocal fluorescent image (63 x magnification) of a polarized SJL-PLP 7 T cell with nanoparticles at the uropod on the pMBMEC monolayer.

3.4. Conclusions

Cell-mediated drug delivery is a promising method to enhance drug targeting by taking advantage of intrinsic cellular properties and using them as an active carrier. The drugs can be transported to the target tissue by chemically attaching nanoparticles to the cell surface. Herein, seven different covalent and non-covalent PLA nanoparticle conjugations strategies were systematically compared. The influence of conjugation chemistry and initial nanoparticle/cell feed ratio on the nanoparticle surface concentration and cell viability was evaluated. The cell surface concentration of nanoparticles greatly impacts cell viability. For all conjugation strategies, it was observed that higher nanoparticle surface concentrations led to decreased viability. Ideally, there is an optimum nanoparticle incubation condition which leads to a high nanoparticle cell surface concentration without impacting cell viability. As found here, this optimum depends on the efficiency of the chosen conjugation strategy. Non-covalent conjugation methods, such as WGA – lectin and biotin – NeutrAvidin are very efficient and require relatively low incubation excesses, which in turn leads to high nanoparticle cell surface concentration with minimal effects on viability. Nanoparticle

quantification by confocal microscopy revealed that at high initial nanoparticle/cell ratios (5000 Nanoparticles/ cell) a maximum surface decoration of 184 ± 56 for WGA nanoparticles/ cell and 176 ± 44 nanoparticles/ cell was achieved. In addition to remaining viable, it is crucial that the nanoparticle immobilization has no impact on cellular functions of the utilized T cells, i.e. in particular crossing endothelial cell barriers, such as the BBB. Nanoparticle attachment via maleimide-thiol coupling, electrostatic adhesion, biotin – NeutrAvidin and WGA – lectin at high initial nanoparticle/cell ratios does not influence the cell binding ability to ICAM-1. Finally it was shown, via a transendothelial migration assay, that nanoparticles conjugated to T cells using the biotin – NeutrAvidin binding motif able to transport across a model BBB carrying nanoparticles. In fact, approximately 80 % of the cells carried nanoparticles post transmigration.

3.5. References

(1) Duncan, R., *Nat. Rev. Cancer* **2006**, *6* (9), 688-701.

(2) Davis, M. E.; Chen, Z. G.; Shin, D. M., *Nat. Rev. Drug Discov.* **2008**, *7* (9), 771-82.

(3) Elsabahy, M.; Wooley, K. L., *Chem. Soc. Rev.* **2012**, *41* (7), 2545-61.

(4) Couvreur, P., *Adv. Drug Del. Rev.* **2013**, *65* (1), 581-596.

(5) Nicolas, J.; Mura, S.; Brambilla, D.; Mackiewicz, N.; Couvreur, P., *Chem. Soc. Rev.* **2013**, *42* (3), 1147-1235.

(6) Ferrari, R.; Sponchioni, M.; Morbidelli, M.; Moscatelli, D., *Nanoscale* **2018**, *10* (48), 22701-22719.

(7) Wilhelm, S.; Tavares, A. J.; Dai, Q.; Ohta, S.; Audet, J.; Dvorak, H. F.; Chan, W. C. W., *Nat. Rev. Mater.* **2016**, *1* (5), 16014.

(8) Danhier, F., *J Control Release* **2016**, *244* (Pt A), 108-121.

(9) Stephan, M. T.; Irvine, D. J., *Nano Today* **2011**, *6* (3), 309-325.

(10) Yoo, J.-W.; Irvine, D. J.; Discher, D. E.; Mitragotri, S., *Nat. Rev. Drug Discovery* **2011**, *10* (7), 521-535.

(11) Su, Y.; Xie, Z.; Kim, G. B.; Dong, C.; Yang, J., *ACS Biomater. Sci. Eng.* **2015**, *1* (4), 201-217.

(12) Fliervoet, L. A. L.; Mastrobattista, E., *Adv. Drug Del. Rev.* **2016**, *106*, 63-72.

(13) Villa, C. H.; Anselmo, A. C.; Mitragotri, S.; Muzykantov, V., *Adv. Drug Del. Rev.* **2016**, *106*, 88-103.

(14) Ayer, M.; Klok, H. A., *J. Controlled Release* **2017**, *259*, 92-104.

(15) Singh, B.; Mitragotri, S., *Biotechnol. Adv.* **2019**; *42*, 107339.

(16) Banskota, S.; Yousefpour, P.; Chilkoti, A., *Macromol. Biosci.* **2017**, *17* (1), 1600361.

(17) Pang, L.; Zhang, C.; Qin, J.; Han, L.; Li, R.; Hong, C.; He, H.; Wang, J., *Drug Deliv.* **2017**, *24* (1), 83-91.

(18) Zhao, Z.; Ukidve, A.; Kim, J.; Mitragotri, S., *Cell* **2020**, *181* (1), 151-167.

(19) Agrahari, V.; Agrahari, V.; Mitra, A. K., *Expert Opin. Drug Delivery* **2017**, *14* (3), 285-289.

(20) Chambers, E.; Mitragotri, S., *Exp. Biol. Med.* **2007**, *232* (7), 958-966.

(21) Chambers, E.; Mitragotri, S., *J. Controlled Release* **2004**, *100* (1), 111-119.

(22) Anselmo, A. C.; Gupta, V.; Zern, B. J.; Pan, D.; Zakrewsky, M.; Muzykantov, V.; Mitragotri, S., *ACS Nano* **2013**, *7* (12), 11129-11137.

(23) Brenner, J. S.; Pan, D. C.; Myerson, J. W.; Marcos-Contreras, O. A.; Villa, C. H.; Patel, P.; Hekierski, H.; Chatterjee, S.; Tao, J.-Q.; Parhiz, H.; Bhamidipati, K.; Uhler, T. G.; Hood, E. D.; Kiseleva, R. Y.; Shuvaev, V. S.; Shuvaeva, T.; Khoshnejad, M.; Johnston, I.; Gregory, J. V.; Lahann, J.; Wang, T.; Cantu, E.; Armstead, W. M.; Mitragotri, S.; Muzykantov, V., *Nat. Commun.* **2018**, *9* (1), 2684.

(24) Zelepukin, I. V.; Yaremenko, A. V.; Shipunova, V. O.; Babenyshev, A. V.; Balalaeva, I. V.; Nikitin, P. I.; Deyev, S. M.; Nikitin, M. P., *Nanoscale* **2019,** *11*, 1636-1646.

(25) Wayteck, L.; Dewitte, H.; De Backer, L.; Breckpot, K.; Demeester, J.; De Smedt, S. C.; Raemdonck, K., *Biomaterials* **2016**, *77*, 243-254.

(26) Stephan, M. T.; Moon, J. J.; Um, S. H.; Bershteyn, A.; Irvine, D. J., *Nat. Med.* **2010**, *16* (9), 1035-41.

(27) Stephan, M. T.; Stephan, S. B.; Bak, P.; Chen, J.; Irvine, D. J., *Biomaterials* **2012**, *33* (23), 5776-87.

(28) Timin, A. S.; Litvak, M. M.; Gorin, D. A.; Atochina-Vasserman, E. N.; Atochin, D. N.; Sukhorukov, G. B., *Adv. Healthcare Mater.* **2018**, *7* (3), 1700818-1700837.

(29) Park, J.; Andrade, B.; Seo, Y.; Kim, M.-J.; Zimmerman, S. C.; Kong, H., *Chem. Rev.* **2018**, *118* (4), 1664-1690.

(30) Abbina, S.; Siren, E. M. J.; Moon, H.; Kizhakkedathu, J. N., *ACS Biomater. Sci. Eng.* **2017**.

(31) Wibroe, P. P.; Anselmo, A. C.; Nilsson, P. H.; Sarode, A.; Gupta, V.; Urbanics, R.; Szebeni, J.; Hunter, A. C.; Mitragotri, S.; Mollnes, T. E.; Moghimi, S. M., *Nat. Nanotechnol.* **2017**, *12* (6), 589-594.

(32) Armstrong, J. P. K.; Shakur, R.; Horne, J. P.; Dickinson, S. C.; Armstrong, C. T.; Lau, K.; Kadiwala, J.; Lowe, R.; Seddon, A.; Mann, S.; Anderson, J. L. R.; Perriman, A. W.; Hollander, A. P., *Nat. Commun.* **2015**, *6* (1), 7405.

(33) Emmetiere, F.; Irwin, C.; Viola-Villegas, N. T.; Longo, V.; Cheal, S. M.; Zanzonico, P.; Pillarsetty, N.; Weber, W. A.; Lewis, J. S.; Reiner, T., *Bioconjugate Chem.* **2013**, *24* (11), 1784-1789.

(34) Cho, J.; Kushiro, K.; Teramura, Y.; Takai, M., *Biomacromolecules* **2014**, *15* (6), 2012-2018.

(35) Jacobs, J.; Byrne, A.; Gathergood, N.; Keyes, T. E.; Heuts, J. P. A.; Heise, A., *Macromolecules* **2014**, *47* (21), 7303-7310.

(36) Xu, M.; Asghar, S.; Dai, S.; Wang, Y.; Feng, S.; Jin, L.; Shao, F.; Xiao, Y., *Int. J. Biol. Macromol.* **2019**, *134*, 1002-1012.

(37) Cao, P.; Mooney, R.; Tirughana, R.; Abidi, W.; Aramburo, S.; Flores, L.; Gilchrist, M.; Nwokafor, U.; Haber, T.; Tiet, P.; Annala, A. J.; Han, E.; Dellinger, T.; Aboody, K. S.; Berlin, J. M., *Bioconjug Chem* **2017**, *28* (6), 1767-1776.

(38) Zheng, Y.; Tang, L.; Mabardi, L.; Kumari, S.; Irvine, D. J., *ACS Nano* **2017**, *11* (3), 3089-3100.

(39) Kolesnikova, T. A.; Kiragosyan, G.; Le, T. H. N.; Springer, S.; Winterhalter, M., *ACS Applied Materials & Interfaces* **2017**, *9* (13), 11506-11517.

(40) Li, L.; Guan, Y.; Liu, H.; Hao, N.; Liu, T.; Meng, X.; Fu, C.; Li, Y.; Qu, Q.; Zhang, Y.; Ji, S.; Chen, L.; Chen, D.; Tang, F., *ACS Nano* **2011**, *5* (9), 7462-7470.

(41) Huang, B.; Abraham, W. D.; Zheng, Y.; Bustamante López, S. C.; Luo, S. S.; Irvine, D. J., *Science Translational Medicine* **2015**, *7* (291), 291ra94-291ra94.

(42) Siriwon, N.; Kim, Y. J.; Siegler, E.; Chen, X.; Rohrs, J. A.; Liu, Y.; Wang, P., *Cancer Immunology Research* **2018**, *6* (7), 812-824.

(43) Wang, S.; Yin, D.; Wang, W.; Shen, X.; Zhu, J.-J.; Chen, H.-Y.; Liu, Z., *Sci. Rep.* **2016**, *6* (1), 22757.

(44) Holden, C. A.; Yuan, Q.; Yeudall, W. A.; Lebman, D. A.; Yang, H., *Int. J. Nanomed.* **2010**, *5*, 25-36.

(45) Saxon, E.; Bertozzi, C. R., *Science* **2000**, *287* (5460), 2007-2010.

(46) Wang, H.; Liu, Y.; Xu, M.; Cheng, J., *Biomater. Sci.* **2019**, *7* (10), 4166-4173.

(47) Zhang, P.; Zhang, X.; Li, C.; Zhou, S.; Wu, W.; Jiang, X., *ACS Applied Materials & Interfaces* **2019**, *11*, 36, 32697–32705.

(48) Thakur, V., Thakur, M., *New York: Jenny Stanford Publishing* **2016**.

(49) Engelhardt, B.; Laschinger, M.; Schulz, M.; Samulowitz, U.; Vestweber, D.; Hoch, G., *J. Clin. Invest.* **1998**, *102* (12), 2096-105.

(50) Wilhelm, C.; Billotey, C.; Roger, J.; Pons, J. N.; Bacri, J. C.; Gazeau, F., *Biomaterials* **2003**, *24* (6), 1001-1011.

(51) Nazarenus, M.; Zhang, Q.; Soliman, M. G.; Del Pino, P.; Pelaz, B.; Carregal-Romero, S.; Rejman, J.; Rothen-Rutishauser, B.; Clift, M. J. D.; Zellner, R.; Nienhaus, G. U.; Delehanty, J. B.; Medintz, I. L.; Parak, W. J., *Beilstein J. Nanotechnol.* **2014**, *5*, 1477-1490.

(52) Verma, A.; Stellacci, F., *Small* **2010**, *6* (1), 12-21.

(53) Tohver, V.; Smay, J. E.; Braem, A.; Braun, P. V.; Lewis, J. A., *Proc. Natl. Acad. Sci. U. S. A.* **2001**, *98* (16), 8950-8954.

(54) McKee, C. T.; Walz, J. Y., *J. Colloid Interface Sci.* **2012**, *365* (1), 72-80.

(55) Yang, B.; Gao, F.; Li, Z.; Li, M.; Chen, L.; Guan, Y.; Liu, G.; Yang, L., *J. Phys. Chem. Lett.* **2020**, *11* (8), 2788-2796.

(56) Cha, J.; Kim, H.; Hwang, N. S.; Kim, P., *ACS Applied Materials & Interfaces* **2018**, *10* (42), 35676-35680.

(57) Reiss, Y.; Hoch, G.; Deutsch, U.; Engelhardt, B., *Eur. J. Immunol.* **1998**, *28* (10), 3086-99.

(58) Steiner, O.; Coisne, C.; Engelhardt, B.; Lyck, R., *J. Cereb. Blood Flow Metab.* **2011**, *31* (1), 315-327.

(59) Sánchez-Madrid, F.; Serrador, J. M., *Nature reviews. Molecular cell biology* **2009**, *10* (5), 353-9.

3.6. Supporting Information

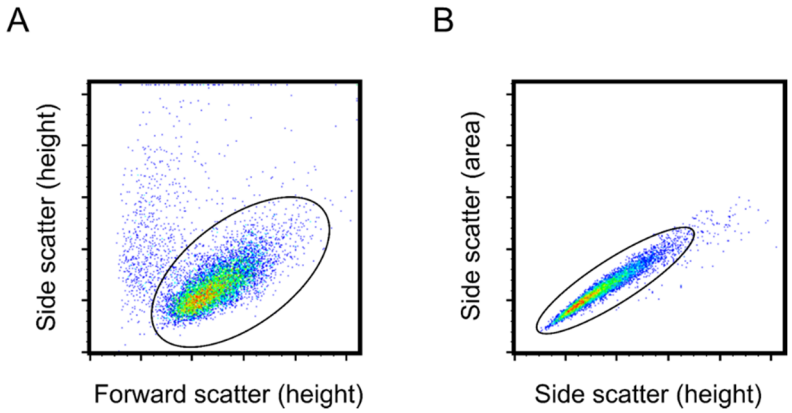

Figure S1: Flow cytometry scatter plots and gating strategy used for flow cytometry analysis. (A) The viable T cell population was selected by plotting height of the side scattered signal versus the height of the forward scattered signal; (B) Multiple cells were excluded from the analysis by plotting the area of the signal obtained from side scatter versus the height of the signal obtained from side scattering.

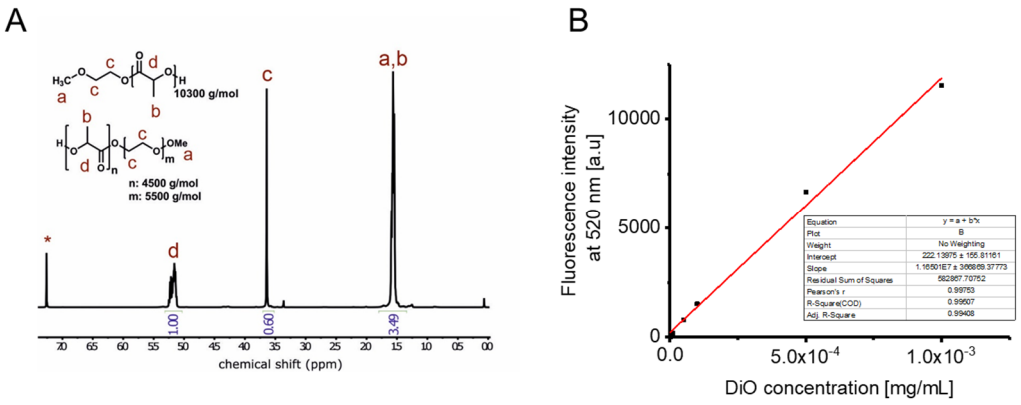

Figure S2: A: ^{1}H-NMR spectrum of lyophilized nanoparticles dissolved in $CDCl_3$. B: Calibration curve of DiO in DMSO (excitation wavelength: 480 nm, emission wavelength: 520 nm.

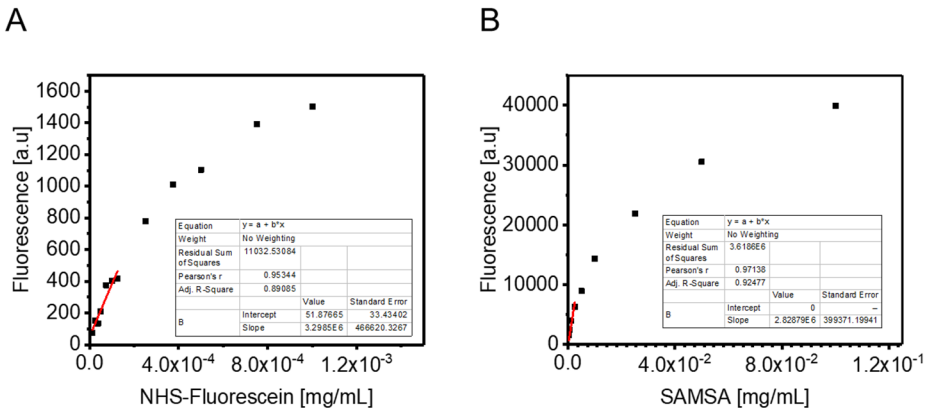

Figure S3: A: Calibration curve of NHS-fluorescein and linear fit in the linear region of the fluorescent signal. B: Calibration curve of SAMSA Fluorescein (5-((2-(and-3)-S-(acetylmercapto) succinoyl) amino) Fluorescein) to determine the thiol surface concentration of nanoparticles.

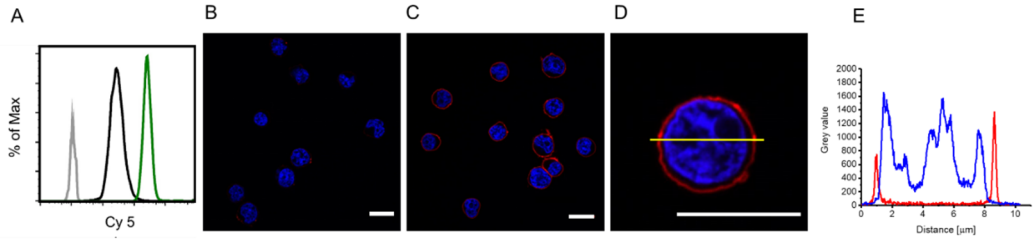

Figure S4: Unmodified cells and TCEP-treated cells were incubated with 20 µM sulfo-cyanine 5 maleimide to show successful surface modification. A: Flow cytometry histogram. Control cells are shown in grey, unmodified and TCEP-treated cells incubated with the fluorescent dye are illustrated in black and green, respectively. B: Confocal microscopy image of unmodified cells incubated with sulfo-cyanine 5 maleimide. C: Confocal microscopy image of TCEP-treated cells incubated with sulfo-cyanine 5 maleimide. D: Image of a single cell using the same conditions as in C. E: Intensity profile of the single cell shown in D. Red: Cy 5 and blue: DAPI. The scale bars represent 10 µm.

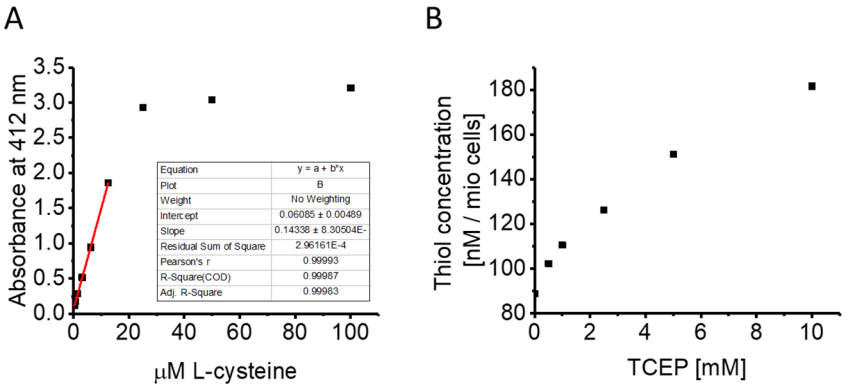

Figure S5: Spectrometric quantification of the thiol surface concentration of Jurkat cells using Ellman's reagent (5,5'-dithiobis-(2-nitrobenzoic acid) (DTNB)). A: Standard absorbance curve after the reaction of L-cysteine with Ellman's reagent and linear progression. B: Calculated thiol surface concentration of cells which were treated with 0, 0.5, 1, 5 or 10 mM TCEP.

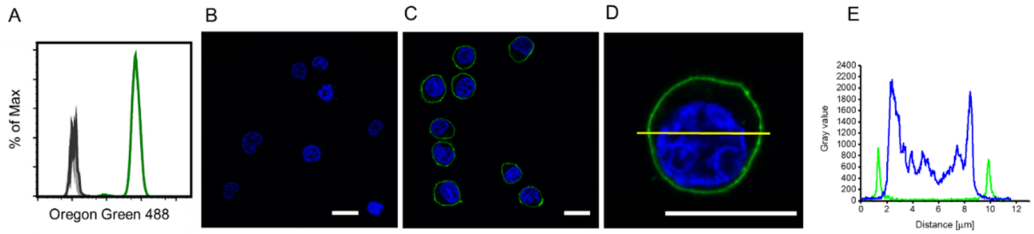

Figure S6: Unmodified cells and Biotin-XX,SSE-treated cells were incubated with 2 µM NeutrAvidin – Oregon Green 488 to show successful surface modification. A: Flow cytometry histogram. Control cells are shown in grey, unmodified and Biotin-XX,SSE-treated cells postmodified with the fluorescent dye are illustrated in black and green, respectively. B: Confocal microscopy image of unmodified cells incubated with Biotin-XX,SSE. C: Confocal microscopy image of Biotin-XX,SSE-treated cells incubated with NeutrAvidin – Oregon Green 488. D: Image of a single cell using the same conditions as in C. E: Intensity profile of the single cell shown in D. Green: Oregon Green 488 and blue: DAPI. The scale bars represent 10 µm.

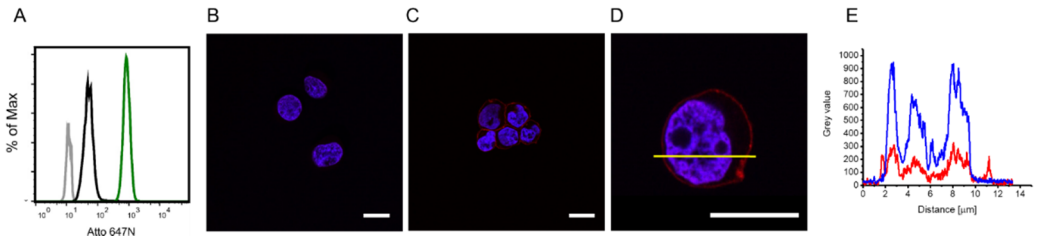

Figure S7: Unmodified cells and NeutrAvidin-coated cells were incubated with Atto 647N-Biotin to show successful surface modification. A: Flow cytometry histogram. Control cells are shown in grey, unmodified and NeutrAvidin-coated cells postmodified with the fluorescent dye are illustrated in black and green, respectively. B: Confocal microscopy image of unmodified cells incubated with Atto 647N-Biotin. C: Confocal microscopy image of NeutrAvidin-coated cells incubated with Atto 647N-Biotin. D: Image of a single cell using the same conditions as in C. E: Intensity profile of the single cell shown in D. Red: Atto 647N and blue: DAPI. The scale bars represent 10 µm.

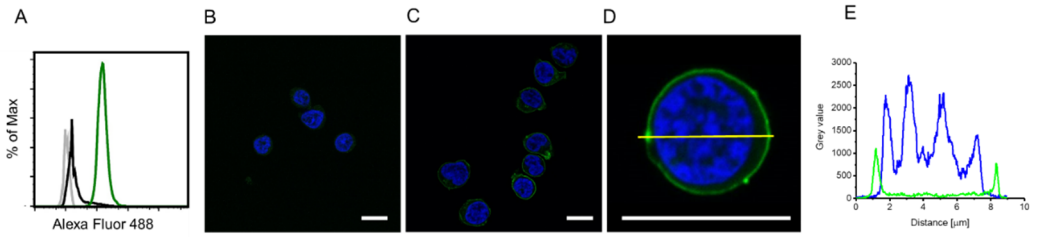

Figure S8: Unmodified cells and N_3-expressing cells were incubated with Alexa Fluor 488 DBCO to show demonstrate the incorporation of azide groups into the cell glycocalyx. A: Flow cytometry histogram. Control cells are shown in grey, unmodified and N_3-cells modified with the fluorescent dye are illustrated in black and green, respectively. B: Confocal microscopy image of unmodified cells incubated with Alexa Fluor 488 DBCO. C: Confocal microscopy image of N_3-cells incubated with Alexa Fluor 488 DBCO. D: Image of a single cell using the same conditions as in C. E: Intensity profile of the single cell shown in D. Green: Alexa Fluor 488 and blue: DAPI. The scale bars represent 10 µm.

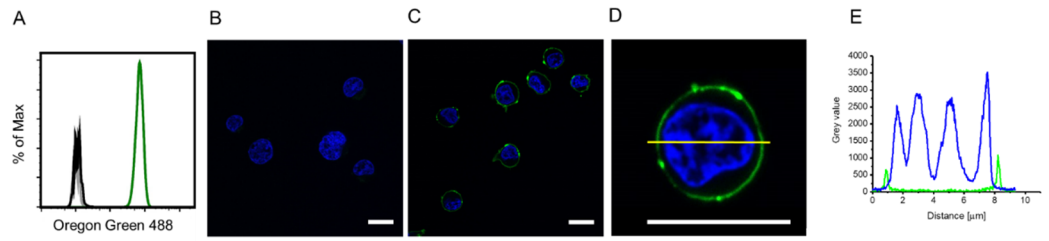

Figure S9: Unmodified cells and biotin cells were incubated with NeutrAvidin, Oregon Green 488 to show demonstrate the incorporation of the biotin moiety into the cell membrane by lipid insertion. A: Flow cytometry histogram. Control cells are shown in grey, unmodified and biotin modified cells stained with the fluorescent dye are illustrated in black and green, respectively. B: Confocal microscopy image of unmodified cells incubated with NeutrAvidin, Oregon Green 488. C: Confocal microscopy image of biotin cells incubated with NeutrAvidin, Oregon Green 488. D: Image of a single cell using the same conditions as in C. E: Intensity profile of the single cell shown in D. Green: Oregon Green 488 and blue: DAPI. The scale bars represent 10 µm.

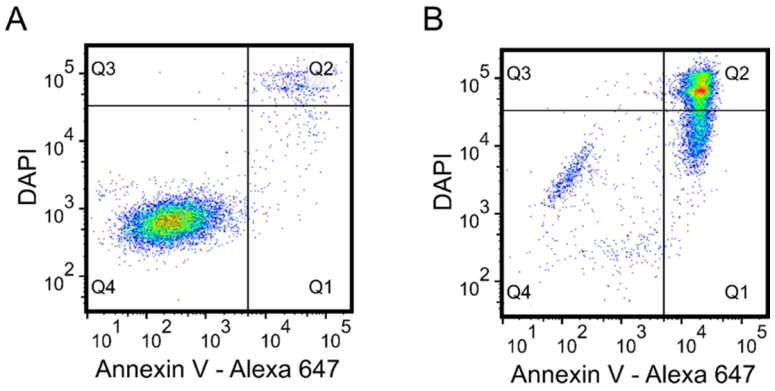

Figure S10: Gating strategy for the Annexin V/ DAPI viability assay. Viable cells were gated as quadrant Q4, early apoptotic cells as quadrant Q1, late apoptotic and necrotic cells as quadrant Q2 and Q3. A: Control cells. B: Staurosporine treated cells.

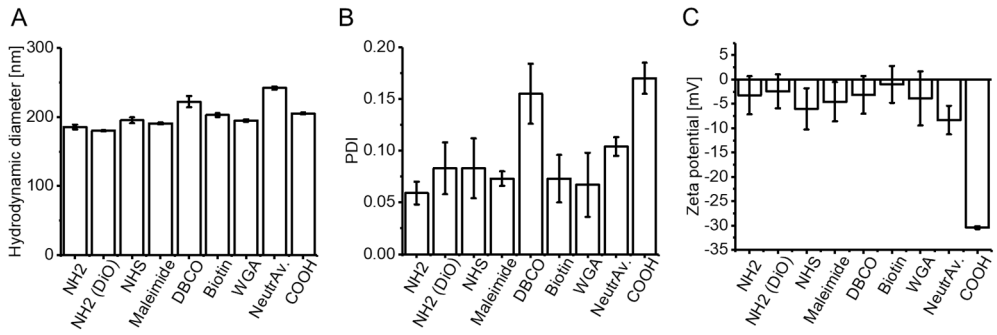

Figure S11: Characterization of PEG-PLA and PLA-COOH nanoparticles using DLS. A) Hydrodynamic diameters, B: PDIs and C: zeta-potentials. All measurement were performed in triplicate and the error bars represent the standard deviations.

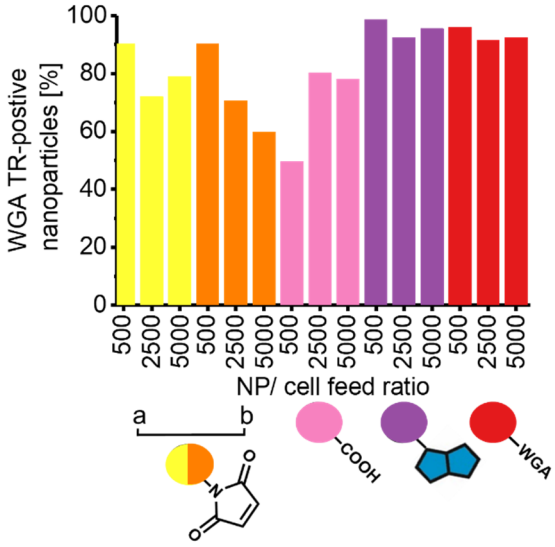

Figure S12: Ratio of nanoparticles which colocalize with the WGA Texas Red membrane stain at initial nanoparticle/cell feed ratio of 500, 2500 and 5000. Yellow: maleimide nanoparticle modified cells, orange: maleimide nanoparticle modified and TCEP treated cells, rose: COOH nanoparticle modified cells and red: WGA nanoparticle modified cells.

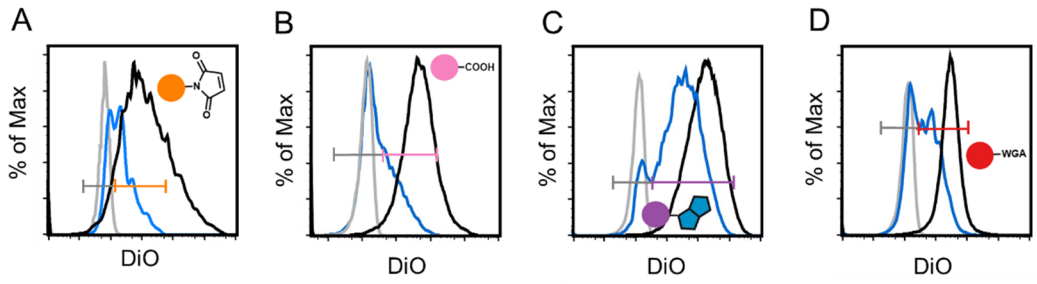

Figure S13: Representative flow cytometry histograms showing nanoparticle- associated fluorescence of SJL-PLP 7 cells before and after transmigration. Control cells are shown in grey, cells directly after the modification with an initial ratio of 5000 NP/ cell in black and transmigrated cells in blue. A: TCEP treated cells were incubated with maleimide PEG-PLA nanoparticles, B: unmodified cells with COOH- PLA nanoparticles, C: NeutrAvidin modified cells were incubated with biotin functionalized PEG-PLA nanoparticles and D: unmodified cells were incubated with WGA functionalized PEG-PLA nanoparticles.

4. Conclusions and Perspectives

The use of cells as drug carrier has efficiently improved the delivery of therapeutics and adjuvants to the brain, lungs and cancer tissue. However, there are still various fundamental questions to be further studied to improve the performance of cell-based polymer nanomedicines. This work shows the importance of an extensive characterization of nanoparticle-decorated cells, elicits certain weaknesses of conventional fluorescent-based methods and shows an alternative fluorescent label-free technique to analyze nanoparticle decorated cells. Most of the techniques used for the analysis of nanoparticle-decorated cells rely on the addition of labels such as fluorescent- or radioactive compounds. The modification of nanoparticles with labels can change the properties of the nanoparticles, alter the nanoparticle-cell interaction or be released from the nanoparticles. It was shown here that fluorescent labels can leach from the nanoparticles generating a false negative result. Fluorescent-label free methods imaging methods provide an alternative imaging strategy to visualize nanoparticles on the cell membrane without the need of labels. In conclusion, the encapsulation of fluorescent or drug molecules has to be closely evaluated in a biological environment to ensure a safe drug transport to the target tissue without premature leakage from the nanoparticles, for example in a burst release.

Although many studies have demonstrated that nanoparticles can be conjugated to cells using covalent and non-covalent interactions, the influence of conjugation chemistry and nanoparticle surface concentration has not been systematically studied in the past. This work aims to show the impact of nanoparticle conjugation chemistry and nanoparticle surface concentration on cell viability, cell proliferation and cell functionality. This work demonstrates the efficient binding of nanoparticles to the cell surface using receptor – ligand interactions. They allow high nanoparticle coverages at low initial nanoparticle/cell feed ratios and therefore very low cell viability impairment. The coupling of WGA nanoparticles to the cell surface leads to the highest nanoparticle surface concentrations, however transendothelial migration of nanoparticle decorated cells reveals a significant loss of nanoparticles. The immobilization of nanoparticles using the NeutrAvidin – biotin motif also leads to a high nanoparticle surface concentration and has been shown to be the most robust conjugation since after transendothelial migration still 80 % of the cells carried nanoparticles. In conclusion, the NeutrAvidin – biotin interactions offers an efficient nanoparticles immobilization strategy, with negligible cell viability impairment, no

impairment of ICAM-1 binding and a high nanoparticle transport rate across a transendothelial barrier.

However, a number of questions still remain unanswered. Does the nanoparticle conjugation efficiency depend on the number of functional groups on the cell surface or on the cell type or its activation state? What role plays the binding affinity and binding valency of ligands – receptor interactions? How can cells be efficiently labeled with nanoparticles (i.e. at a high nanoparticle conversions)? Further studies should aim to answer these questions and provide an improved comprehension of the interaction between nanoparticles and the cell surface at a molecular level.

To optimize and standardize the characterization of nanoparticle- modified cells as well as the deliberate exploitation of the chemical nature of cells are fundamental for the development of more advanced cell- mediated drug delivery systems.

Tanja Thomsen

Av. F.C.-de-la-Harpe 10
CH - 1007 Lausanne
+41(78) 634 33 83
tanjthomsen@gmail.com
Skype ID: ttanjathomsen

Education

Swiss Federal Institute of Technology, Lausanne (EPFL)
PhD in Material Science (2015 – present)

University of Stuttgart (Germany)
Master of Science in Chemistry (2012 – 2014)

Christian-Albrecht University of Kiel (Germany)
Bachelor of Science in Chemistry (2009 – 2012)

Core Experience

Polymers Laboratory (EPFL) (2015 – present)

Cell- mediated drug delivery across the blood-brain barrier (*Doctoral thesis).*

- Multidisciplinary project to develop a novel drug delivery strategy. The research combined Pharmaceutical Sciences (polymer nanoparticle preparation and characterization) with Chemistry (bioconjugation reactions) and Biology (live cell nanoparticle conjugation, extensive characterization of nanoparticle – cell conjugates and evaluation in an *in vitro* blood-brain barrier model).
- The project was carried out in a multidisciplinary environment with the Theodor Kocher Institute (University of Bern) for Neuroimmunobiology and the Optics Laboratory at EPFL.

Polymeric Materials Laboratory (University of Stuttgart) (2014)

Polymer synthesis of redox - active materials for electrochemical devices, such as solar cells and batteries *(Master thesis*).

- Implementation of a new synthesis strategy to control polymer structure – property relationships at the molecular and mesoscopic scale in films.

Additional Experience

Polymers Laboratory (EPFL) (2015 – present)

- Teaching assistant for Polymer Chemistry and Macromolecular Engineering Master course and supervision of project Master students.
- Presentations in international conferences (posters and talk).
- Lab manager for a lab used by multiple groups: responsible for lab organization, maintenance of instruments, monitoring inventory and ordering of lab supplies.
- Communication and presentation of complex scientific topics to a broad audience as a participant in the "My thesis in 180 Seconds" final at EPFL (spring 2020).

Languages

English: Fluent, spoken and written (C2)
French: Intermediate, spoken (B1) and written (A2)
German: Native language

Technical Skills

Life Sciences skills	Cell culture, Viability assay, Proliferation assay, Binding assay, Flow cytometry and Confocal microscopy.
Chemistry skills	Organic synthesis, Polymer Chemistry, Bioconjugation Chemistry, Nanoparticle / micelle preparation and purification.
Analytical skills	Size exclusion chromatography (SEC), Nuclear magnetic resonance (NMR), Dynamic light scattering (DLS), UV-Vis spectroscopy, Fluorescence spectroscopy, Fourier transform infrared spectroscopy (FTIR), Differential scanning calorimetry (DSC) and Cyclic voltammetry (CV).
IT skills	Adobe Illustrator, Photoshop, CorelDRAW, Imaris, FlowJo, Image J, Origin, MATLAB, TopSpin, MestReNova NMR, ChemDraw Bio and MS Office Professional (XP, W10; PC and Mac).
Project management	Laboratory logistics and safety, coordination of courses and supervision of students.

Scientific Publications

- Thomsen, T.; B. Ayoub, A.; Psaltis, D.; Klok, H.-A. *Fluorescence-based and Fluorescent label-free Characterization of Polymer Nanoparticle Decorated T cells. Biomacromolecules* **2020***,* in press. DOI: 10.1021/acs.biomac.0c0096.
- Thomsen, T.; Reissmann, R.; Kaba, E.; Engelhardt, B.; Klok, H.-A. *Chemical conjugation strategies of nanoparticles to T lymphocytes and their influence on viability and functional properties.* In preparation.